

Stellingen

1. Stellingen met het onderschrift 'dit proefschrift' gaan voorbij aan het doel van stellingen bij een proefschrift.
2. Elk systeem kan worden beschreven als zijnde fractaal op een zekere lengteschaal terwijl geen enkel systeem fractaal is op alle lengteschalen.
L. Bremer, proefschrift Landbouwniversiteit Wageningen, 1992.
3. Voor kolloïdale deeltjes die volledig bedekt zijn met polymeer voorspellen evenwichtstheoriën een attractie tussen de deeltjes als desorptie van het polymeer mogelijk is. Aangezien ze in de praktijk stabiel zijn bewijst dit dat er een kinetische barrière is tegen aggregatie van zulke deeltjes.
4. Bij afwezigheid van de 'disjoining pressure' in de vloeistoffilms in een schuim zorgt drainage voor een zeer snelle afbraak van het schuim.
R. Tuinier, C. G. J. Bisperink, C. van den Berg, A. Prins, *J. Colloid Interface Sci.* **179** (1996) 327.
5. Bij de evolutie van micro-organismen speelt zout een belangrijke rol.
K. Kawada, *Adv. Colloid Interface Sci.* **71** (1997) 299.
6. Bij het begrijpen van de 'Big Bang' lopen wetenschappers tegen een singulariteit aan zodat in dit geval het begin het einde is.
S.W. Hawking, R. Penrose, *Scientific American* **275** (1996) 60.
7. Zolang er veel mensen zijn die geloven in paranormale verschijnselen is het van belang dat er wetenschappers zijn die paranormale pretenties onderzoeken op hun juistheid.
J. Utts, *Statistical Science*, **6** (1991) 363.
8. De geografisch discutabele aanduiding van Wageningen als 'Food Valley' zou vervangen moeten worden door 'Food Hill'. De ambities van het 'Technologisch TOP Instituut Voeding' worden door deze term ook beter gedekt.
9. De uitdrukking 'alles went behalve een vent' mag worden geïnterpreteerd als blijk van waardering voor het verrassende gedrag van mannen.
10. De hoogte van het budget van een universitaire onderzoeksgroep zou af moeten hangen van de onderwijslast, het prestatieniveau van de onderzoeksgroep en de maatschappelijke relevantie van het onderzoek.

Promotoren: Prof. Dr. M.A. Cohen Stuart
hoogleraar fysische chemie, met bijzondere aandacht voor de
kolloïdchemie (LUW)
Prof. Dr. G.J. Fleer
persoonlijk hoogleraar bij het laboratorium voor Fysische Chemie en
Kolloïdkunde (LUW)

Co-promotoren: Dr. C.G. de Kruif (NIZO food research), Ede
Dr. Ir. P. Zoon (NIZO food research), Ede

1100001. 2502.

An exocellular polysaccharide and its interactions with proteins

Remco Tuinier

Proefschrift

ter verkrijging van de graad van doctor

op gezag van de rector magnificus

van de Landbouwniversiteit Wageningen,

dr. C.M. Karszen,

in het openbaar te verdedigen

op vrijdag 4 juni 1999

des namiddags te half twee in de Aula

van g64115

Tuinier, Remco

An exocellular polysaccharide and its interactions with proteins
(Een exocellulair polysaccharide en de interacties met eiwitten)

Remco Tuinier. -[S.l. : s.n.]

Thesis Wageningen - with refs. - with summary in Dutch

Subject headings: polysaccharide, protein, rheology, scattering, depletion interaction.

ISBN 90 5808 04 98

Cover design: Jeannette Kröner

Fotografie: Henk van Brakel, Jan Klok en Fanny Weinbreck

Het onderzoek dat is beschreven in dit proefschrift is financieel mogelijk gemaakt door de
Associatie van Biotechnologisch Onderzoek Nederland (ABON).

BIBLIOTHEEK
LANDBOUWUNIVERSITEIT
WAGENINGEN

'... and inside every turning leaf
is the pattern of an older tree
the shape of our future
the shape of all our history ...'

Gordon Sumner (Sting) in 'I was brought to my senses,' 1996.

Dedicated to the memory of Cyril Renaud (1972-1998)

Contents

Chapter 1	Introduction	1
	Polysaccharides	1
	Sources of polysaccharides	3
	Model descriptions of polysaccharides	6
	Rheology of exocellular polysaccharides	7
	Interactions between polysaccharides and proteins	7
	Colloidal components in milk	9
	Whey proteins	10
	Casein micelles	10
	Emulsions	11
	Outline of this thesis	11
	References	13
Chapter 2	Isolation and physical characterization of an exocellular polysaccharide	15
	Abstract	15
	Introduction	16
	Theory	17
	Static light scattering	18
	Dynamic light scattering	19
	Polymer chain dimensions in dilute solution	20
	Materials and methods	21
	EPS production	21
	EPS isolation	22
	Purification	23
	EPS analysis	23
	Gel permeation chromatography	23
	Dynamic light scattering	24
	Results and discussion	24
	Conclusions	29
	References	30
Chapter 3	Concentration and shear-rate dependence of an exocellular polysaccharide	33
	Abstract	33
	Introduction	34
	Theory	35
	Concentration dependence of the zero-shear viscosity	35
	Shear-rate dependence	37
	Experimental	40
	Results and discussion	40
	Intrinsic viscosity	40
	Concentration dependence of the zero-shear viscosity	41
	Shear-rate dependence	43
	Conclusions	47
	References	48

Chapter 4	Viscoelastic properties of a polysaccharide produced by a <i>Lactococcus lactis</i>	49
	Abstract	49
	Introduction	50
	Theory	50
	Oscillatory flow	50
	Relaxation times	51
	Relation between the storage modulus and normal stresses	52
	Materials and methods	53
	Results and discussion	54
	Description of dynamic moduli	54
	Concentration dependence of the moduli	55
	Relationship between static and oscillatory shear flow	57
	Conclusions	60
	References	61
Chapter 5	Depletion induced phase separation of aggregated whey protein colloids by an exocellular polysaccharide	63
	Abstract	63
	Introduction	64
	Theory	65
	Static scattering	65
	Analysis of molar mass and radius of gyration	65
	Influence of interactions on the scattered intensity	66
	Dynamic light scattering (DLS)	67
	Depletion interaction theory	67
	Phase separation kinetics	70
	Methods and materials	72
	Experimental techniques	72
	Small-Angle Neutron Scattering (SANS)	72
	Size exclusion chromatography-static light scattering (SEC-SLS)	72
	Dynamic light scattering (DLS)	72
	Small-angle light scattering (SALS)	72
	Material	73
	Exocellular polysaccharide	73
	Aggregated whey protein colloids (AWCs)	73
	Characterization of the AWC-aggregates	74
	AWC/EPS mixtures	75
	Results and discussion	75
	Attractions	75
	Small-angle neutron scattering (SANS)	75
	Dynamic light scattering	80
	Phase diagram	81
	Phase separation kinetics	84
	Conclusions	88
	Appendix	88
	References	91

Chapter 6	Depletion interaction of casein micelles and an exocellular polysaccharide	93
	Abstract	93
	Introduction	94
	Theory	95
	Depletion interaction theory	95
	Adhesive hard sphere model	97
	Scattering techniques	98
	Dynamic light scattering	98
	Small-angle neutron scattering (SANS)	99
	Turbidity measurement	100
	Experimental methods	101
	Material	101
	Scattering techniques	102
	Dynamic light scattering	102
	Small-Angle Neutron Scattering (SANS)	102
	Turbidity measurement	102
	Results and discussion	103
	Self-diffusion	103
	Structure factors	105
	Turbidity	111
	Conclusions	113
	References	113
Chapter 7	Phase behavior of casein micelles/exocellular polysaccharide mixtures; experiment and theory	115
	Abstract	115
	Introduction	116
	Theory	118
	Depletion interaction theories	118
	Vrij theory	118
	Lekkerkerker theory	121
	Adhesive hard sphere model	123
	Phase separation from self-diffusion	124
	Experimental	125
	Results and discussion	126
	Observations and phase diagram	126
	Theoretical description	129
	The Vrij model	129
	Lekkerkerker theory	129
	Phase diagram from self-diffusion	130
	Conclusions	131
	Appendix	132
	References	134

Chapter 8	Phase separation, creaming, and network formation of oil-in-water emulsions induced by an exocellular polysaccharide	137
	Abstract	137
	Introduction	138
	Theoretical background	139
	Creaming in O/W emulsions	139
	The viscosity of weakly aggregated dispersions	141
	Materials	143
	Methods	143
	Preparation of the emulsion mixtures	143
	Experimental techniques	143
	Emulsion stability	144
	Results and discussion	145
	Phase diagram	145
	'Gel'-region	147
	Demixing kinetics	148
	Rheology	153
	Conclusions	155
	References	156
Chapter 9	Practical implications and future work	159
	Viscosity of EPS solutions	159
	Dynamic rheological properties of EPS solutions	161
	EPS and its interactions with proteins	162
	Suggestions for future work	165
	References	167
	Summary	169
	Samenvatting	172
	List of symbols	176
	List of publications	181
	Dankwoord	182
	Curriculum Vitae	184

1

General introduction

Polysaccharides

According to the Oxford dictionary a polymer is 'a compound whose molecule is formed from a large number of repeated units of one or more compounds of low molecular mass'. In simple words this means that polymers are multiples of connected monomers. An important class of polymers are polysaccharides, consisting of connected monosaccharides. The most common units occurring in polysaccharides are glucose, galactose, and mannose; somewhat less common are xylose, rhamnose and arabinose. Most monosaccharide molecules have a pentagonal or hexagonal carbon ring structure with an oxygen atom as one of the corners. The chemical structure of a β -D-glucose molecule is given in Figure 1.

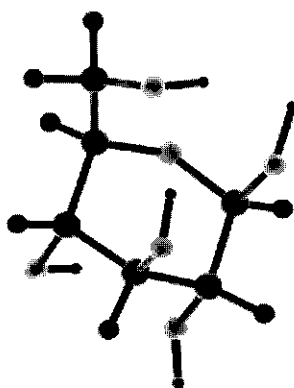


Figure 1 Ball and stick model of β -D-glucose.

The oxygen- (light gray), carbon (gray) and hydrogen (dark gray) atoms can be recognized by the number of covalent bonds. Most monosaccharide molecules have a pentagonal or (as in Figure 1) hexagonal carbon ring structure with an oxygen atom as one of the corners. In hexosaccharides the carbon atoms are numbered from 1 to 6. The five carbon atoms in the ring are numbered from 1 to 5, where C1 and C5 are linked to the oxygen in the ring. The C6 atom is linked to the C5 carbon atom. In amino sugars an -NH_2 group replaces an -OH group, as is the case in glucosamine and galactosamine.

Chemically, polysaccharides are thus carbohydrates consisting of sugar (monosaccharide) residues, covalently linked together via glycosidic bonds. Such linkages of the sugar residues can occur through, for instance, α - or β - (1 \rightarrow 3), (1 \rightarrow 4) or (1 \rightarrow 6) bonds. When the polysaccharide consists of only one type of monosaccharide the polysaccharide is denoted as a homopolysaccharide whereas it is called a heteropolysaccharide when it consists of two or more different sugar residues. Variation in linkage and sugar composition leads to a large number of types of polysaccharides. Within a polysaccharide the sugar may be present in the backbone or as a side group, linked to a backbone monosaccharide. Polysaccharides can be either linear or branched. A polysaccharide is denoted as branched when it contains one or more points where three or more chains emanate.

A special feature of polysaccharides is that they often carry ionizable groups, such as carboxyl groups (replacing -OH groups) in, for instance, carboxymethylcellulose (CMC). This then makes the polysaccharide also a polyelectrolyte. The properties of polyelectrolytes strongly depend on the ionic strength of the solution. The charged groups on the polyelectrolyte attract counterions and repel co-ions. At low ionic strength ($< \sim 10^{-2}$ M) internal electrostatic repulsion makes the polyelectrolyte more rigid than its neutral analogue. With increasing ionic strength the charges become more screened and at high ionic strength the behavior of a solution of polyelectrolytes resembles that of neutral polymers. Sometimes, counterions may act as a 'glue' connecting the polyelectrolyte segments, thereby inducing gelation of the polyelectrolyte solution.

Charged polysaccharides can be divided into two groups - weak and strong polyelectrolytes - depending on the value of the dissociation constant of the ionizable group. If all ionizable groups dissociate at pH values above 2, the polyelectrolyte is denoted as strong, whereas it is weak when only a part of the groups dissociate. Strong polyelectrolytes carry e.g. $\sim\text{SO}_3^-$ (as in carrageenans and glycosaminoglycans such as in heparin) or $\sim\text{HPO}_4^-$ groups, as in the polysaccharide described in this thesis, whereas a weak polyelectrolyte carries weak acid groups, e.g. a $\sim\text{COO}^- / \text{COOH}$ group (as in pectins and CMC) or pyruvate groups such as in xanthan. The properties of weak polyelectrolytes are strongly pH-dependent.

In this thesis I describe various properties of a particular type of polysaccharide which is present naturally in acidified milk products. The polysaccharide is a strong polyelectrolyte. The focus is on two main subjects. Firstly, the relation between the primary structure, the molecular parameters (molar mass, radius of gyration) and the rheological behavior in aqueous solution is investigated. Secondly, the interactions of the polysaccharide with proteins, as relevant in many food products, are studied.

Sources of polysaccharides

Polysaccharides are ubiquitous in biological systems. In industry, polysaccharides have become frequently used biopolymers. They constitute about 60% of the industrial water-soluble polymers [1]. The vast majority of polysaccharides is from vegetable sources, in particular from cellulose as present in plants. Below, some aspects of plant polysaccharides are first considered, after which polysaccharides produced by bacteria are discussed, the latter are relevant for this thesis.

Plants, and in particular plant cell walls, consist of polysaccharides such as celluloses, xyloglucans and pectins. These substances provide a rigid structure as found, for instance, in tree trunks. Cellulose is the most abundant organic material on earth. A remarkable manifestation of the presence of plant polysaccharides is in the seas and oceans. In the littoral polysaccharides are harvested from thousands of varieties of seaweed. Algal polysaccharides, such as agar, alginates, and carrageenan probably give the seaweed the strength needed to withstand the varying stresses due to tides and waves. In plants, carbohydrate polymers can also serve as energy storage units; starch is a well-known example.

In Gram-positive bacteria the bacterial cell wall consists of peptidoglycan, a polysaccharide with covalently linked peptide groups. Peptidoglycan forms a solid barrier which protects the underlying protoplast, resists turgor (osmotic pressure shocks), and helps to maintain the shape of the cell. As well as being a component of bacteria themselves, polysaccharides can also be excreted by the bacterial cells. In the 19th century it was discovered that the bacterium *Leuconostoc mesenteroides* is able to produce a glucan, later named dextran, which became of importance in the food industry, especially as a viscosifier. Nowadays, various microbial polysaccharides, e.g. xanthan and gellan, are used industrially and can be found in various products in which an increased viscosity is needed. Quite often, a relatively low concentration (<1%) is sufficient to increase the fluid viscosity significantly [2].

Polysaccharides produced by micro-organisms can be divided into three categories. Firstly, capsular polysaccharides (CPSs) are firmly attached to the cells and not extractable in cold water [3]. Secondly, loosely associated material (LAM) can be detached from the wall of the bacterial cells by external forces, such as shear. Thirdly, extra- or extracellular polysaccharides (EPSs) are excreted into the surrounding medium. In some cases polysaccharides are produced in-situ in food products, notably in acidified milk products, such as yogurt and viliiii. The 'slimy' or 'ropy' flow behavior of such products is usually attributed to the presence of polysaccharides.

Lactic acid bacteria (and yeasts) are the most important industrial micro-organisms [4]. Already in ancient Egypt fermentation was deliberately used for food preparation, albeit without

the knowledge of the role of micro-organisms. Several micro-organisms are used for the fermentation of milk and for wine-making and these organisms have received much attention over the last decades. The work of microbiologists and genetic engineers on genera such as streptococci and lactobacilli, and especially the *Lactococcus lactis* has contributed to new developments in fermentation. Increasing knowledge on the metabolism of lactic acid bacteria has enabled many steps in fermentation processes to be optimized. For instance, in butter production the essential metabolites, lactic acid and diacetyl, can be produced in special fermentations and are added to the churned cream [5]. This enhances the control over the production process. Since the catabolism of sugar and the biosynthesis of cell wall material are almost separate metabolic pathways, lactic acid bacteria are ideally suited for metabolic engineering [6]. It is therefore possible to engineer overproduction of various interesting metabolites such as alcohol, acetoin, diacetyl [7] and EPS.

The presence of 'slime-producing' micro-organisms in milk was first recognized some 150 years ago by Ehrenberg [8]. At the beginning of this century Buchanan and Hammer [9] discovered that in-situ production of *Bacterium bulgaricum* increased the viscosity of (slimy) milk. Ropy cultures as they were called have been recognized as a means to increase the viscosity of the product [10]. Attempts have been made to understand the influence of EPS on the rheological properties of yogurt [11,12]. Van Marle and Zoon [13] determined the concentration of EPS in various yogurts and measured the apparent viscosity as a function of shear rate. There did not seem to be a direct relationship between the overall EPS concentration and the rheological properties of yogurt, contrary to common belief. However, the various yogurt cultures appeared to affect the protein network structures of the yogurt gel, presumably by the excretion of EPS. Also, different cultures probably produce EPSs with different primary structures and physical properties.

In this thesis the role of EPS in (acidified) milk products was investigated by studying the physical properties of an EPS and its interactions with the main components in dairy products. The chemical structure of the repeating unit of this EPS is given in Figure 2 (see Chapter 2 for details). A better understanding of the physical properties of EPSs may facilitate the control of the desired and undesired properties of fermented dairy products and may lead to a more directed role in (new) dairy products. EPSs from lactic acid bacteria are produced by 'food-grade' cultures and are produced *in situ* during fermentation of the product. As a result EPS does not have to be declared as an added 'artificial' ingredient. It might also be cost-effective if no additional thickeners need to be used.

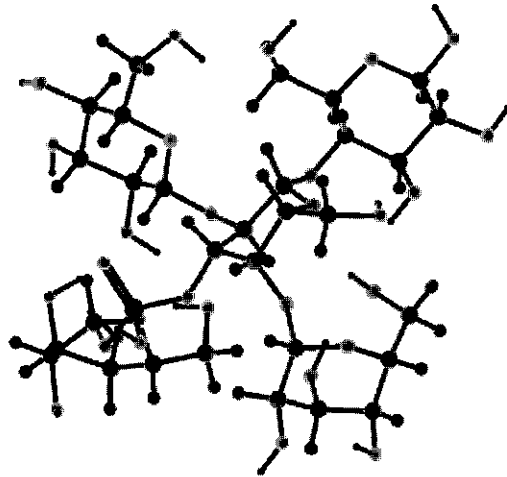


Figure 2 Molecular dynamics snapshot image of the repeating unit of B40 EPS. The central galactose group lies in the center, connected to the backbone glucoses (upper and lower right), the rhamnose group (upper left) and the phosphate group (lower left; recognizable by its double bond with an oxygen), which is again connected to another galactose group.

Systematic physical characterization of EPS produced by a lactic acid bacterium has hardly been performed until now. This thesis therefore focuses on the physical characterization of an EPS. We selected the EPS from the lactic acid bacterium *Lactococcus lactis* subsp. *cremoris* strain B40. The EPS-producing B40 strain was chosen since it increases the viscosity of fermented milk, the primary structure of its EPS is known, and isolation and characterization of the gene cluster for the production of its EPS has been started [14]. Knowledge of the chemistry of the polysaccharide facilitates the physical characterization and knowledge of the genetic engineering of EPS production might open new perspectives for adjusting the chemistry, molar mass or concentration of the EPS.

Model descriptions of polysaccharides

In this thesis the focus is on the physical properties of a particular EPS. Only limited attention will be paid to polysaccharide chemistry although it is of course realized that the primary structure is at the base of the physical properties. Polysaccharides contain many internal glycosidic linkages and their overall shape in solution is the result of bond rotations about the oxygens bridging the monosaccharides.

Many polysaccharides in aqueous solution are flexible since the thermal energy is larger than the energy barriers required to achieve backbone rotation. Such polysaccharides have a fluctuating three-dimensional conformation and are called random coil polymers. Compared to simple molecules, such coils are complex systems due to their many degrees of freedom. Kuhn [15], however, showed that the description of polymer molecules can be simplified by using proper statistical averages. Flory [16] said: 'Polymers...are susceptible to treatment that is simple, yet rigorous and exact,' thereby indicating that a good description is possible without the detailed chemistry. Following Kuhn, Flory [17] and Volkenstein [18] further developed the description of flexible polymers. The concepts of Kuhn, Flory and Volkenstein are still at the base of polymer physics. Since the 1930's much work has been done in polymer physics and various important achievements are reviewed in references [15,17-27]. The achievements described in these textbooks show that the molecular theory of polymers in solution has developed rapidly.

A restriction in such approaches is that the polymers must have enough flexibility: the number of freely flexible segments, usually referred to as Kuhn segments, must be larger than 10. Occasionally, specific interactions, may restrict the flexibility of a polymer and fix the polymer in an ordered shape, called a helix. Then, the relative orientations of two neighboring monosaccharides can be defined by two dihedral angles [28]. Starting with the possible configurations of the neighboring monosaccharides one can compute the most probable conformation of the entire chain using molecular dynamics simulation. An example is the work of Brant [29,30], who obtained good agreement for the helix conformation of simple polysaccharides between calculated structure and X-ray scattering data. Examples of polysaccharides which tend to form helices are pectins, xanthans, gellans and some of the carrageenans, which can be extracted from red seaweed [31]. As the investigated polysaccharides from *Lactococcus lactis* subsp. *cremoris* are all random coil polymers, a description of rods, helix-polymers and semi-flexible polymers is less relevant and will be omitted.

Rheology of exocellular polysaccharides

If a 'new' EPS is isolated it is necessary to characterize this EPS in various ways in order to test its capability as thickening agent. A clear physico-chemical basis for selection criteria is, however, lacking. In recent years several research groups have isolated EPSs from a large variety of strains. Rheological tests are required when one wants to know whether the EPS can replace polysaccharides which are used in practice. In references [32-34] it is indicated what kind of rheological measurements are performed on the obtained EPS solutions. It is rather straightforward to measure the flow curve (viscosity as a function of shear rate) [32]. Such flow curves are often interpreted with an empirical power-law model [32,34]. Although power-law models may give a good mathematical fit of the measured data, the physical meaning of the parameters obtained is limited, if any. The intrinsic viscosity is a central parameter in the description of the viscosity of polymer solutions, which can be measured in the very dilute regime [33]. By normalization over the intrinsic viscosity the concentration dependence of the viscosity of many flexible polysaccharides can be described by a single master curve [34]. Since the intrinsic viscosity depends only on the molar mass and on the size of the polymer in solution, it follows that the molecular parameters (molar mass and radius of gyration) of the polymer determine the rheology. From this it follows that it would be possible to describe the rheological behavior on the basis of molecular characteristics only. This route will be explored in this thesis.

Interactions between polysaccharides and proteins

Most food products in which polysaccharides can be found contain fat, oil particles and/or proteins which may interact with the polysaccharides. Knowledge of the individual components is not sufficient to describe the properties of a food product containing not only a polysaccharide but also other biopolymers and dispersed particles. Therefore the second part of this thesis concerns the interactions with some of the most common food colloids: protein aggregates (Chapter 5), protein associates (Chapters 6 and 7) and emulsion droplets covered with proteins (Chapter 8).

When a protein solution is mixed with a solution of polysaccharides the behavior of the mixture depends on whether the two biopolymers are segregative (the biopolymers repel each other and are denoted as incompatible) or associative (the biopolymers attract one another). The main trends of mixing polysaccharides and proteins are (highly) schematically illustrated in Figure 3.

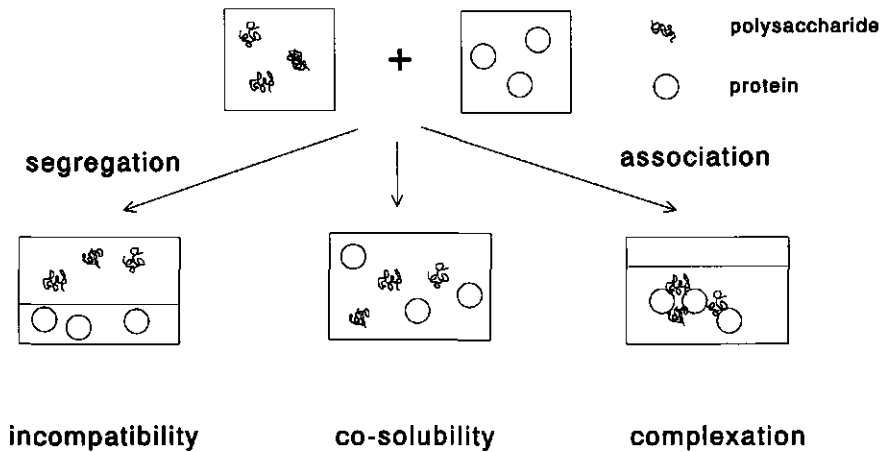


Figure 3 Main trends in the behavior of protein/polysaccharide mixtures.

For very dilute solutions the system is stable since the mixing entropy dominates and proteins and polysaccharides are co-soluble. Upon increasing the concentration of the biopolymers the system may become unstable, depending on the type of interaction. As a rule proteins and polysaccharides tend to segregate [35]. In the case of segregation a reduction of the polymer concentration near the protein particle is found. This reduction of the polymer concentration is due to a loss of conformational entropy of polymers near an interface. A reduction of polymer concentration near an interface is called depletion. Exceeding a certain polymer concentration leads to a phase separation into a protein-enriched and a polysaccharide-enriched phase (see Figure 3). A special case is a segregative interaction between very large polymers and relatively small colloidal spheres. For such systems the reduction of conformational entropy is small. Then the concentration needed for phase separation is very high or not attainable in practice.

A mixture of polysaccharides and proteins can also be unstable when associative interactions are operational. In that case the polysaccharides adsorb onto the protein surfaces. If the amount of polymer is not large enough to completely cover the protein, a polysaccharide

may adsorb onto more than one protein surface, thereby bridging two or more protein particles. Such a process is also called complex coacervation, denoted as such by Bungenberg de Jong [36]. Complex coacervation can be found for instance in mixtures of casein micelles and low-methoxyl pectin [37]. The mechanism is also denoted as bridging flocculation. When the proteins are fully covered the proteins are repulsive which imparts colloidal stability. This can be important if the proteins are initially unstable. Then the polysaccharide can act as stabilizer. In summary, polysaccharides either adsorb onto proteins or induce effectively attractions between colloidal particles.

Attractions between proteins as induced by non-adsorbing polysaccharides eventually leads to phase separation as depicted in Figure 3. In colloid physics phase separation is a well-known phenomenon. Phase transitions in colloidal suspensions can be understood by treating colloidal particles thermodynamically equivalent to molecules. Perrin [38] used equilibrium theories developed for molecular systems to describe colloidal suspensions. Nowadays it is generally recognized that colloidal suspensions can be regarded as supramolecular fluids of particles in a continuous background [39,40]. Concentrated colloidal suspensions exhibit states analogous to those of molecular systems, such as gas, liquid and crystal. When attraction between colloidal particles is absent only a fluid and crystal phase can be observed, corresponding to the phase states of atoms at high temperatures and high densities [40,41]. By increasing the effective attraction between the colloids by adding non-adsorbing polymers (as by lowering the temperature in molecular systems), a colloidal fluid may phase separate into a colloidal gas and a colloidal solid for short-ranged attractions or into a colloidal gas and liquid for long-ranged attractions [40].

Colloidal components in milk

In this study colloid physics approaches based upon the ideas and models in the previous section will be used. As the polysaccharide studied in this thesis can be found in dairy products, the focus is on the interactions and phase behavior of EPS with colloidal components in milk. There are three distinctly different types of particles in the colloidal size range in milk. Those particles are fat globules ($\sim 1 \mu\text{m}$), casein micelles ($\sim 0.1 \mu\text{m}$) and whey proteins ($\sim 0.01 \mu\text{m}$). Smaller molecules (numbering more than 100,000 species in milk) are considered as part of the continuous phase (background).

Whey proteins

Milk contains approximately 3.5 wt% of proteins. The proteins which do not precipitate at pH 4.6 are called serum or whey proteins and constitute 0.6 wt% of the milk. These whey proteins comprise of a diverse group of globular proteins, with a diameter in the order of 5 nm, which are sometimes present as (oligomeric) association structures [42]. In the cheese-making process these proteins are by-products. However, the whey proteins are nutritious and are well suited for food technological applications. When whey proteins are exposed to a heat treatment, they denature, aggregate and can give rise to very viscous solutions or gels, depending on the initial protein concentration, pH and salt concentration [43,44].

Casein micelles

By far the largest fraction of proteins in milk is made up of caseins, which exist in fresh milk as association colloids called casein micelles (depicted in Figure 4). The casein micelles consist of four different casein proteins (α_{s1} -, α_{s2} -, β - and κ -), calcium phosphate and calcium citrate. Casein micelles are quite stable: one can boil milk or add sodium chloride without inducing flocculation.

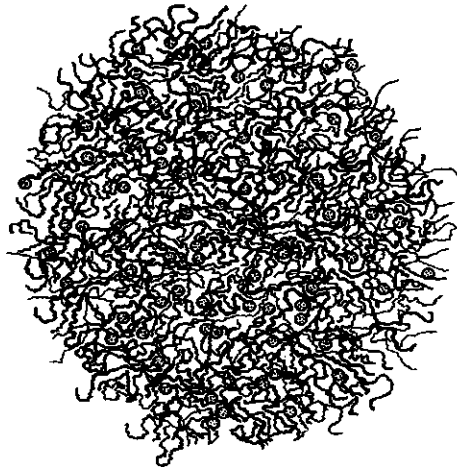


Figure 4 Schematic picture of a casein micelle.

The (z-averaged) hydrodynamic radius of casein micelles as determined by dynamic light scattering is about 140 nm [45]. Hansen *et al.* [46] studied the size of casein micelles with small-angle neutron scattering and found a (weight-averaged) radius of 100-120 nm. Recently, De Kruif [47] analyzed the size distribution of casein micelles in skim milk and found a (number-averaged) radius of 100 nm. These data show that casein micelles are not very polydisperse. At the surface of the casein micelles κ -casein molecules are located. They can be regarded as a kind of block copolymers; they contain a hydrophobic part associated with the interior of the casein micelle and a hydrophilic part, which is negatively charged and protrudes into the solvent, serving as a steric stabilization layer

Emulsions

Most fat in milk (>99%) is present in the form of fat globules or droplets contain also a small amount of other components. The milk fat particles are surrounded by a membrane consisting of polar lipids and proteins, including many enzymes [42]. Fat globules are the largest particles in milk (diameter ~ 4 μm). As present in milk, fat particles are very complex, consisting of a large variety of lipids due to the many types of fatty acids in milk. This variety divides milk fat into a solid fraction and a liquid fraction. Further, the surfaces of milk fat globules are covered with milk proteins, phospholipids, cholesterol and other compounds [42]. In order to understand the mechanism of the interactions between EPS and the colloidal particles in milk, an oil-in-water emulsion was chosen as a simpler model emulsion. The effect of EPS on the properties of such an emulsion, consisting of oil droplets covered with whey proteins, was studied. Since the oil droplets in the model system are covered with proteins this is also a study of polysaccharide-protein interactions. It will be shown that polysaccharides induce attractions between the droplets, and the effect of attractions and demixing on the creaming rate and the rheology of the emulsions will be described.

Outline of this thesis

The aim of this work was to investigate the physico-chemical role of *in-situ* produced polysaccharides in acidified milk products. Much work has been done on EPS chemistry, see for instance references [48-50]. However, knowledge of the chemistry of EPSs does not enable an understanding of the differences between the physical properties of various types of acidified milk products containing various EPSs. The work described in this thesis serves as a tool to better understand the physico-chemical role of EPSs.

This thesis is divided in two parts; the first part concerns the characterization of the EPS and the second part focuses on the interactions of EPS with milk proteins. Part one first continues with an investigation on the physical properties of the EPS. In Chapter 2 the isolation, purification, and analysis of the molecular properties of EPS from *L.lactis* B40 are described. The molar mass (distribution), the (averaged) radius of gyration and the hydrodynamic radius of the EPS in solution are determined using light scattering techniques. Chapter 3 deals with the concentration dependence and the shear thinning behavior of the viscosity of the EPS solutions. It will be shown that the viscosity can be described in terms of the concentration, shear rate and intrinsic viscosity, which in turn, only depends on the molar mass and size of the EPS. The dynamic rheological properties of the EPS are focused on in Chapter 4. The Rouse model, based on molecular parameters, allows a good description of the dynamic moduli as a function of the frequency of the EPS solutions. It is shown that the elasticity becomes quite significant at high EPS concentrations.

The second part of the thesis is devoted to the interactions between EPS and the most relevant colloidal (protein) particles present in milk products. In Chapter 5 the interactions with whey proteins are investigated. Although native whey proteins are co-soluble with EPS, aggregated whey protein colloids (AWCs) attract one another upon adding EPS due to depletion interaction, leading to a phase separation at high EPS concentration. Scattering techniques allow a measurement of these attractions and can be described quantitatively with theoretical predictions for depletion interaction. The phase boundary is also described theoretically. The phase separation process can be described as a spinodal decomposition, as shown by small-angle light scattering data. The interactions between the EPS and casein micelles are treated in Chapter 6. Dynamic light scattering, neutron scattering, and turbidity measurements are used to show that EPS effectively induces attractions between casein micelles. The measurements can be described with depletion interaction theory. The phase behavior of mixtures of EPS and casein micelles is the subject of Chapter 7. Depletion interaction theories are used to calculate the phase boundary and compared with the experimental phase boundary. The effect of adding the EPS to an oil-in-water emulsion, stabilized with whey proteins, is reported in Chapter 8. The phase diagram is given and shows that at high EPS concentration there is a 'gel' region, where a network of aggregating oil droplets is formed which does not phase separate. The kinetics of phase separation in the unstable region is measured and described theoretically. Finally, in Chapter 9 various practical implications of this research project will be discussed.

Acknowledgment

The author thanks Dr. Harry S. Rollema, NIZO food research, for his help with the Molecular Dynamics simulations, and Dr. Gerhard A. de Ruiter, NIZO food research, for a critical reading of the manuscript of this Chapter.

References

- [1] Linton, J.D., In: 'Novel Biodegradable Microbial Polymers' E.A. Dawes (Ed.) NATO ASI Series, Ser.E, Applied Sciences Vol.186, Kluwer, Dordrecht, pp. 311, 1990.
- [2] O'Donnell, C.D., *Dairy Foods*, **93** (1990) 47.
- [3] Sutherland, I.W., *Ann. Rev. Microbiol.*, **39** (1985) 243.
- [4] Sibakov, M., Hugenholtz, J., *Finn. J. Dairy Sci.*, **51** (1995) 1.
- [5] Veringa, H.A., Slomp, M., van den Berg, G., Escher, J.T.M., *Voedingsmiddelentechnologie* **24** (1991) 13.
- [6] Hugenholtz, J., *FEMS Microbiol. Rev.*, **112** (1993) 165.
- [7] Marrugg, J.D., Toonen, M.Y., Verhue, W.M., Verrips, C.T., Process for the preparation of α -acetolactic acid (1992) EP 0500188.
- [8] Ehrenberg, O., *Verhandl. d. Berl. Akad.* **34** (1840) 202.
- [9] Buchanan, R.E., Hammer, B.W., *Res. Bul. Ia. Agr. Exp. Sta.*, **22** (1915) 205.
- [10] Galesloot, T.E., Hassing, F., *Dairy Sci. Abstr.*, **30** (1968) 370.
- [11] Schellhaas, S.M., Morris, H.A., *Food Microstructure*, **4** (1985) 279.
- [12] Van Marle, M.E., PhD Thesis Twente University, 1998.
- [13] Van Marle, M.E., Zoon, P. *Neth. Milk Dairy J.*, **49** (1995) 47.
- [14] van Kranenburg, R., Marugg, J.D., van Swam, I.I., Willem, N.J., de Vos, W.M., *Mol. Microbiol.*, **24** (1997) 387.
- [15] Kuhn, W., *Kolloid Z.*, **68** (1934) 2.
- [16] Flory, P.J., *Chemical and Engineering News*, April 8, 1974.
- [17] Flory, P.J., 'Principles of Polymer Chemistry,' Cornell University Press, New York, 1953.
- [18] Tanford, C.H., 'Physical chemistry of macromolecules,' Wiley, New York, 1961.
- [19] Volkenstein, M.V., 'Configurational Statistics of Polymeric Chains,' Interscience New York, 1963.
- [20] Flory, P.J., 'Statistical Mechanics of Chain Molecules,' Interscience New York, 1969.
- [21] Ferry, J.D., 'Viscoelastic Properties of Polymers,' Wiley, Second edition, 1970.
- [22] Yamakawa, H., 'Modern theory of polymer solutions', Harper and Row Publ., New York, 1971.
- [23] De Gennes, P.G., 'Scaling Concepts in Polymer Physics,' Cornell University Press, New York, 1979.
- [24] Vinogradov, G.V., Malkin, Ya., 'Rheology of Polymers,' Springer-Verlag, 1980.

- [25] Doi, M., Edwards, S.F., 'The Theory of Polymer Dynamics,' Clarendon Press, 1986.
- [26] Freed, K.F., 'Renormalization Group Theory of Macromolecules,' Wiley, New York, 1987.
- [27] Fler, G.J., Cohen Stuart, M.A., Scheutjens, J.M.H.M., Vincent, B., Cosgrove, T., 'Polymers At Interfaces,' Harper & Row, 1993.
- [28] Rees, D.A., *MTP Internat. Rev. Sci. Org. Chem. Series One*, **7** (1973) 251.
- [29] Brant, D.A., *Carbohydr. Polym.*, **2** (1982) 165.
- [30] Brant, D.A., *Q. Rev. Biophys.*, **9** (1976) 527.
- [31] De Ruiter, G.A., Rudolph, B., *Trends Food Sci. Techn.* **8** (1997) 389.
- [32] Fishman, M.L., Cescutti, P., Felt, W.F., Osman, S.F., Hoagland, P.D., Chau, H.K., *Carbohydr. Pol.*, **32** (1997) 213.
- [33] Eteshola, E., Gottlieb, M., Arad, S., *Chem. Engin. Sci.*, **51** (1996) 1487.
- [34] Lapasin, R., Prici, S., 'Rheology of Industrial Polysaccharides: Theory and Applications,' Blackie Academic, 1995.
- [35] Grinberg, V.Ya., Tolstoguzov, V.B., *Food Hydrocoll.* **11** (1997) 145.
- [36] Bungenberg de Jong, H.G., Chapters 8 & 10 in: 'Colloid Science, Vol. 2, Reversible Systems' H.R. Kruyt (Ed.), Elsevier, Amsterdam, 1949.
- [37] Tokaev, E.S., Gurov, A.N., Rogov, I.A., Tolstoguzov, V.B., *Die Nahrung*, **31** (1987) 825.
- [38] Perrin, J. *Compt. Rend.*, **158** (1914) 1168.
- [39] Vrij, A., Nieuwenhuis, E.A., Fijnaut, H.M., Agterof, W.G.M., *Faraday Disc. Chem. Soc.* **65** (1978) 101.
- [40] Poon, W., Pusey, P.N., Lekkerkerker, H.N.W., *Physics World*, April (1996) 27.
- [41] Hansen, J.P., McDonald, I.R., 'Theory of simple liquids,' Academic Press, New York, 1986.
- [42] Walstra, P., Jenness, R., 'Dairy Chemistry and Physics,' Wiley, New York, 1984.
- [43] Hoffmann, M.A.M., Roefs, S.P.F.M., Verheul, M., Van Mil, P.J.J.M., De Kruif, C.G., *J. Dairy Res.* **63** (1996) 423.
- [44] Verheul, M., Roefs, S.P.F.M., *Food Hydrocolloids*, **12** (1998) 17.
- [45] Bauer, R., Hansen, M., L.Ogendal, Lomholt, S., K.Qvist., *J. Chem. Phys.* **103** (1995) 2725.
- [46] Hansen, S., Bauer, R., Lomholt, S.B., Quist, K.B., Pedersen, J.S., Mortensen, K., *Eur. Biophys. J.* **24** (1996) 143.
- [47] De Kruif, C.G., *J. Dairy Sci.* **81** (1998) 3019.
- [48] Gruter, M., Leeflang, J., Kuiper, J.P., Kamerling, J.P., Vliegthart, J.F.G., *Carbohydr. Res.*, **239** (1993) 209.
- [49] Robijn, G.W., Thomas, J.R., van den Berg, D.J.C., Haas, H., Kamerling, J.P., Vliegthart, J.F.G., *Carbohydr. Res.*, **276** (1995) 137.
- [50] van Casteren, W.H.M., Dijkema, C. Schols, H.A., Beldman, G., Voragen, A.G.J., accepted for publication in *Carbohydr. Pol.*, 1998.

2

Isolation and physical characterization of an exocellular polysaccharide

Abstract

The physical properties of a polysaccharide produced by the lactic acid bacterium *Lactococcus lactis* subsp. *cremoris* strain NIZO B40 were investigated. Separation of the polysaccharide from most low molar mass compounds in the culture broth was performed by filtration processes. Residual proteins and peptides were removed by washing with a mixture of formic acid, ethanol, and water. Gel permeation chromatography (GPC) was used to size-fractionate the polysaccharide. Fractions were analyzed by multi-angle static light scattering in aqueous 0.10 M NaNO₃ solutions from which a number- (M_n) and weight-averaged (M_w) molar mass of $(1.47 \pm 0.06) \cdot 10^3$ and $(1.62 \pm 0.07) \cdot 10^3$ kg/mol, respectively, were calculated so that $M_w/M_n \approx 1.13$. The number-averaged radius of gyration was found to be 86 ± 2 nm. From dynamic light scattering an apparent z-averaged diffusion coefficient was obtained. Upon correcting for the contributions from intramolecular modes by extrapolating to zero wave vector a hydrodynamic radius of 86 ± 4 nm was calculated. Theoretical models for random coil polymers show that this z-averaged hydrodynamic radius is consistent with the z-averaged radius of gyration, 97 ± 3 nm, as found with GPC.

Introduction

In the last decade the interest in polysaccharides produced by micro-organisms had significantly increased [1]. The main investigations are directed towards the biosynthesis [2-4], growth conditions [5] or chemical analysis [6-8] of these exocellular polysaccharides (further denoted as EPSs); physical characterization of these biopolymers has received less attention. An overview of work done on EPSs produced by lactic acid bacteria is given by Cerning [9]. The interest in EPS was stimulated by the discovery that polysaccharides are present in various types of yogurt. Because of the thickening capacity of polysaccharides, attempts have been made to relate the rheological properties of yogurt to the EPS concentration. However, van Marle and Zoon [10] did not find a simple relationship between the EPS concentration and the rheological properties of stirred yogurt made with various cultures. The yogurt cultures appeared to affect the protein network structures of the yogurt gel. Also, different cultures probably produce EPSs with different primary structures and physical properties. These aspects are still under investigation.

The foregoing gives us good reasons to pay more attention to the role of EPSs in dairy products. The main interest in EPSs from lactic acid bacteria arises from the fact that these polysaccharides are produced by 'food-grade' cultures. If the EPS is produced *in situ*, during processing of the product, it does not have to be considered as an additional 'artificial' ingredient. It might also be cost-effective if no additional thickeners need to be used. In order to better understand the thickening mechanism, knowledge of the physical properties of the isolated polysaccharides is required. Systematic physical analysis of an EPS produced by a lactic acid bacterium has hardly been performed until now. This motivated the present work.

The EPS of *Lactococcus lactis* subsp. *cremoris* strain NIZO B40, hereafter referred to as EPS, was chosen for the present study because it has interesting thickening properties. The structure of the repeating unit was analyzed by van Casteren *et al.* [11] and is given in Figure 1. The structure consists of a backbone in which the repeating unit contains three $\beta(1\rightarrow4)$ -linked monosaccharides, namely two D-glucose (Glc) residues and one D-galactose (Gal) unit. The galactose residue carries two side groups. Carbon atom C3 is linked to a phosphoric acid group of which one oxygen atom is bound to the C1 of an α -D-galactose. The backbone galactose also has a covalent bond with an α -L-rhamnose (Rha) residue through a (1 \rightarrow 2) bond. The chemical structure of the EPS indicates that it is similar to an EPS produced by *Lactococcus lactis* subsp. *cremoris* SBT 0495, studied by Nakajima *et al.* [12].

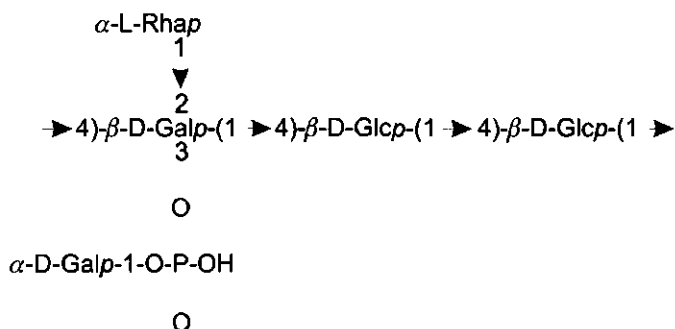


Figure 1 Chemical structure of B40 EPS. The *p*'s refer to the fact that all monosaccharides are present in the pyranose form.

We describe a method of producing and concentrating EPS on a pilot-plant scale, followed by a purification step. The polysaccharide was then separated by gel permeation chromatography (GPC) and the molar mass and size of the various fractions were measured by static light scattering. These experiments yielded the primary physical properties such as radius of gyration and the molar mass (distribution) of the polysaccharide. In addition, the isolate was studied by dynamic light scattering, which yielded the hydrodynamic radius.

Theory

In order to determine the molecular size and molar mass of EPS we have used both static and dynamic light scattering. A central parameter in any scattering experiment is the scattering wave vector Q . This quantity is defined as the vectorial difference between the wave vectors of the scattered and incident beam:

$$|Q| \equiv \frac{4\pi n}{\lambda_0} \sin\left(\frac{\theta}{2}\right) \quad 1$$

where λ_0 is the wavelength of the incident beam in vacuo, θ the angle under which scattered light is detected and n the refractive index of the continuous phase.

Static light scattering

An expedient quantity in light scattering is the Rayleigh ratio $R(Q)$, defined as:

$$R(Q) = \frac{I(Q)r^2}{I_0} \quad 2$$

where $I(Q)$ is the scattered intensity, i.e., the amount of energy scattered per unit volume across a unit area ($J.m^{-5}$) at a distance r between the scattering volume and the detector, at a wavevector Q . The quantity I_0 is the intensity of the (vertically polarized) primary beam ($J.m^{-2}$). For monodisperse sols, consisting of solid particles, $R(Q)$ is related to the structure factor $S(Q,c)$ and to the particle form factor $P(Q)$ by [13]:

$$R(Q) = KcMP(Q)S(Q,c) \quad 3$$

where c represents the particle concentration, M the molar mass and where the material constant K is given by:

$$K = \frac{2\pi^2 n_0^2}{\lambda_0^4 N_{AV}} \left(\frac{dn}{dc} \right)^2 \quad 4$$

where N_{AV} is Avogadro's number, n_0 the refractive index of the solvent, and dn/dc the refractive index increment. For a Gaussian polymer coil the form factor was derived by Debye [14]:

$$P(Q) = \frac{2}{Q^4 R_g^4} [\exp(-Q^2 R_g^2) - (1 - Q^2 R_g^2)] \quad 5$$

with R_g is the radius of gyration of the statistical coil. At $Q = 0$, the structure factor is related to the osmotic compressibility. Expanding the osmotic compressibility in a virial series then gives the following approximate expression for the inverse structure factor $S(0,c)^{-1}$ [13,15]:

$$S(0,c)^{-1} = 1 + 2B_2 Mc + 3B_3 Mc^2 + \dots \quad 6$$

where B_2 and B_3 are the second and third virial coefficients, respectively. At very low concentration the contribution of the higher-order terms as well as the Q -dependence can be neglected, or $S(Q,c) \approx 1$ for any type of particle. Combination of equations 3,5 and 6 then yields for low QR_g :

$$\frac{Kc}{R(Q)} \approx \frac{1}{M} \left(1 + \frac{Q^2 R_g^2}{3} \right) \quad 7$$

Hence, measurement of $R(Q)$ as a function of Q yields the molar mass ($Q \rightarrow 0$) and the radius of gyration (Q dependence). By analyzing several narrow fractions of a polymer by light

scattering the relation between R_g and M can be studied. Another measure of the size of polymer coils is the hydrodynamic radius which is related to the diffusion coefficient of a polymer. The latter can be determined by dynamic light scattering (DLS).

Dynamic light scattering

In a suspension the particles diffuse through the solvent due to Brownian motion. This random motion causes the scattered intensity to fluctuate. Information on the dynamic properties of the particles can be obtained by measuring the frequency of the intensity fluctuations in time. This can be performed by determining the intensity auto-correlation function $G^{(2)}(Q, \tau)$, which is defined as [15, 16]:

$$G^{(2)}(Q, \tau) = \langle I(Q, t) \cdot I(Q, t + \tau) \rangle \quad 8$$

where $I(Q, t)$ is the intensity at a wave vector Q at time t . The auto-correlation function correlates the measured fluctuating intensities $I(Q)$ at t with those at $(t + \tau)$. At very long time scales ($\tau \rightarrow \infty$) there is no correlation left and $G^{(2)}(Q, \tau)$ equals $\langle I^2 \rangle$. Dividing the intensity auto-correlation function by its long-time value gives the normalized auto-correlation function $g^{(2)}(\tau)$:

$$g^{(2)}(\tau) = \frac{G^{(2)}(Q, \tau)}{G^{(2)}(Q, \infty)} \quad 9$$

which, for monodisperse sols, is related to the diffusion coefficient D :

$$g^{(2)}(\tau) = 1 + \beta \exp(-2Q^2 D \tau) \quad 10$$

Here, β is a constant linked to the signal-to-noise ratio of the apparatus used. For polydisperse systems $g^{(2)}(\tau)$ does not decay purely exponentially. For such systems Koppel [17] expanded $\ln(g^{(2)}(\tau) - 1)$ in a series of cumulants:

$$\frac{1}{2} \ln[g^{(2)}(\tau) - 1] = \frac{1}{2} \ln \beta - \Gamma_1 \tau + \frac{1}{2!} \Gamma_2 \tau^2 - \dots + \frac{(-1)^n}{n!} \Gamma_n \tau^n \quad 11$$

where Γ_1 , Γ_2 and Γ_n are the first, second and n th order cumulants. In theory, any required number of cumulants can be determined; in practice reasonably narrow distributions can be analyzed adequately by using a second-order cumulant fit. Then from Γ_1 the diffusion coefficient can be calculated. For non-rigid particles with internal motions, such as flexible polymers, D is an apparent diffusion coefficient which depends on Q . For linear flexible polymers Burchard [18] derived the following equation for the first cumulant:

$$\Gamma_1 = Q^2 \langle D \rangle_z (1 + C Q^2 R_g^2 - \dots) \quad 12$$

where $\langle D \rangle_z$ is the z -averaged diffusion coefficient and C is a quantity which depends on branching and polydispersity. Equation 12 shows that the apparent diffusion coefficient Γ_1/Q^2

increases with Q , which corresponds to the fact that at higher Q -values the diffusion of polymer segments within the molecules are studied. In general, increasing Q means that smaller length scales are probed.

The theory of Burchard *et al.* [19] predicts an increase of C with polydispersity and a decrease with branching. For non-branched monodisperse random coil chains their theory predicts $C \approx 0.17$. However, experimental results for the value of C are not conclusive [20-22]. Regardless of the precise value of C , extrapolation of Γ_1/Q^2 to zero Q gives $\langle D \rangle_2$. From this diffusion coefficient the hydrodynamic radius R_H of the EPS molecules is calculated with the Stokes-Einstein relation:

$$D = \frac{k_B T}{6\pi\eta_s R_H} \quad 13$$

where k_B is the Boltzmann constant and η_s the solvent viscosity.

Polymer chain dimensions in dilute solution

In the theoretical sections it has been demonstrated how the radius of gyration and the hydrodynamic radius can be determined with scattering methods. Freire *et al.* [23] did Monte Carlo simulations from which they calculated both R_H and R_g . In the long chain length limit they found for $\xi = R_g/R_H$ a value of 1.27 ± 0.02 . When long-range interactions between the segments is introduced ξ has the same value. These results have been confirmed by the renormalization group theory [24].

So far, we have shown how the molar mass and size of a polymer molecule can be analyzed. Next, we discuss the relation between the molecular size and molar mass. For long flexible chains the random walk model was introduced by Kuhn [25]. The root-mean-square end-to-end distance, $\langle R^2 \rangle^{1/2}$, follows from the number N_K of Kuhn segments and the length l_K of such a segment as [26]:

$$\langle R^2 \rangle = \alpha^2 l_K^2 N_K \quad 14$$

where α is the linear expansion coefficient. For long chains the radius of gyration R_g equals $\langle R^2 \rangle^{1/2}/\sqrt{6}$. Since N_K is proportional to the molar mass, R_g is proportional to $M^{0.5}$. However, real chains with N segments, each of length l , cannot be directly regarded as purely random walks. The values for l and N can be translated to l_K and N_K by demanding equal contour lengths for the Kuhn chain and the real chain:

$$L \equiv lN = l_K N_K \quad 15$$

When R_g has been measured, the quantity l_k can then be calculated from equation 14 as $l_k = \langle R \rangle^2 / L = 6R_g^2 / L$ and N_k follows as L / l_k . A prerequisite for the validity of this approach is that N_k must not be too small ($N_k > 10$). For a polymer in a good solvent α depends also (weakly) on N . Flory [26] derived an expression which relates the expansion coefficient α to N :

$$\alpha^5 - \alpha^3 \sim (1 - 2\chi)N^{\frac{1}{2}} \quad 16$$

where χ is the Flory-Huggins segment-solvent interaction parameter; it is equal to 0.5 for a poor (θ)-solvent and it is zero for a good solvent. According to equation 16, for high α (good solvent) the expansion coefficient scales with the number of segments as $\alpha \sim N^{0.1}$. Then, from equation 14 it follows that $R_g \sim N^{0.6}$ for high α . More generally, we can write:

$$R_g \sim M^{\nu} \quad 17$$

where for flexible chains the exponent ν is in between 0.5 (θ -solvent) and 0.6 (good solvent).

The approach given above applies to solutions of uncharged polymer molecules. However, B40 EPS is a polyelectrolyte above pH 2 since the repeating unit contains a phosphate group. At high ionic strength, however, all charges of polyelectrolytes are screened and the behavior is quasi-neutral. At intermediate ionic strengths the charges may contribute to a higher α and chain stiffness [27,28]. We determined $R_g(M)$ for the EPS and compared the results with equation 17.

Materials and methods

EPS production

A pre-inoculum of 1% of the strain *Lactococcus lactis* subsp. *cremoris* NIZO B40 was made in M17-medium, based upon a recipe of Terzaghi and Sandine [29], for 16 hours at 30°C. The pre-inoculum was used to inoculate (1%) a whey permeate medium, which consists of 350 L whey permeate, 7 kg lactose, 7 L (25%) yeast extract (Bio Springer) and 3 L of a 40% sodium phosphate buffer solution. All concentrations are given in mass percent. The medium was sterilized before inoculation by a HTST (high temperature-short time) treatment at 140°C for 20 seconds by passing it through a tubular heat exchanger, and placed in a 500 L fermenter which was kept under N_2 pressure. The incubation time was 20 hrs at 30°C. The initial pH was 6.5; it decreased during incubation but was held constant at 5.8 by adding the required amount of 33% NaOH solution. After fermentation the culture broth was heated to 50°C to improve the detachment of the EPS from the walls of the microbial cells.

EPS isolation

The first step in the isolation of EPS from the broth (see Figure 2) was centrifugation to separate particles having sizes larger than microns (mainly bacteria and cell debris). This was performed with a Westfalia centrifuge with a pressure difference of 4 bar and, as for all further filtrations, at 50°C. The supernatant was microfiltered over a ceramic membrane (Ceraiver Membraiox) with a pore size of 1.4 µm to a concentration factor of 10. The microfiltrate was additionally ultrafiltered with a polysulfone (Romicon DM 10) membrane with a molar exclusion limit of 10 kDa, again to concentrate 10 times.

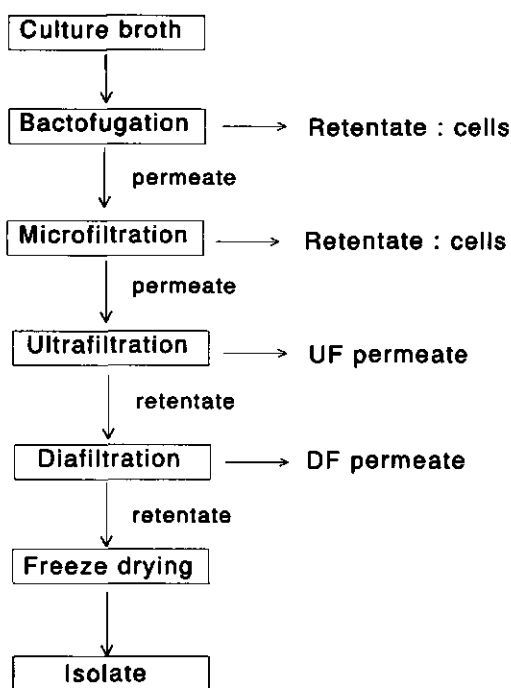


Figure 2 Flow scheme of the EPS isolation process.

Subsequently, the retentate was diafiltered with the same ultrafiltration equipment with 20 volumes deionized water, after which the product was freeze dried. The freeze-dried powder was stored at 5°C. All further analysis was performed at room temperature. The remaining powder contained 63% EPS, 18% proteins, 8% ash, 6% mannan-rich material [11] and 5% water.

Purification

The freeze-dried product needed some additional purification because Kjeldahl analysis showed the presence of nitrogen (protein) containing impurities and UV transmission (at 280 nm) gave evidence of aromatic groups. Moreover, the first results for the relation between the molar mass and the radius of gyration (as measured by GPC and static light scattering) were erratic. Probably, small aggregates, which gave deviating light scattering results, were present.

Various purification methods, such as gel permeation on a preparative column, additional dialysis, lab-scale ultrafiltration, and ethanol precipitation, did not give satisfactory results. Milas *et al.* [30] and Fouissac *et al.* [31] used ethanol precipitation and ethanol washing to remove aggregates of polysaccharides. It is assumed that these aggregates are formed during the freeze-drying process [32]. In our system, these aggregates could not be eliminated by ethanol.

We developed a washing method in which 0.5 g freeze-dried powder is suspended in 500 mL 80% ethanol solution containing 0.1% formic acid. We used formic acid as a buffer at low pH (pH 3.0) in order to make the proteins more soluble in ethanol solutions. This suspension was led through a column with a sintered glass filter at the bottom, and washed by leading 1 L of the ethanol-water-formic acid mixture through the filter (the polysaccharide did not pass the filter). Then the powder was washed with 96% ethanol. Finally, the remaining ethanol was evaporated. The addition of 0.1% formic acid greatly improved the light scattering results. Higher concentrations (up to 3%) did not affect the final result. UV analysis showed that the washing method decreased the amount of proteins. After purification by washing the EPS the amount of proteins was decreased. After purification the sample contained 72% EPS, 6% proteins, 9% ash, 7% mannan and 6% water. Further washing did not change the end result. We assume that this smaller fraction of impurities will not affect our results since both the proteins and mannan are much smaller than the large EPS molecules. The monosaccharide composition of the EPS was not affected by the washing method.

EPS analysis

- Gel permeation chromatography

Gel permeation or size exclusion chromatography (GPC) was performed using TSK-gel 6000 PW columns (Phenomenex). The molar exclusion limit as stated by the supplier is $8 \cdot 10^3$ kg/mol. A pre-column (PWH TSK-gel, Phenomenex) was used to give a crude first separation and to protect the column. The gel permeation separation was carried out at room temperature with 0.10 M NaNO_3 as the eluent.

The eluent from the column was analyzed on-line by RI (refractive index) detection (ERC-7510 detector from ERMA optical works), by UV transmission at a wavelength of 280 nm, and by static light scattering (SLS). Integration of the RI signal was used to determine the polysaccharide concentration in the fractions; dextran and pullulan were used as standards. The on-line UV transmission measurements were made with a LKB 2140 rapid spectral detector. Static light scattering was performed with a Wyatt Technology DAWN apparatus with a 5 mW He-Ne laser ($\lambda_0 = 632.8$ nm). The laser is linearly polarized and has a narrow beam diameter to enhance the intensity. The DAWN contains 18 intensity detectors at scattering angles ranging from 3.3° to 158.3° . After a few initial experiments we decided to exclude angles 3.3° - 36.1° and 158.3° , since the signal-to-noise ratio at these angles was too low for an accurate measurement. Hence, we used 12 angles to analyze the samples, giving a Q-range from 10.0 to $25.6 \mu\text{m}^{-1}$. Finally, the refractive index increment needed for the material constant K (equation 4) was measured using a Carl Zeiss refractometer. We obtained a value of 0.135 ± 0.005 mL/g in 0.10 M NaNO_3 .

- Dynamic light scattering

Dynamic light scattering experiments were performed using a Spectra Physics 275 mW Ar laser with a wavelength of 514.5 nm. In this apparatus, the light beam is focused on the axis of the goniometer using a lens. The sample cuvette housing is kept at a temperature of 25°C . The goniometer can be set at the required scattering angle. The detected intensity is processed by a digital ALV-5000 correlator to give the auto-correlation function defined in equation 9. We analyzed the data using a second-order cumulant fit. The experiments were performed at various EPS concentrations in 0.10 M NaNO_3 . In order to obtain a qualitatively adequate cumulant fit an intensity (expressed as photon count rate) of at least 10^4 Hz is required. For that reason concentrations lower than approximately 0.2 g/L could not be analyzed accurately.

Results and discussion

After 20 hours of fermentation at 30°C (pH=5.8) the culture broth contained $6.5 \cdot 10^8$ colony forming units per mL, as determined by colony counting on GMA (glycerol phosphate milk agar) plates. The EPS production was about 0.37 g/L before heating to 50°C . After 2 hours at 50°C the culture broth contained 0.49 g/L EPS.

The washed EPS isolate was brought on the GPC column and the fractions were analyzed by SLS. A typical GPC result is plotted in Figure 3. The molar mass and radius of gyration decrease as a function of elution volume, because in a GPC experiment the larger molecules pass the column faster than the shorter ones. The results are very reproducible.

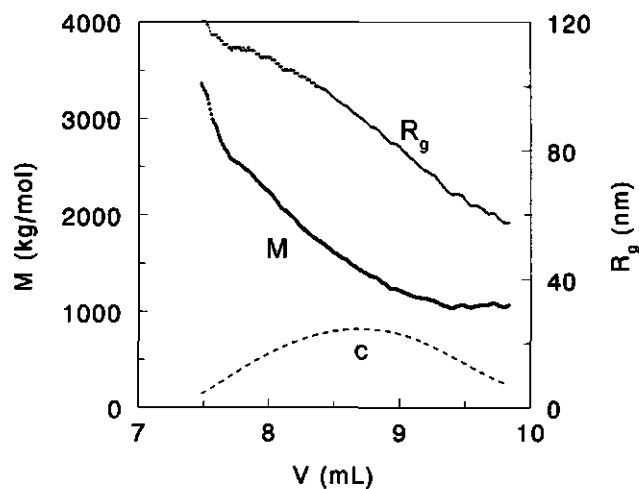


Figure 3 GPC results for B40 EPS in 0.10 M NaNO₃. The data for the molar mass M and radius of gyration R_g are given as a function of the elution volume V . The dashed curve represents the polymer concentration c in arbitrary units.

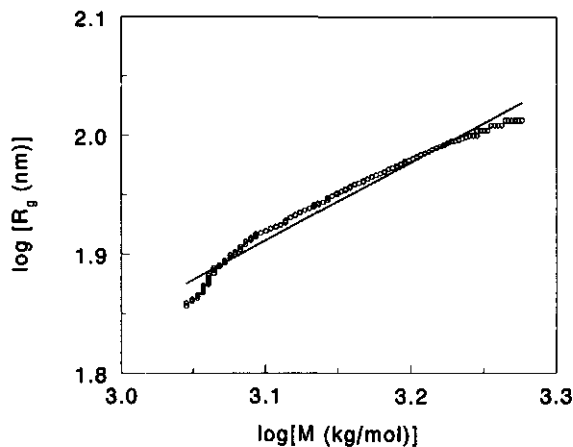


Figure 4 The dependence of the radius of gyration on the molar mass.

In Figure 3 the noise is somewhat larger at the tail ends of the distribution since the polymer concentration is rather low at the tails. The bulk of the material has a molar mass in the range $1\text{-}3 \cdot 10^6$ g/mol and a radius of gyration in the range 60-120 nm.

The radius of gyration is plotted as a function of the molar mass on a double logarithmic scale in Figure 4. Best fits of the fractions with the highest polymer concentrations yield an exponent $\nu \approx 0.57 \pm 0.02$, which approaches the theoretical value $\nu = 0.6$ for flexible polymer molecules in a good solvent.

After calibration of the data plotted in Figure 3, the distributions of the molar mass and radius of gyration are obtained; they are plotted in Figure 5 (a) and (b), respectively. From these, the number- and weight-averaged molar masses were calculated as $(1.47 \pm 0.06) \cdot 10^3$ and $(1.62 \pm 0.07) \cdot 10^3$ kg/mol, respectively, and the number- and weight-averaged radii of gyration as 86 ± 2 and 91 ± 2 nm, respectively. The z-averaged radius of gyration was found to be 97 ± 3 nm. The polydispersity index M_w/M_n is thus 1.13, which is surprisingly low in comparison to that of most synthetic polymers. However, the real polydispersity of the sample could be somewhat higher since we eliminated the tails of the distribution where the error in the scattering intensities were too large. The size distribution of the molar mass can be described as a Schulz-Flory distribution [26]. A best fit of this distribution depicted as a dashed curve is given in Figure 5 (a).

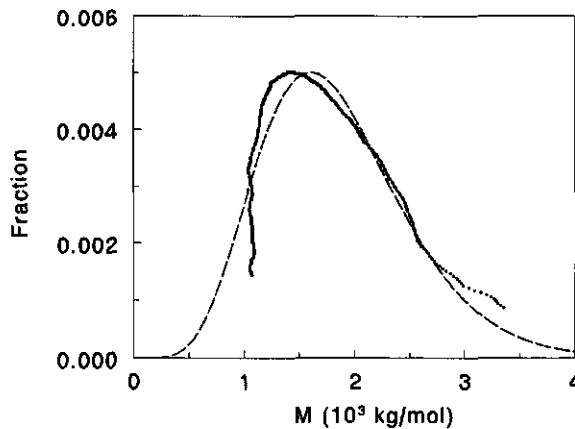


Figure 5 (a) The size distribution of the molar mass of B40 EPS molecules.

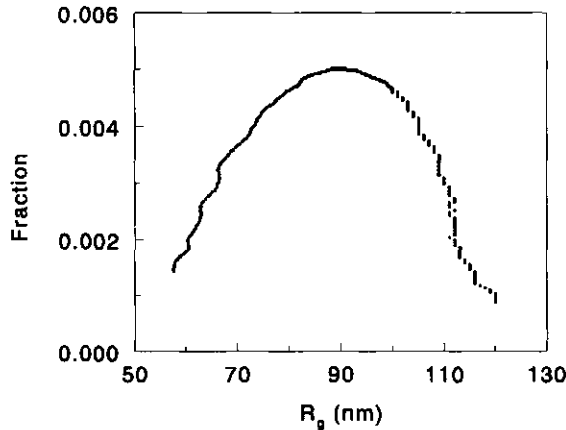


Figure 5 (b) The size distribution of the radius of gyration of B40 EPS molecules.

By regarding an EPS molecule as a Kuhn chain we can obtain information about the Kuhn length and the chain stiffness. In order to calculate the Kuhn length of B40 EPS molecules from equation 14, values for l and N are required. We took N as the number of repeating units. The molar mass M_0 of the repeating unit is 873 g/mol, which gives $N = M_r/M_0 = 1.68 \cdot 10^3$ repeating units. Each repeating unit contains three backbone monosaccharides. The β -glucose groups are estimated to have a length (distance between the linkage oxygens) of 0.554 nm [33], and the β -galactose group has a length of 0.453 nm [33], due to the kink it introduces in the chain. Then, $l = 1.561$ nm and for the contour length L we find $L = 2.63$ μ m. It has to be remarked that the side groups in the chain may affect the value of the lengths mentioned.

In a first simple approach we set $\alpha = 1$ (θ -solvent). With $R_g = 86 \pm 2$ nm, $l_k = 6R_g^2/L$ follows as $l_k = 16.9 \pm 1.5$ nm, and from equation 15 we find $N_k = 156 \pm 20$. This means that 33 ± 3 monosaccharide backbone units (about 11 repeating units) are required to mimic a freely rotational Kuhn segment. For a commercial polysaccharide thickener such as CMC Davis [34] measured a Kuhn length of 10.8 nm at high ionic strength. For hyaluronate, Fouissac *et al.* [31] found an l_k value of 12 ± 3 nm. These values indicate that B40 EPS has a rather stiff chain. Since $\nu = 0.57$, it follows that $\alpha > 1$. The value for l_k would then be lower than calculated above by a factor α^2 ; similarly N_k would become higher by the same factor. For the moment, we can

only conclude that the values given above for l_k and N_k are upper and lower estimates, respectively.

A parameter which directly gives information on thickening properties of a polymer solution is the intrinsic viscosity, which depends on the hydrodynamic volume of a polymer molecule. The hydrodynamic radius of polymer molecules can be measured by dynamic light scattering. Therefore, we measured the first cumulant as a function of Q for the EPS molecules in solutions with a ionic strength of 0.10 M by DLS. In Figure 6, Γ_1/Q^2 (also called 'apparent' diffusion coefficient) is plotted as a function of Q^2 . The data can be described with equation 12. The diffusion coefficient $\langle D \rangle_z$ was calculated from the intercept of Γ_1/Q^2 as a function of Q^2 and from the slope C can be calculated by using equation 12. For C we found a value of 0.15, which is close to the theoretical value of 0.17 [19].

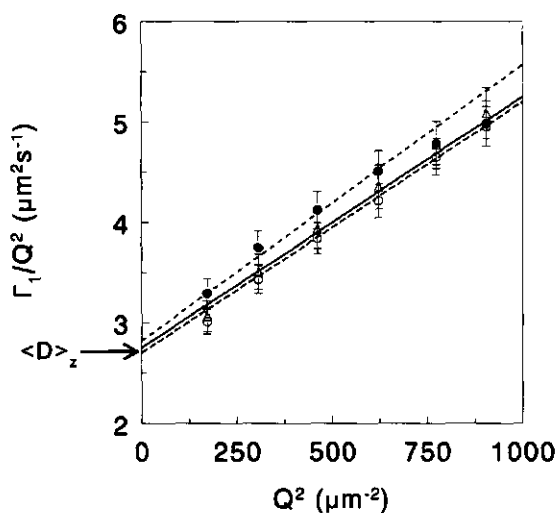


Figure 6 Apparent diffusion coefficient Γ_1/Q^2 as a function of Q^2 . Extrapolation to $Q^2 = 0$ gives $\langle D \rangle_z$. The data are given for polymer concentrations of 0.20 g/L (Δ), 0.25 g/L (\bullet) and 0.30 g/L (\circ).

By using equation 13, the z-averaged R_H can be calculated from $\langle D \rangle_z$. For the solvent viscosity, we used the viscosity of water at 298 K (0.8904 mPa·s). The extrapolated values give a z-averaged hydrodynamic radius of 86 ± 4 nm. This value can be compared with the z-averaged radius of gyration, 97 ± 3 nm, which yields a ratio $\xi = R_g / R_H = 1.13 \pm 0.09$. This value is close to 1.26-1.28 as reported theoretically [23,24] and experimentally for synthetic polymers [35].

The results in Figure 6 are given for three concentrations; 0.20, 0.25 and 0.30 g/L. It is assumed that these concentrations are small enough to neglect hydrodynamic interactions between the polymer molecules. The overlap concentration, M_w/V_p , with V_p being the volume per mole polymer ($= N_{AV} \cdot 4/3 \cdot \pi \cdot R_g^3$), which equals 1.0 g/L, is much higher than 0.30 g/L. Therefore, we can consider the system as being sufficiently dilute to study the diffusion of individual EPS molecules.

Conclusions

We have shown how EPS can be isolated on a pilot-plant scale using membrane filtration processes. The freeze-dried isolate contains impurities from proteins. After dissolving the isolate in aqueous solution some aggregates remain in the solution. A washing method yields a purified sample, which can be analyzed properly by a combination of static light scattering and GPC. The number-averaged molar mass was determined as $1.47 \cdot 10^6$ g/mol and the polydispersity index was found to be 1.13, which is relatively low in comparison with most synthetic polymers. The number-averaged radius of gyration R_g was measured as 86 ± 2 nm. By analyzing various fractions the relation between R_g and M ($R_g \sim M^{0.57}$) was determined and it follows that B40 EPS can be described as a random coil in a good solvent. The z-averaged hydrodynamic radius R_H , determined by dynamic light scattering, is 86 ± 4 nm. The relation between R_H and R_g is consistent with theoretical results for random coil polymer molecules.

Acknowledgments

The authors thank Guido Sala for performing the GPC/SLS analysis. Ellen Looijesteijn, Dr. Mark Smith, Fedde Kingma, and Carolien van der Horst of NIZO food research are acknowledged for their help in developing the EPS production process. Elly Faber, Department of Bio-Organic Chemistry, Utrecht University, is thanked for calculating the length of the backbone monosaccharides.

References

- [1] Sutherland, I.W., *Ann. Rev. Microbiol.*, **39** (1985) 243.
- [2] Finan, T.M., Hirsch, A.M., Leigh, J.A., Johansen E., Kuldau, G.A., Deegan, S., Walker, G.C., Signer, E.R., *Cell*, **40** (1985) 869.
- [3] Dillard, J.P., Yother, J., *Mol. Microbiol.*, **12** (1994) 959.
- [4] Stingle, F., Neeser, J.R., Mollet, B., *J. Bacteriol.*, **178** (1996) 1690.
- [5] Crescenzi, V., *Biotechnol. Prog.*, **11** (1995) 251.
- [6] Gidley, M.J., Dea, I.C.M., Eggleston, G., Morris, E.R., *Carbohydr. Res.*, **160** (1987) 381.
- [7] Doco, T., Wieruszkeski, J.-M., Fournet, B., Carcano, D., Ramos, P., Loones, A., *Carbohydr. Res.*, **169** (1990) 313.
- [8] Robijn, G.W., van den Berg, D.J.C., Haas, H., Kamerling, J.P., Vliegthart, J.F.G., *Carbohydr. Res.*, **276** (1995) 117.
- [9] Cerning, J., *FEMS Microbiology Reviews*, **87** (1990) 113-130.
- [10] Van Marle, M.E., Zoon, P. *Neth. Milk Dairy J.*, **49** (1995) 47.
- [11] van Casteren, W.H.M., Dijkema, C. Schols, H.A., Beldman, G., Voragen, A.G.J., accepted for publication in *Carbohydr. Pol.*, 1998.
- [12] Nakajima, H., Hirota, T., Toba, T., Itoh, T., Adachi, S., *Carbohydr. Res.*, **224** (1992) 245-253.
- [13] Kerker, M., 'Scattering of light and other electromagnetic radiation,' Academic Press, New York, 1969.
- [14] Debye, P., In: 'Light scattering from dilute polymer solutions,' D.McIntyre, F.Gornick (Eds.), Gordon and Breach, 1964.
- [15] Lyklema, J., 'Fundamentals of Colloid and Interface Science,' Chapter 7, Academic press, 1991.
- [16] Dhont, J.K.G., 'An Introduction to Dynamics of Colloids,' Elsevier Science, Amsterdam, 1996.
- [17] Koppel, D.E., *J. Chem. Phys.*, **57** (1972) 4814.
- [18] Burchard, W., *Adv. Polymer. Sci.*, **48** (1983) 1.
- [19] Burchard, W., Schmidt, M., Stockmayer, W.H., *Macromolecules*, **13** (1980) 1265.
- [20] Adam, M., Delsanti, M., *Macromolecules*, **10** (1977) 1229.
- [21] Jones, J., Caroline, D., *J. Chem. Phys.*, **37** (1979) 187.
- [22] Han, C.C., *Polymer*, **20** (1979) 259.
- [23] Freire, J.J., Rey, A., Garcia de la Torre, J., *Macromolecules*, **19** (1986) 457.
- [24] Freed, K.F., 'Renormalization Group Theory of Macromolecules,' Wiley, New York, 1987.
- [25] Kuhn, W., *Kolloid Z.*, **68** (1934) 2.
- [26] Flory, P.J., 'Principles of Polymer Chemistry,' Cornell University Press, New York, 1953; 'Statistical Mechanics of Chain Molecules,' Interscience New York, 1969.
- [27] Odijk, T., *J. Polym. Sci. Polym. Phys. Ed.*, **15** (1977) 477.

- [28] Skolnick, J., Fixman, M., *Macromolecules*, **10** (1977) 944.
- [29] Terzagi, B.E., Sandine, W.E., *Appl. Microbiol.*, **29** (1975) 807-813.
- [30] Milas, M., Rinaudo, M., Knipper, M., Schuppiser, J.L., *Macromolecules*, **23** (1990) 2506.
- [31] Fouissac, E., Milas, M., Rinaudo, M., Borsali, R., *Macromolecules*, **25** (1992) 5613.
- [32] Rinaudo, M., personal communication.
- [33] calculated by using the program Insight II, Biosym MS I, San Diego, California, U.S.A.
- [34] Davis, R.M., *Macromolecules*, **24** (1991) 1149.
- [35] Burchard, W., Schmidt, M., *Macromolecules*, **14** (1981) 210.

3

Concentration and shear-rate dependence of an exocellular polysaccharide

Abstract

The viscosity of an exocellular polysaccharide (EPS) produced by the bacterium *Lactococcus lactis* subsp. *cremoris* B40 was studied in aqueous solution at an ionic strength of 0.10 M. Firstly, the zero-shear viscosity was determined as a function of the concentration. From the data in the low concentration range the intrinsic viscosity was determined. In addition the shear-thinning behavior was measured at several concentrations. The intrinsic viscosity and the concentration dependence of the (zero-shear) viscosity of the B40 EPS could be predicted from the molar mass and the hydrodynamic radius. The shear rate at which the viscosity starts to decrease scales with polymer concentration in accordance with the Rouse theory. Combining existing theories it is shown that it is possible to predict the viscosity and shear-thinning behavior as a function of polymer concentration, molar mass, and hydrodynamic radius of the polymer.

Introduction

Water-soluble natural polymers such as polysaccharides have gained much interest because of their functional properties in a variety of products. In food products polysaccharides are often used to provide a thickening effect. The corresponding enhancement of the viscosity leads to a better mouthfeel of food products. In this study the viscosity of an exocellular polysaccharide (EPS) produced by the food-grade lactic acid bacterium *Lactococcus lactis* subsp. *cremoris* code B40 was investigated; we denote the polysaccharide as B40 EPS. The chemical structure was reported earlier [1]. The interest in EPS arises from the fact that these polysaccharides can be produced *in situ* in dairy products during fermentation so that a thickening agent is incorporated in the product in a natural way. Thickening polymers play a role in several food products, such as yogurt.

The viscosity and shear-thinning behavior are important properties in view of the role of B40 EPS as a thickener in dairy products. For instance, in chocolate milk the viscosity has to be high at zero shear rate to prevent sedimentation of the cocoa particles, whereas the viscosity has to decrease during pouring and drinking. This implies that the viscosity must start to decrease at a shear rate of about $10 \cdot 10^3 \text{ s}^{-1}$. Polysaccharides can be used for this purpose, since they exhibit strong shear-thinning behavior.

We have focused on the viscosity and the shear-thinning behavior of B40 EPS in solutions of ionic strength of 0.10 M, which is a typical value for the ionic strength (isotonic value) in many food products. For example, milk has an ionic strength of 0.08 M. The EPS contains negatively charged phosphate groups, which can be regarded as being quasi-neutral since they are highly screened at an ionic strength of 0.10 M (the Debye length is only 1 nm) and the radius of gyration is independent at ionic strengths exceeding 0.03 M.

In a previous study [2] we determined various molecular parameters of B40 EPS. Gel permeation chromatography was used to fractionate the polysaccharide. Fractions were analyzed by static light scattering in aqueous 0.10 M NaNO_3 solutions and this yielded a number- (M_n) and weight-averaged (M_w) molar mass of $(1.47 \pm 0.06) \cdot 10^3$ and $(1.62 \pm 0.07) \cdot 10^3$ kg/mol, respectively. The polydispersity index M_w/M_n equals 1.13, which indicates a relatively monodisperse sample. The averages of the radius of gyration were found to be 86 ± 2 nm (number average), 91 ± 2 nm (weight average) and 97 ± 3 nm (z-average). From dynamic light scattering experiments we determined a (z-averaged) hydrodynamic radius of 86 ± 4 nm. In this study we establish the relation between these molecular quantities and the rheological properties of B40 EPS solutions.

Theory

Concentration dependence of the zero-shear viscosity

For spherical particles dispersed in a solvent, the relative viscosity η_r (with respect to the solvent), can generally be written as a virial expansion:

$$\eta_{r0} = \frac{\eta_0}{\eta_s} = 1 + \frac{5}{2} v_{sp} c + C_1 v_{sp}^2 c^2 + \dots \quad 1$$

where the subscript 0 refers to the limit of zero shear. The quantity η_0 is the dynamic viscosity in the Newtonian plateau regime, η_s the viscosity of the solvent, v_{sp} the specific volume of the dispersed spherical particles and C_1 is a constant which reflects the hydrodynamic interactions between the particles. For polymer solutions four concentration regimes can be distinguished [3,4]: 1, very dilute; 2, dilute; 3, semi-dilute; and 4, entangled. We characterize the crossovers between these regimes by the concentrations c_{12} , c_{23} and c_{34} .

In the very dilute regime the concentration is sufficiently low to neglect the third and higher terms of equation 1. As shown by Einstein, the Newtonian intrinsic viscosity $[\eta]_0$ for a dispersion of spheres equals $5/2 \cdot v_{sp}$. Polymer solutions can be described as dispersions of 'fluffy' spheres with an effective hydrodynamic radius R_H , defined as the friction coefficient of such a sphere divided by $6 \cdot \pi \cdot \eta_s$. Since the molar volume of such fluffy spheres is $4/3 \cdot \pi \cdot R_H^3 \cdot N_{AV}$, the intrinsic viscosity can be written as:

$$[\eta]_0 = \frac{5}{2} \frac{4\pi R_H^3}{3} \frac{N_{AV}}{M} \quad 2$$

where N_{AV} is Avogadro's number. Debye and Bueche [5] derived this equation under the implicit assumption that the coils are non-free draining. For free-draining coils the numerical pre-factor will be smaller than the Einstein factor 5/2. In the very dilute regime $[\eta]_0$ can be determined by extrapolating $(\eta_{r0}-1)/c$ to zero concentration.

In the dilute regime the polymer molecules interact hydrodynamically, but there is still a low probability of intermolecular segment-segment contact. This regime is often described by the first three terms of the Huggins equation [6]:

$$\eta_{r0} = 1 + [\eta]_0 c + k' [\eta]_0^2 c^2 + \dots \quad 3$$

which is another way of writing equation 1. In this equation, the Huggins constant k' is a measure of pairwise hydrodynamic interactions between the macromolecules. Experimentally, k' has values of 0.3-0.4 for polymers in good solvents and 0.5-0.8 for polymers in theta solvents. The cross-over between the very dilute and dilute regimes is in the concentration

range where the third term of equation 3 can no longer be neglected with respect to the second term. We therefore choose c_{12} as the concentration at which the third term of equation 3 is 10 times smaller than the second term. Hence, c_{12} equals $0.1/(k'[\eta]_0)$.

The onset of the semi-dilute region is characterized by the concentration where the polymer chains start to overlap hydrodynamically. The cross-over from dilute to semi-dilute can therefore be defined as the concentration where $[\eta]_0 c$ equals 1, so $c_{23} = 1/[\eta]_0$. In the semi-dilute regime, there is a large probability of intermolecular segment-segment contact, which strongly increases the friction when a shear rate is applied on such a solution. The complex behavior in the semi-dilute regime is given by the Martin equation [7]:

$$\eta_{r0} = 1 + [\eta]_0 c e^{k'c[\eta]_0} \quad 4$$

which may be expanded to give a power series of which equation 3 gives the first terms.

For $c[\eta]_0 \gg 1$, physical segment-segment 'knots' will dominate the interactions in polymer solutions [4]. In that regime, the polymer concentration is so high that the polymer chains are entangled. Bueche [8] (see also [9,10]) derived the following scaling relation for sufficiently long entangled chains:

$$\eta_{r0} \sim c^{7/2} \quad 5$$

Later, Graessley [11] confirmed this result. Both approaches are based upon the fact that $\eta_{r0} \sim \xi c$, where ξ is the friction coefficient which is a constant in dilute solution. However, ξ starts to depend on c when the chains entangle. It can be shown [8-11] that ξ depends on c as $\xi \sim c^{-2.5}$ in the entangled regime, which then leads to equation 5. Using a reptation model, De Gennes [12] arrived at $\eta_{r0} \sim c^{1.54}$ which is an almost identical result.

For various polysaccharides, such as dextran, carboxymethylamylose, aliginate, κ -carrageenan, and hyaluronate, Morris *et al.* [13] observed a strong increase of the viscosity above $c[\eta]_0 \approx 4$. Above that concentration these authors found experimentally $\eta_{r0} \sim c^{3.3 \pm 0.3}$, which is in reasonable agreement with the theoretical scaling exponents. Lapsin and Pricl [14] review various experimental values found for the exponent and most lie in the same range. Therefore, we assume the fourth regime to be entered at approximately $c_{34} = 4/[\eta]_0$.

An important observation of Morris *et al.* [13] is that a plot of the specific viscosity $\eta_{r0} - 1$ as a function of $c[\eta]_0$ yields a master curve for the polysaccharides mentioned above. A similar result was later found for instance by Robinson *et al.* [15], Fouissac *et al.* [16] and Milas *et al.* [17]. This means that the zero-shear viscosity of the polysaccharides can be described in terms of $[\eta]_0$ only: all specific information of the individual polysaccharides is accounted for in $[\eta]_0$ which, in turn, depends on R_H and M . This finding leads to the conclusion that the concen-

tration dependence of the viscosity of these polysaccharides can be described in terms of these two molecular parameters only.

Shear-rate dependence

Shear-thinning (viscosity decreasing with increasing shear rate) is a well-known property of polymer solutions. In Figure 1 the general behavior is sketched. At sufficiently low shear rates the solution exhibits Newtonian behavior and the viscosity has a constant, high value, the zero-shear viscosity η_0 . At such shear rates the relaxation time needed for rearrangement of the chain segments of the polymer is smaller than the distortion time.

When the shear rate $\dot{\gamma}$ increases, the distortion time decreases and when this time becomes smaller than the longest relaxation time the dissipation and, consequently, the viscosity decreases. The shear rate $\dot{\gamma}_R$ at which the viscosity starts to decrease is related to the longest relaxation time. The latter can be calculated with Rouse theory [18]. More or less arbitrarily, we define $\dot{\gamma}_R$ as the shear rate at which the viscosity is equal to 95% of η_0 . At very high shear rates a constant low viscosity is reached, which we denote as η_∞ . The general picture sketched in Figure 1 applies at any polymer concentration c . The parameters η_0 and η_∞ depend on c and both increase with increasing polymer concentration. The parameter $\dot{\gamma}_R$ decreases with increasing polymer concentration.

When shear is applied, the polymer chains will be extended under an angle of 45° with the flow field, whereas they are compressed in the perpendicular direction. This effect was also recently demonstrated in molecular dynamics simulations by Pierleoni and Ryckaert [19]. This orientation and elongation causes a decrease in energy dissipation (fewer solvent molecules will interact with the polymer molecules due to shearing), which is manifested as a lower viscosity. This viscosity reduction can be calculated when the dynamics of the polymer molecule are known as a function of shear rate.

To this end, we use the approach of Bueche [20] who considered a polymer molecule as a collection of beads and springs (see also [10]). The model of Bueche can be criticized in the sense that for bead-spring models one usually does not find shear-rate thinning. However, since the model which works out well for many (synthetic) polymer solutions [21] and does not need empirical fit parameters we apply it here. In bead-spring models the beads can rotate freely and the springs connecting the beads are Hookean. The distance between two adjacent beads is assumed to be equal to the Kuhn length l_k , and the number of beads is taken to be the number N_k of Kuhn segments in the chain.

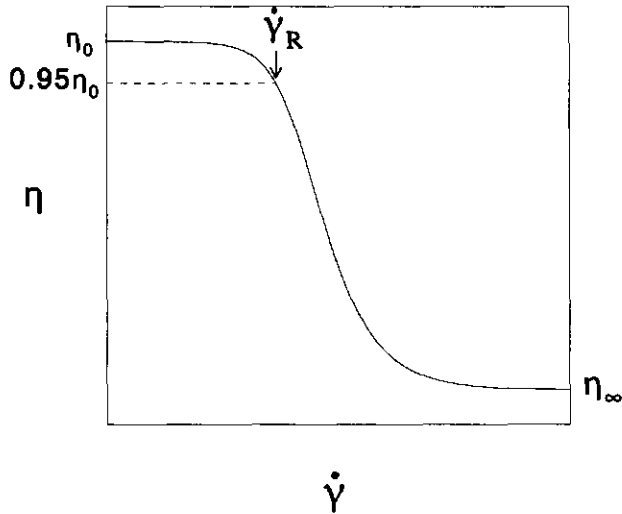


Figure 1 Schematic picture of the shear-thinning behavior of polymer solutions. Symbols are explained in the text.

The quantities l_k and N_k can be calculated by requiring the same contour length L for the equivalent Kuhn chain and the real chain: $l_k N_k = l N = L$, where l is the length of a monomeric unit of the polymer and N the number of those units in the chain. When the radius of gyration R_g is measured independently (e.g. from static light scattering), l_k can be calculated from $R_g = \alpha l_k N_k^{0.5} / 6^{0.5}$ or

$$l_k = 6 R_g^2 / \alpha^2 L \tag{6}$$

where α is the linear expansion coefficient which depends on the solvent quality. From l_k , N_k follows as $N_k = L / l_k$.

By regarding the polymer molecules as bead-spring systems, Bueche [20] replaced the dynamics of a polymer molecule by the dynamics of a set of masses connected by Hookean springs in series. The displacements of the beads are calculated using a relaxation time spectrum. Bueche's final result is [20]:

$$\frac{\eta - \eta_s}{\eta_0 - \eta_s} = 1 - \frac{6}{\pi^2} \sum_{p=1}^{N_k} \frac{\lambda^2}{p^2 (p^4 + \lambda^2)} \left(2 - \frac{\lambda^2}{p^4 + \lambda^2} \right) \tag{7}$$

where $p = 1, 2, \dots, N_k$, and the dimensionless shear rate λ is defined as $\dot{\gamma} \tau_1$, where τ_1 is the longest relaxation time. As expected, $\eta = \eta_0$ for $\dot{\gamma} = 0$. The leading term in the summation is the first ($p = 1$):

$$\frac{\eta - \eta_s}{\eta_0 - \eta_s} \approx 1 - \frac{6}{\pi^2} \frac{\lambda^2}{(1 + \lambda^2)} \left(2 - \frac{\lambda^2}{1 + \lambda^2} \right) \quad 8$$

which shows that the viscosity is about $\eta_0/2$ when $\dot{\gamma} = \tau_1^{-1}$. For higher values of $\dot{\gamma}$, the approximation according to equation 8 becomes increasingly inaccurate because then higher p values also contribute; hence η_∞ depends on N_k .

For monodisperse samples, Bueche's theory is in reasonable agreement with experimental data for many polymers, such as polystyrene, polyethylene, and carboxymethylcellulose [22]. Middleman [22] modified Bueche's theory to account for the effect of polydispersity. The correction factor for the viscosity becomes more than 10 percent only when the polydispersity index M_w/M_n exceeds 4/3; therefore, for our system it is reasonable to assume that we do not need such a correction.

Furthermore, we need an expression for the longest relaxation time τ_1 . Here we use the theory of Rouse [18], who developed a generalized Maxwell model from which the relaxation times of polymer chains can be calculated. Rouse resolved all motions of parts of the polymer chain into a series of normal modes. These normal modes can be seen as a series of discrete standing waves caused by a sinusoidal vibration which is applied to the bead-spring chain. When a bead is displaced from its equilibrium position, two types of forces act on the bead: hydrodynamic forces resulting from viscous interaction with solvent and Brownian forces which tend to return the chain to a state of maximum entropy. Rouse [18] derived expressions for the spectrum of relaxation times τ_p , each of which represents a normal mode:

$$\tau_p = \frac{6(\eta_0 - \eta_s)M}{p^2 \pi^2 RTc} \quad 9$$

The longest relaxation time ($p = 1$) is often called the Rouse time. The lowest modes (longest relaxation times) are the most relevant. Hence, in equation 7 there is only a significant effect of the value of N_k when it is lower than 10 (very rigid chains). When the coils do not interact no concentration dependence on the relaxation times is expected; in that case the ratio $(\eta_0 - \eta_s)/c = [\eta]_0 \eta_s$ is a constant. For the longest relaxation time ($p = 1$) equation 9 then reads:

$$\tau_1 = \frac{6 \eta_s [\eta]_0 M}{\pi^2 RT} \quad 10$$

At higher concentrations the relaxation times increase since the rearrangements of entanglements are slower than the internal correlation times of segments within an individual

chain. In equation 9 this effect is accounted for in η_0 , which increases more than linearly with increasing c .

Experimental

B40 EPS was produced and isolated as described in Ref.[2]. The ionic strength of all solutions was 0.10 M NaCl. Ubbelohde capillary (Schott-Geräte) measurements were used to determine the intrinsic viscosity $[\eta]$ of B40 EPS solutions in the (very) dilute range (0.020-0.60 g/L). The kinematic viscosity was calculated taking into account the Hagenbach correction. The solution density, needed to convert the kinetic into the dynamic viscosity, was measured using an Anton-Paar apparatus. The viscosity as a function of shear rate for various B40 EPS concentrations (0.020-6.5 g/L) was measured with a Rheometrics RFSII rheometer for the higher shear rate range (2-1000 s^{-1}) and with a Contraves LS40 for the low shear range (10⁻²-80 s^{-1}). The Rheometrics rheometer was equipped with a double slit cylinder (radii from inside out 28.94, 29.514, 31.992 and 34.00 mm, respectively, effective bob length 30.8 mm). The Contraves apparatus was equipped with a single slit cylinder (inner and outer radius 5.501 and 6.005 mm, respectively, and a bob length of 8.116 mm). All measurements were made at 298 K.

Results and discussion

Intrinsic viscosity

The specific viscosity $\eta_{sp} = \eta_r - 1$ as a function of B40 EPS concentration, obtained with an Ubbelohde capillary, is plotted in Figure 2 (filled symbols). The dependence is approximately linear below 0.20 g/L. From this part of the graph $[\eta]$ was calculated as 1.9 ± 0.1 m³/kg. This value cannot be taken as the zero-shear limit $[\eta]_0$. The average shear rate in the capillary is about 10³ s^{-1} , and the shear rate near the capillary wall is around $1.5 \cdot 10^3$ s^{-1} . According to equation 10 the longest relaxation time is 10⁻³ s, indicating that $\dot{\gamma}_R$ (see Figure 1) is around 10³ s^{-1} . The relative viscosity as measured with capillary viscometry is therefore not only a function of concentration but also of shear rate.

Results obtained with the Contraves low-shear viscometer are given in Figure 2 as the open symbols. In this case the shear rate is in the range 1-80 s^{-1} , where the viscosity is shear rate independent.

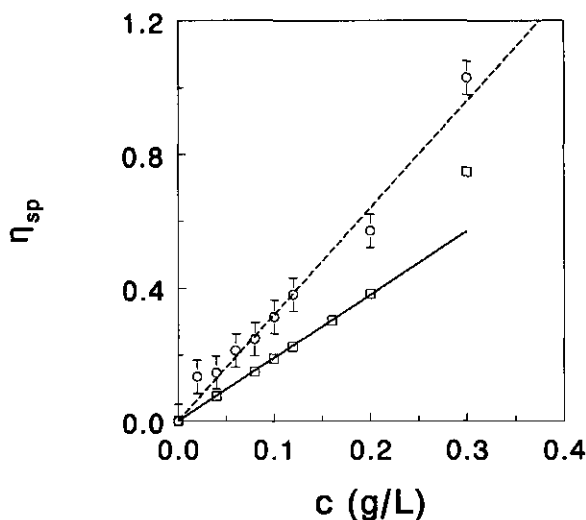


Figure 2 Comparison of the specific viscosities measured by low-shear rheometry (circles) with those measured using a Ubbelohde capillary (squares) at low concentrations.

The measured specific viscosities obtained from the Contraves measurements were higher than those obtained by capillary rheometry and yield $[\eta]_0 = 3.2 \pm 0.2 \text{ m}^3/\text{kg}$. This result corroborates that the shear rate in the capillary is above the zero-shear range.

The experimental $[\eta]_0$ can be compared with theory by using equation 2, giving $[\eta]_0 = 2.8 \pm 0.5 \text{ m}^3/\text{kg}$ by inserting the hydrodynamic radius of 86 nm and $M = 1.47 \cdot 10^3 \text{ kg/mol}$ (as found previously [2]). This is rather close to the experimental value $3.2 \pm 0.2 \text{ m}^3/\text{kg}$. We note here that equation 2 requires the number-averaged R_{H+} . From dynamic light scattering however a z-averaged hydrodynamic radius is found which is larger than the number average.

Concentration dependence of the zero-shear viscosity

The zero-shear viscosities of B40 EPS solutions were measured over a wide concentration range. The results are plotted in Figure 3 (data points), where the polymer concentration is normalized by multiplication with the experimental $[\eta]_0$.

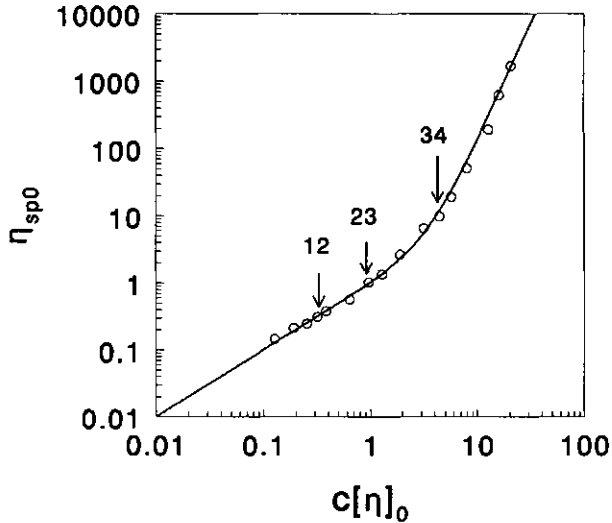


Figure 3 The concentration dependence of the specific viscosity of B40 EPS solutions. The concentration is normalized by multiplication with $[\eta]_0$. Symbols give the experimental data; the solid curve corresponds to equation 11. The arrows give the cross-over concentrations c_{12} , c_{23} and c_{34} , as defined in the text.

This normalized plot closely resembles the master curve of Morris *et al.* [13] for various polysaccharides and for those reviewed by Lapasin and Prici [14]. In order to describe both our results and those of Morris *et al.* [13] we propose the equation:

$$\eta_{sp0} = [\eta]_0 c + \frac{1}{25} ([\eta]_0 c)^{7/2} \quad 11$$

The first-order term of the concentration dependence of equation 11 is the same as in equation 3. The exponent 7/2 of the second term is the scaling exponent from Bueche's theory (equation 4) and is close to the experimental exponent 3.3 ± 0.3 given by Morris *et al.* [13]. The factor 1/25 in equation 11 is an empirical fitting parameter, which determines the crossovers from very dilute ($\eta_0 \sim c^1$) to entangled ($\eta_0 \sim c^{7/2}$) regimes. In Figure 3 this dependence according to equation 11 is plotted as the solid curve. The experimental data are very well described by this curve.

With $[\eta]_0 = 3.2 \text{ m}^3/\text{kg}$, the cross-over concentrations for the various regimes can be estimated : $c_{12} \approx 0.10 \text{ g/L}$ (where k' is taken as 0.3), $c_{23} \approx 0.31 \text{ g/L}$ and $c_{34} \approx 1.25 \text{ g/L}$. These concentrations (multiplied by $[\eta]_0$) are indicated in Figure 3 by the arrows. Indeed, below c_{12} (very dilute regime) $\eta \sim c^1$, and above c_{34} (entangled regime) $\eta \sim c^{7/2}$.

Shear-rate dependence

In Figure 4 the viscosity as a function of shear rate is shown for four concentrations (g/L): 1.8 and 2.5 (Figure 4 a) and 4.0 and 6.5 (Figure 4 b). The full curves in Figure 4 will be discussed later. The data points in these plots show that the shear rate $\dot{\gamma}_R$ at which the viscosity starts to decrease becomes lower for higher concentrations, which agrees with equation 7.

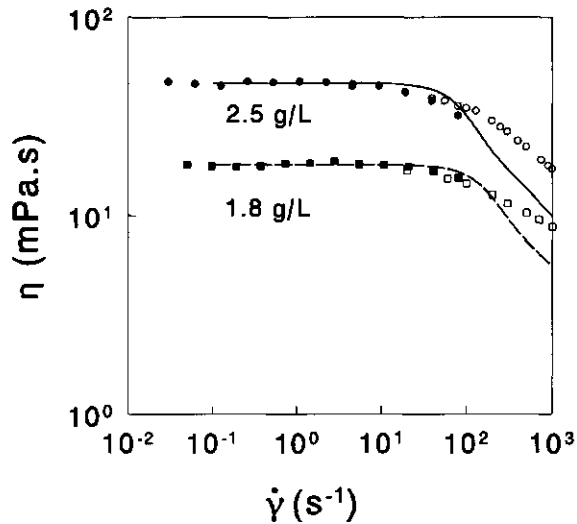


Figure 4 (a) The shear-rate dependence of the apparent viscosity of 1.8 (squares) and 2.5 (circles) g/L B40 EPS in in 0.10 M NaCl solutions. Open symbols are data points measured with the Rheometrics equipment; closed symbols represent data obtained with the Contraves rheometer. The curves are model predictions as discussed in the text.

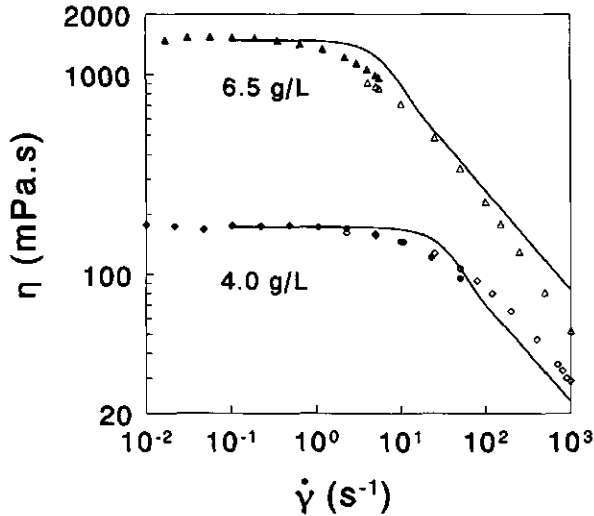


Figure 4 (b) As Figure 4 (a) but for concentrations 4.0 and 6.5 g/L.

We determined $\dot{\gamma}_R$ values at various concentrations and have plotted the results in Figure 5. In the entangled regime $\dot{\gamma}_R$ scales with c as $\dot{\gamma}_R \sim c^{-2.6}$ (we used the data above 2.5 g/L for this experiment). In this regime $\eta_0 \gg \eta_s$ and equations 5 and 9 can be combined to give $\tau_1 \sim c^{2.5}$. Since $\dot{\gamma}_R$ is inversely proportional to the longest relaxation time these equations predict $\dot{\gamma}_R \sim c^{-2.5}$, which is rather close to the experimental exponent. Combination of the result from the reptation approach of De Gennes with the Rouse relaxation time yields $\dot{\gamma}_R \sim c^{-2.75}$, which is also consistent with experiment. In fact, the experimental exponent is in between the two theoretical values.

The viscosity at various shear rates was calculated by using equations 7,9 and 11. Figure 6 shows some theoretical curves to illustrate the main trends. The curves of Figure 6 apply to a polymer with a molar mass of 10^3 kg/mol consisting of 100 beads ($N_k = 100$). The intrinsic viscosity is chosen as $1 \text{ m}^3/\text{kg}$. The relative viscosity is plotted for three polymer concentrations as a function of shear rate, over a broad range of shear rates as encountered in practice. We observe the typical shear-thinning behavior for polymer solutions: a constant viscosity at low shear rates and a decrease at higher shear rates.

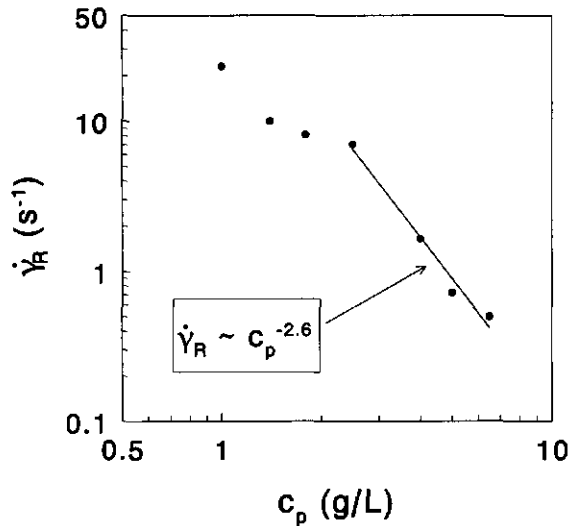


Figure 5 Shear rate at which the viscosity starts to decrease as a function of B40 EPS concentration.

As to the concentration dependence, at every shear rate the viscosity is higher at higher concentrations, and the value of $\dot{\gamma}_R$ is lower in more concentrated solutions. These theoretical plots illustrate that the theoretical η_r depends strongly on the concentration, which agrees with experimental results.

The next step is the input of the appropriate parameters for B40 EPS in the model (see equations 7 and 9). The zero-shear intrinsic viscosity was taken as $3.2 \text{ m}^3/\text{kg}$, M_n equals $1.47 \cdot 10^5 \text{ kg/mol}$ [2], and the solvent viscosity is $0.8904 \text{ mPa}\cdot\text{s}$ [23]. The Kuhn length was calculated from equation 6 for $\alpha=1$, as in Chapter 2, giving $l_k = 17 \text{ nm}$ and $N_k = 156$.

In Figures 4 (a) and (b) the theoretical curves for B40 EPS solutions, obtained from equations 7 and 9 with the parameters given above, are plotted as the solid curves. The theoretical and experimental curves have the same general shape and the data are of the same order of magnitude. For the lower concentrations 1.8 and 2.5 g/L (Figure 4 a) the decrease of the viscosity at high $\dot{\gamma}$ according to the Bueche-Rouse theory is stronger than found experimentally. This might be due to the fact that excluded-volume effects are neglected in the model.

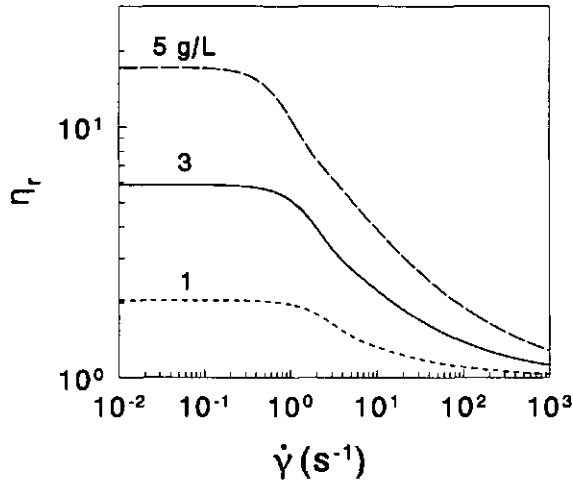


Figure 6 Relative viscosity for three polymer concentrations as a function of shear rate according to equation 7 for a polymer with $M = 10^5$ kg/mol and $N_k = 100$.

Previously [2], we showed that the chains are swollen due to this excluded-volume effect. It is generally known that the excluded volume plays only a role at low concentrations. Indeed, the model predictions are better for 4.0 and 6.5 g/L (Figure 4 b). Taking into account experimental uncertainties, we can conclude that the model describes the shear-thinning of B40 EPS solutions fairly well.

The Bueche-Rouse theory shows how the rheological behavior of solutions of flexible polysaccharides with a low degree of polydispersity can be predicted, which is useful for understanding the relation between the structure of (exocellular) polysaccharides and their suitability as a thickening agent. One could criticize the fact that the springs in the Bueche-Rouse model are considered to be Hookean. Bird *et al.* [25] tried to improve on this aspect by using springs which mimic finite extensibility. Warner [26] calculated the flow-induced stresses by dilute solutions of finitely extendible non-linear elastic dumb-bells. However, this model does not give a good description for experimental data at low shear rates [27]. Moreover, it is not consistent when dynamic and static rheological properties are compared [27]. In the very dilute

regime the Fixman model [28,29], which takes excluded-volume effects into account, might be used to improve the theory. However, for the moment the simple model as treated above is adequate.

Conclusions

Measurement of the zero-shear viscosity of solutions of polymers of high molar mass, such as exocellular polysaccharides, cannot be performed with Ubbelohde capillary viscometers, because the shear rates in the capillary are too high for this purpose. For true zero-shear results, one needs an appropriate low-shear rheometer. The concentration dependence of the viscosity of the EPS solutions as well as other solutions of flexible polysaccharides at low shear rates can be predicted rather well with an equation containing the intrinsic viscosity $[\eta]_0$ as the main parameter. In turn, $[\eta]_0$ is determined by the hydrodynamic radius and molar mass. This means that the zero-shear viscosity behavior can be directly related to molecular parameters. The combination of the Rouse theory for the longest relaxation time and Bueche's theory for the shear rate dependence rather accurately predicts the experimental results for B40 EPS solutions in the entangled region.

Acknowledgments

Professor J. Mellema, Department of Rheology of Twente University, is thanked for making accessible the Contraves rheometer.

References

- [1] Nakajima, H., Hirota, T., Toba, T., Itoh, T., Adachi, S., *Carbohydr. Res.*, **224** (1992) 245.
- [2] Tuinier, R., Zoon, P., Olieman, C., Cohen Stuart, M.A., G.J. Fleer, De Kruif, C.G., *Biopolymers* **49** (1999) 1; Chapter 2 of this thesis.
- [3] Berry, G.C., *J. Rheol.*, **40** (1996) 1129.
- [4] Macosko, C.W. Ed., '*Rheology. Principles, measurements and applications*,' VCH Publishers, New York, 1994.
- [5] Debye, P., Bueche, A.N., *J. Chem. Phys.*, **16** (1948) 573.
- [6] Huggins, M.L., *J. Am. Chem. Soc.* **64** (1942) 2716.
- [7] Spurlin, H.M., Martin, A.F., Tennent, H.G., *J. Polym. Sci.* **1** (1946) 63.
- [8] Bueche, F., '*Physical properties of polymers*,' Interscience, 1962.
- [9] Ferry, J.D., '*Viscoelastic Properties of Polymers*,' Wiley, Second edition, 1970.
- [10] Vinogradov, G.V., Malkin, Ya., '*Rheology of Polymers*,' Springer-Verlag, 1980.
- [11] Graessley, W.W., *J. Chem. Phys.* **47** (1967) 1942.
- [12] De Gennes, P.G., *Macromolecules*, **9** (1976) 594.
- [13] Morris, E.R., Cutler, A.N., Ross-Murphy, S.B., Rees, D.A., Price, J., *Carbohydr. Polymers*, **1** (1981) 5.
- [14] Lapasin, R., Prici, S., '*Rheology of Industrial Polysaccharides: Theory and Applications*,' Blackie Academic, 1995.
- [15] Robinson, G., Ross-Murphy, S.B., Morris, E.R., *Carbohydr. Res.*, **107** (1982) 17.
- [16] Fouissac, E., Milas, M., Rinaudo, M., *Macromolecules*, **26** (1993) 6945.
- [17] Milas, M., Roue, I., Berry, G.C., *J. Rheol.*, **40** (1996) 1155.
- [18] Rouse, P.E., *J. Chem. Phys.* **21** (1953) 1272.
- [19] Pierleoni, C., Ryckaert, J-P., *Macromolecules*, **28** (1995) 5097.
- [20] Bueche, F., *J. Chem. Phys.* **22** (1954) 1570.
- [21] Middleman, S., '*The Flow of High Polymers*,' Interscience Publ., New York, 1968.
- [22] Middleman, S. *J. Appl. Polym. Sci.* **11** (1967) 417.
- [23] '*Handbook of chemistry and physics*,' 45th edition, Chem.Rubber Co., Cleveland (Ohio), 1964.
- [24] Granath, K.A., *J. Colloid Sci.* **13** (1958) 308.
- [25] Bird, R.B., Warner, H.R.Jr., Evans, D.C., *Adv. Polymer Sci.* **8** (1970) 1.
- [26] Warner, H.R.Jr., *Ind. Eng. Chem. Fundam.* **11** (1972) 379.
- [27] Graessley, W.W., *Adv. Polymer Sci.* **16** (1974) 1.
- [28] Fixman, M., *J. Chem. Phys.* **42** (1965) 3831.
- [29] Fixman, M., *J. Chem. Phys.* **45** (1966) 793.

4

Viscoelastic properties of a polysaccharide produced by a *Lactococcus lactis*

Abstract

The viscoelastic properties of a well-characterized model exocellular polysaccharide (EPS) produced by the lactic acid bacterium *Lactococcus lactis* subsp. *cremoris* strain B40 were investigated. Dynamic rheological measurements were performed as a function of frequency and EPS concentration. The dynamic properties could be described by the bead-spring model of Rouse. Concentrated EPS solutions have a significant elasticity ($G' > G''$) at high frequencies. The relatively high G' values at high concentrations and high frequencies are indicative of significant normal stress differences and we suggest that these normal stresses may explain the contribution of EPSs to the ropy behavior of yogurts.

Introduction

In-situ production of exocellular polysaccharides (EPSs) in yogurt gives rise to a better texture of the product [1] and therefore the properties of these EPSs are of special interest. The production of EPSs can lead to a ropy consistency [2-4]. Ropiness or sliminess is characterized by a thread-like behavior on pouring the yogurt. Consequently, the bacterial strains which are used as starters for ropy yogurts are called ropy strains [4]. From the surface of a ropy yogurt one can easily pull out a thread of the yogurt and pouring the yogurt shows these threads as well. These phenomena imply that ropy yogurts are able to generate normal stresses upon elongation.

Previously [5,6] we have analyzed various physical properties of an EPS produced by the lactic acid bacterium *Lactococcus lactis* subsp. *cremoris* NIZO B40. It was shown that in a 0.10 M salt solution the EPS behaves as a flexible chain with excluded volume [5]. Both the concentration and the shear-rate dependence of the viscosity of solutions of this EPS have been described theoretically [6]. As is well known, concentrated polymer solutions also exhibit elastic properties which are related to normal stresses. In order to investigate the elastic properties and the relation between elastic and viscous properties we report the viscoelastic properties of EPS solutions and we show how the simple model of Rouse [7], based on molecular properties of polymers, gives a good description of the measurements.

Theory

Oscillatory flow

The viscoelastic properties of a material can be determined by measuring the stress response in an oscillating shear field [8]. In such a dynamic experiment a periodic sinusoidal strain is imposed on the system and the concomitant shear stress is determined as a function of time. A single experiment allows a determination of both the elasticity and the viscosity. From mechanical analogues of viscoelastic materials, such as the Maxwell element [9], one can derive for the storage and loss moduli, G' and G'' , respectively, the following dependences on the frequency ω for a multi-element Maxwell model:

$$G'(\omega) = \sum_{i=1}^N G_i \frac{\omega^2 \tau_i^2}{1 + \omega^2 \tau_i^2} \qquad G''(\omega) = \sum_{i=1}^N G_i \frac{\omega \tau_i}{1 + \omega^2 \tau_i^2} \qquad 1$$

where G_i is the strength of the relaxation with relaxation time τ_i . The ratio G''/G' is called $\tan \delta$, with the loss angle δ . From Lodge's constitutive equation [10] it can be derived that, in the limit of low frequencies, G' and G'' are related to stationary shear flow by [8]:

$$\lim_{\omega \rightarrow 0} \frac{G'}{\omega^2} = \frac{\psi_{1,0}}{2} \qquad \lim_{\omega \rightarrow 0} \frac{G''}{\omega} = \eta_0 \qquad 2$$

where η_0 is the zero-shear viscosity and $\psi_{1,0}$ is the first normal stress coefficient, which equals $N_1/\dot{\gamma}^2$ at low shear rate $\dot{\gamma}$, with N_1 the first normal stress difference. These expressions underline the relationship of Coleman and Markovitz [8,11], which says that steady shear flow and sinusoidal shear deformations can be directly related. We will check whether the relationship of Coleman and Markovitz applies for our system.

Relaxation times

Equation 1 gives a (Maxwell) continuum mechanics description of the viscoelastic properties of polymer solutions but does not contain molecular information. These are stored in the moduli G_i and the relaxation times τ_i . In order to obtain expressions for these quantities one needs a molecular model which describes the relaxation of polymer coils upon deformation. We have found that our system can be described best by the Rouse model.

In the model of Rouse [7] a polymer molecule is described as a chain consisting of springs which are connected by beads. It is assumed that there is only hydrodynamic interaction between the beads and the solvent molecules. The number of springs is usually set equal to the number of Kuhn segments N_k . The energy dissipation of such a bead-spring system in a shear flow field results from hydrodynamic forces acting upon the beads and the restoring tendency of the chain to diffuse towards a random state. The motions of these bead-spring systems can be subdivided into independent relaxation modes. Every mode has a characteristic relaxation time τ_p . The longest relaxation time τ_R is given by the first mode ($p=1$):

$$\tau_R = \frac{6(\eta_0 - \eta_s)M}{\pi^2 RTc} \qquad 3$$

where c equals the polymer concentration, η_s the viscosity of the solvent, M the molar mass of the polymer molecule, R the gas constant, T the temperature and η_0 the zero-shear viscosity. For the EPS of *L. lactis* strain B40 we have shown [6] that the concentration dependence of the zero-shear viscosity can be described with:

$$\frac{\eta_0}{\eta_s} = 1 + [\eta]_0 c + \frac{1}{25} ([\eta]_0 c)^{3.5} \qquad 4$$

where $[\eta]_0$ is the zero-shear intrinsic viscosity.

Higher-order relaxation times (for $p < N_k/5$) can be calculated using $\tau_p = \tau_1/p^2$. For a good description of the relaxations of a polymer molecule under shear, Fixman [12] showed that it is sufficient to consider the 10 longest relaxation times. Under simple shear, the moduli in

the Rouse bead-spring systems are all equal to cRT/M , which follows from volume averaging [13]. Consequently, we replace equation 1 with:

$$G'(\omega) = \frac{cRT}{M} \sum_{p=1}^{N_K} \frac{\omega^2 \tau_p^2}{1 + \omega^2 \tau_p^2} \quad 5$$

$$G''(\omega) = \omega \eta_s + \frac{cRT}{M} \sum_{p=1}^{N_K} \frac{\omega \tau_p}{1 + \omega^2 \tau_p^2} \quad 6$$

where the relaxation times can be calculated from equation 3 and $\tau_p = \tau_R/p^2$.

Zimm [14] extended the Rouse model by adding hydrodynamic interactions between the beads of the polymer. At low concentrations the theory of Zimm gives a good description for polymer solutions with a narrow size distribution [15]. In the entangled region the Rouse theory gives a better description of the experimental data, especially for high molar mass polymers. This is explained by a screening of the hydrodynamic interactions between the beads with increasing concentration and chain length [15]. All theories mentioned were developed for ideal chains but they can be applied to polymers in a good solvent since experimental results for $G'(\omega)$ and $G''(\omega)$ hardly depend on the solvent quality [15].

At very high polymer concentrations and in polymer melts the relaxation behavior of the system is governed by entanglements. For a highly entangled system the entanglements can be regarded as topological constraints which only enable snake-like motions (reptations) of a polymer chain in a 'tube' [16,17]. The model of Doi and Edwards [17] gives a poorer description of our measured data, both qualitatively and quantitatively. The Doi-Edwards theory predicts a different relaxation domain than is observed experimentally. This means that the investigated solution does not satisfy the reptation conditions; the entanglement density is not high enough to assume that the polymers only exhibit snake-like motions.

Relation between the storage modulus and normal stresses

The relation between G'/ω^2 and $N_1/\dot{\gamma}^2$ as satisfied by equation 2 makes a connection between the elastic component as measured in oscillatory shear flow, G' , and the first normal stress difference N_1 in static shear flow. Significant first normal stress differences lead to the Weissenberg effect, i.e. rod-climbing behavior of solutions. Later, we will use equation 2 to make a connection between the measured G' and the thread-like behavior of the EPS solutions in order to speculate on the relation between sliminess or ropiness and normal stresses, as measured via the storage modulus. By combining equations 2, 3 and 5 the normal stress difference can be expressed as:

$$N_1 = \dot{\gamma}^2 \frac{36}{\pi^4} \frac{(\eta_0 - \eta_s)^2 M}{RTc} \quad 7$$

From equation 4 we can see that η_0 only depends on the polymer concentration and $[\eta]_0$, which in turn depends on the molar mass and the hydrodynamic radius of the polymer [18]. The normal stress difference thus only depends on polymer concentration, shear rate and molecular properties of the polymer.

Materials and methods

EPS was produced on pilot-plant scale. A pre-inoculum of 1% of the strain *Lactococcus lactis* subsp. *cremonis* NIZO B40 was made and used to inoculate a whey permeate medium, which consisted of whey permeate, lactose, yeast extract and a sodium phosphate buffer solution. The EPS production was described previously [5]. After fermentation the culture broth was centrifuged, microfiltered and ultrafiltered. Subsequently, the retentate was diafiltered with deionized water, after which the EPS product was freeze-dried.

Dynamic rheological measurements were carried out with a Carri-med rotational rheometer (TA-instruments, type CSL²500 A/G H/R). Temperature control was established by connection with a Julabo F25 cooling/heating bath. We used a double concentric cylinder geometry in order to achieve a maximum torque domain. The frequency domain was 0.1-250 rad/s. The signal-to-noise ratio was too small below 1 Pa for a reliable measurement. The most concentrated EPS solution (10 g/L) was used to detect the linear region. We found that G' became non-linear above $\gamma=0.3$, where γ is the deformation, and G'' lost its linearity with γ above 0.8. Therefore we chose $\gamma=0.1$ during the experiments.

In order to achieve a broad frequency spectrum we changed the temperature in the range from 5.0° to 50.0°C and made use of the time-temperature superposition principle proposed by Williams *et al.* [19], which states that one is allowed to shift experimental data horizontally over the log-frequency scale in such a way that they match data for the same system at another temperature under the restriction that there are no conformational transitions or supramolecular structure formations under the shifting operations [20]. The temperature T_0 to which the data were shifted is called the reference temperature.

Results and discussion

Description of dynamic moduli

For several EPS concentrations we measured G' and G'' as a function of the frequency ω and in Figure 1 we report the results for a concentration of 10.0 g/L (ionic strength 0.10 M) at various temperatures: 5.0, 20.0 and 50.0°C (they covered the measurements at 10 and 30°C). By making use of time-temperature superposition we shifted all curves to that of 20.0°C. It can be seen that the superposition is successful; the data points from the various temperatures follow rather accurately a single curve. The shapes of the curves are characteristic for concentrated polysaccharide solutions [20]. With increasing concentration both moduli increase. The elastic contribution increases more strongly than the viscous one at higher concentrations. This means that upon making the solution more viscous by adding EPS, one also makes a system more elastic. We now compare the measured curves with theory as presented in the theoretical section.

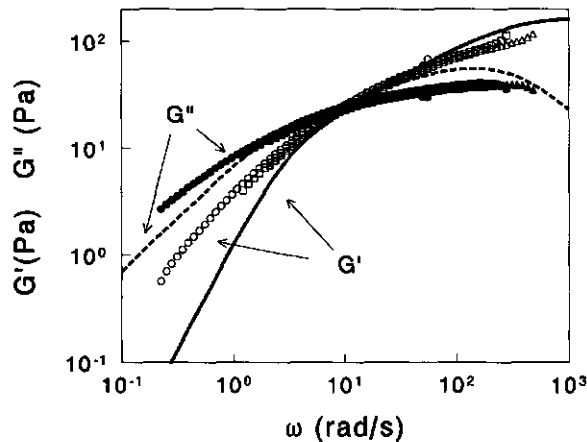


Figure 1 Dynamic shear loss (G'' ; closed symbols) and storage (G' ; open symbols) moduli as a function of the frequency of a 10 g/L EPS solution in 0.10 M NaCl as obtained from time-temperature superposition to 20.0°C. The different symbols refer to measurements at different temperatures (5 (triangles), 20 (squares), and 50°C (circles)). The solid and dashed curves are model predictions from the Rouse theory.

In Figure 1 the result for the Rouse theory (equations 3-6) for a polymer concentration of 10 g/L is plotted. The solid curve corresponds to G' and the dashed curve to G'' . From separate measurements on dilute solutions, we know the intrinsic viscosity $[\eta]_0$ (3.2 m³/kg [6]) and the molar mass (1.47·10³ kg/mol [5]). We used only the lowest 10 relaxation modes as suggested by Fixman [12]. Above $\omega=5$ rad/s the predicted G' values (solid curve) correspond reasonably well with the experimental data; note that there are no adjustable parameters. At lower frequencies the theoretical prediction is poorer and the limiting behavior $G' \sim \omega^2$ is not yet achieved. This may be due to polydispersity effects. The Rouse theory assumes that the polymers are monodisperse. Kokini *et al.* [21] showed that polydispersity of polysaccharides shifts the G' of polysaccharide solutions to higher values at low frequencies.

The calculated loss moduli from the Rouse theory (dashed curve) agree quite well with the experimental data points; the deviation at low frequencies is only small. At high frequencies ($\omega > 10^2$) the theoretical curve passes through a maximum, which is also found experimentally, albeit at a slightly higher frequency. The position of the maximum in the theoretical value of G'' strongly depends on the number of relaxation modes taken into account; the restrictions to 10 modes may be responsible for the discrepancy between theory and experiment at high frequencies. Furthermore, polydispersity tends to broaden the relaxation spectrum and therefore smooth out the maximum of G'' in the experimental curve [21].

We conclude that our system can be described reasonably by the simple model using 10 relaxation modes, without invoking adjustable parameters. There might be models which give a more quantitative description, such as the Oldroyd eight-constant model [22] or the BKZ model [23], but the disadvantage of such models is that they contain many parameters that cannot be determined independently and have to be fitted to the rheological data. Such models have obviously less predictive power.

Concentration dependence of the moduli

We measured the dynamic shear moduli at various concentrations and some representative measurements at 25°C are plotted in Figure 2 (a) for $G'(\omega)$ and in 2 (b) for $G''(\omega)$. The curves are again calculated from the theory of Rouse. It is seen that the theoretical curves satisfactorily describe the measured data points. Especially the G'' predictions match the experimental data rather accurately. We may therefore conclude that the Rouse model adequately describes the dynamic rheological properties of our EPS solutions.

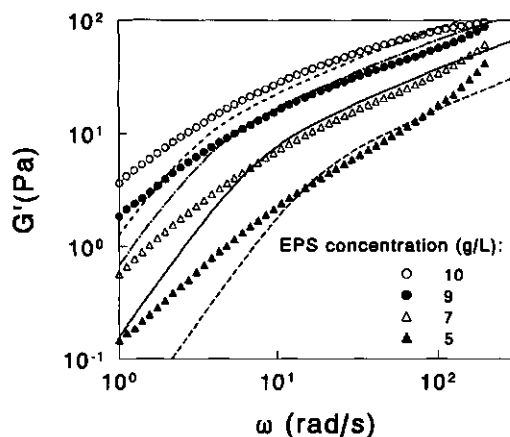


Figure 2 (a) Experimentally determined dynamic storage modulus (symbols) of EPS solutions in 0.10 M NaCl at various concentrations as indicated as a function of the frequency. The curves are calculated from the Rouse theory. The measurements were made at 25.0 ± 0.5 °C.

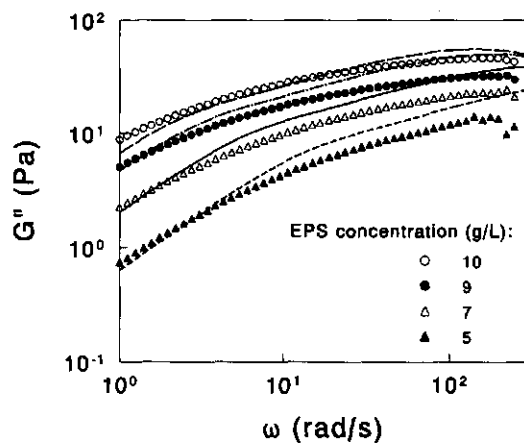


Figure 2 (b) Dynamic loss modulus (symbols) of EPS solutions in 0.10 M NaCl at various concentrations as indicated as a function of the frequency. The curves are calculated from the Rouse theory. The measurements were made at 25.0 ± 0.5 °C.

In order to compare the elastic and loss moduli as a function of frequency and concentration we have plotted $\tan\delta = G''/G'$ as a function of frequency for the four EPS concentrations in Figure 3. The curves clearly show that $\tan\delta$ strongly decreases with increasing concentration and increasing frequency. Increasing the EPS concentration or decreasing the time scale thus makes the solution more elastic. The point where $\tan\delta$ becomes smaller than unity marks the onset of the elasticity-dominated regime.

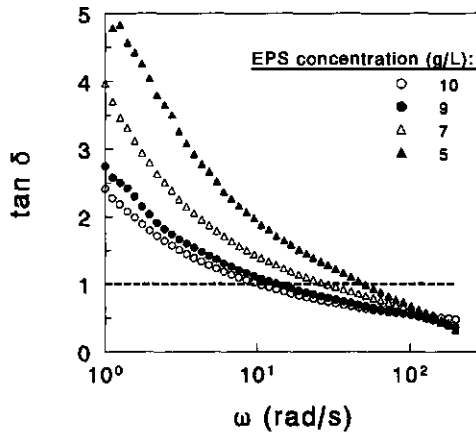


Figure 3 Loss tangent ($\tan\delta$) as a function of the frequency of EPS solutions in 0.10 M NaCl at 5, 7, 9 and 10 g/L as indicated. The measurements were made at 25.0 ± 0.5 °C. The dashed horizontal line identifies the point where $G' = G''$.

Relationship between static and oscillatory shear flow

The relationship of Coleman and Markovitz states that the $\eta'(\omega)$ curve from a dynamic shear experiment should be similar to the $\eta(\dot{\gamma})$ curve from a static shear experiment [11]. In Figure 4, $\eta'(\omega)$ for $c=6.5$ g/L is shown together with the $\eta(\dot{\gamma})$ flow curve determined earlier [6]. In this figure we have included the Rouse prediction for $\eta'(\omega)$ calculated from equations 4-6 with the intrinsic viscosity of 3.2 m³/kg as measured previously [6]. The curves show that the behavior of $\eta'(\omega)$ and $\eta(\dot{\gamma})$ match quite well. As before, the Rouse model describes the measurements well. The results given in Figure 4 show that the relationship of Coleman and Marovitz applies to the investigated EPS solution.

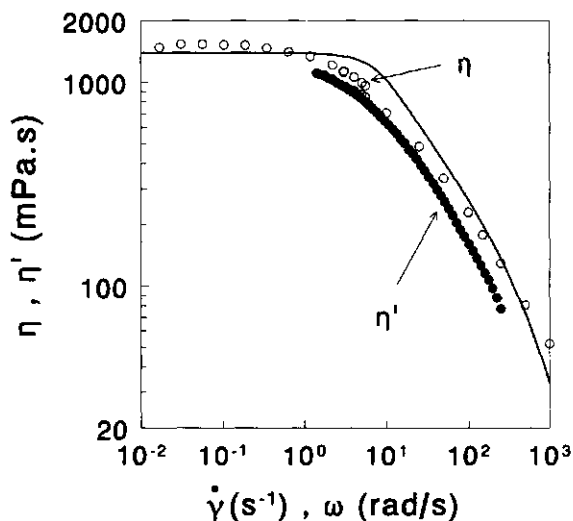


Figure 4 Comparison of the shear-rate dependence of the viscosity [5] with the dynamic viscosity as a function of the frequency of a 6.5 g/L EPS in 0.10 M NaCl solution. Open symbols are data points obtained from static shear measurements and closed symbols were obtained from dynamic rheological measurements. The solid curve represents the Rouse prediction for $\eta'(\omega)$.

This gives a strong argument in support of the use of the relation $G'/\omega^2 = N_e/f\dot{\gamma}^2$ at infinitely low frequencies. Experimentally, $N_e/f\dot{\gamma}^2$ can be calculated from G'/ω^2 by extrapolation to $\omega \rightarrow 0$. In Figure 5 we plot G'/ω^2 as a function of ω . Equation 5 shows that at low frequencies G'/ω^2 should equal $cRT[\tau_R^2/(1+\omega^2\tau_R^2)]/M$; a fit using this relation was made for the lowest measured frequencies in order to estimate $[G'/\omega^2]_{\omega=0}$. The calculated $[G'/\omega^2]_{\omega=0}$ ($=N_e/f\dot{\gamma}^2$) values are plotted as a function of the concentration in Figure 6. The dashed line represents the relation $N_e/f\dot{\gamma}^2 = cRT\tau_R(c)^2/M$, which follows from equation 5 for $\omega \rightarrow 0$. The experimental data agree reasonably well with the theoretical prediction. The experimental $[G'/\omega^2]_{\omega=0}$ values are somewhat higher which can be explained from the fact that the measured G' values in the low-frequency range are smaller than the predicted ones due to polydispersity of the EPS.

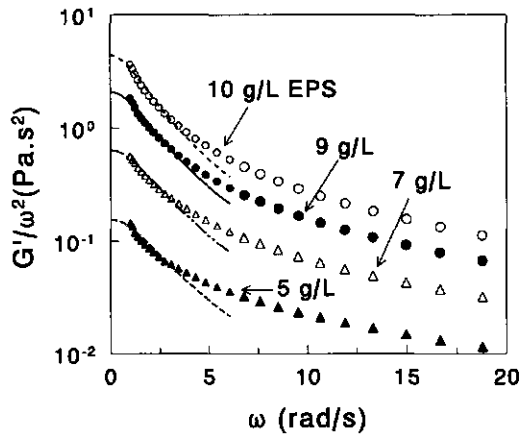


Figure 5 Dynamic storage modulus normalized over the squared frequency as a function of the frequency of EPS solutions in 0.10 M NaCl at various concentrations as indicated. The curves are best fits to the relation $G'/\omega^2 = cRT[\tau_R^2/(1+\omega^2\tau_R^2)]/M$ as explained in the text.

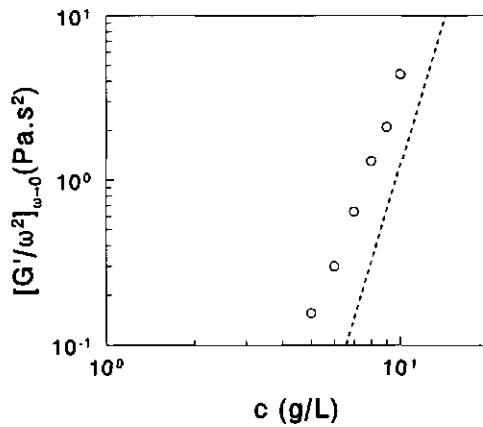


Figure 6 Dynamic storage modulus normalized over the squared frequency as a function of the EPS concentration. Open symbols refer to the experimentally determined G'/ω^2 values from extrapolation as shown in Figure 5. The dashed line is the theoretical prediction from the theory of Rouse.

On the basis of the results presented we can now comment on a possible explanation for the ropy behavior of EPS-containing yogurts. Ropy behavior is usually tested by (poorly defined) elongation of the yogurt. When the normal stress is large enough to compensate the weight of the yogurt film one calls the yogurt ropy. For a typical thread length of 1 cm, the stress required to prevent the film from falling equals approximately 100 Pa. For 10 g/L EPS and a typical shear rate of 10 s^{-1} the normal stress difference equals $\sim 100 \text{ Pa}$, which is thus enough to prevent the yogurt thread from falling. Typical average EPS concentrations in yogurt are of the order of 100 mg/L. However, in yogurt a large fraction of the volume is occupied by casein micelles, thus leaving only a small volume of continuous phase for EPS. As a consequence, EPS is concentrated in the continuous phase of yogurt. We therefore suggest that the elasticity of the EPS solutions is sufficient to cause the ropy behavior of yogurts.

Conclusions

The viscoelastic properties of concentrated solutions of an EPS produced by the lactic acid bacterium *Lactococcus lactis* subsp. *cremoris* NIZO B40 can be described by the Rouse model. Further the relationship of Coleman and Markovitz applies to our system since the viscous part of the complex viscosity as a function of the frequency compares well with the shear-rate dependence of the viscosity.

With increasing polymer concentration the elastic component strongly increases and dominates the viscous one at high frequencies. It is shown that this agrees with significant normal stress differences. In yogurt, the average concentration of EPS is rather small. One might conclude that normal stresses are thus negligible. However, it should be realized that yogurt contains a large effective volume fraction of casein micelles, so that the EPS may be effectively concentrated by a factor of about 10^2 . This then explains the rheological characteristics of 'ropy' yogurt.

References

- [1] van Marle, M.E., 'Structure and rheology of stirred yoghurt,' PhD Thesis, Twente University, ISBN 9036510805, 1998.
- [2] Schellhaass, S.M., Morris, H.A., *Food Microstructure*, 4 (1985) 279.
- [3] Ceming, J., Bouillanne, C., Desmazeaud, M., Landon, M., *Biotech. Lett.*, 8 (1986) 625.
- [4] Rawson, H.L., Marshall, V.M., *Int. J. Food Sci. Techn.*, 32 (1997) 213.
- [5] Tuinier, R., Zoon, P., Olieman, C., Cohen Stuart, M.A., G.J. FLeer, De Kruijff, C.G., *Biopolymers* 49 (1999) 1.
- [6] Tuinier, R., Zoon, P., Cohen Stuart, M.A., G.J. FLeer, De Kruijff, C.G., submitted; Chapter 3.
- [7] Rouse, P.E., *J. Chem. Phys.* 21 (1953) 1272.
- [8] Macosko, C.W. (Ed.): 'Rheology. Principles, measurements and applications,' VCH Publishers, New York, 1994.
- [9] Maxwell, J.C., *Phil. Trans.*, 157 (1867) 49.
- [10] Lodge, A.S., *Trans. Faraday Soc.*, 52 (1956) 120; *Rheol. Acta*, 7 (1968) 379.
- [11] Coleman, B.D., Markowitz, H., *J. Appl. Phys.*, 35 (1964) 1.
- [12] Fixman, M., *J. Chem. Phys.*, 42 (1965) 3831; *J. Chem. Phys.*, 45 (1966) 793.
- [13] Kramers, H.A., *Physica*, 11 (1944) 1.
- [14] Zimm, B.H., *J. Chem. Phys.* 24 (1956) 269.
- [15] Ferry, J.D., 'Viscoelastic Properties of Polymers,' Wiley, Second edition, 1970.
- [16] De Gennes, P.G., *J. Chem. Phys.*, 55 (1971) 572.
- [17] Doi, M., Edwards, S.F., 'The Theory of Polymer Dynamics,' Clarendon Press, 1986.
- [18] De Gennes, P.G., 'Scaling Concepts in Polymer Physics,' Cornell University Press, New York, 1979.
- [19] Williams, M.L., Landel, R.F., Ferry, J.D., *J. Amer. Chem. Soc.* 77 (1955) 3701.
- [20] Lapasin, R., Prici, S., 'Rheology of Industrial Polysaccharides: Theory and Applications,' Blackie Academic, 1995.
- [21] Kokini, J.L., Wang, C-F., Huang, H., Shrimanker, S., *J. Text. Stud.*, 26 (1995) 421.
- [22] Oldroyd, J.G., *Rheol. Acta* 1 (1961) 337.
- [23] Bernstein, B., Kearsley, E.A., Zapas, L.J., *Trans. Soc. Rheol.*, 7 (1963) 391.

Depletion induced phase separation of aggregated whey protein colloids by an exocellular polysaccharide

Abstract

An attractive interaction, commonly referred to as depletion interaction, is induced between aggregated-whey-protein colloid (AWC) particles when they are mixed with exocellular polysaccharides (EPSs) from a lactic acid bacterium. This interaction originates from a loss of conformational entropy of the EPSs near the surfaces of neighboring AWC particles and leads to a phase separation at high enough EPS and AWC concentrations. The effect of the depletion interaction on the properties of the mixtures of EPS and AWC particles is first studied in the stable, i.e. one-phase region. The strength of attractions is characterized by using small-angle neutron scattering (SANS) and dynamic light scattering (DLS). The SANS results can be described quantitatively by a theoretical model for depletion interaction. From Ornstein-Zernike plots we derive the position of the spinodal. The DLS results can be described qualitatively quite well by using a recently derived expression for the wavevector (Q)-dependent diffusion coefficient as a function of the correlation length.

Further the experimental phase boundary is determined and compared with a mean-field theory that evaluates the free energy of a mixture of colloids and large non-adsorbing polymers. The calculated spinodal was found to be consistent with the experimentally determined position of the phase boundary.

Spinodal phase separation kinetics is investigated by small-angle light scattering (SALS). At low Q a scattering peak was detected which shifted to lower Q 's with time in agreement with other experimental data and theoretical predictions for spinodal decomposition. Both the scaling of the scattered intensity with Q and the scaling of the Q -position of the peak with time agree with theoretical predictions.

Introduction

The properties of exocellular polysaccharides (EPSs) by food grade micro-organisms, produced during fermentation of milk and products as yogurt [1,2], is an important topic for product development but is also of scientific interest. The EPSs have a significant influence on the rheological properties of fermented milk products [3], but the underlying mechanisms are not yet understood. Adding EPS to a dairy product makes the final product a biopolymer mixture containing polysaccharides and proteins. Both types of biopolymers affect the structure and texture of food products. Upon mixing two such biopolymers in an aqueous solution they are either associative or segregative. When the biopolymers are mutually segregative the mixture is said to be incompatible. Incompatibility is a very common phenomenon in polymer solutions as well as in protein-polysaccharide mixtures [4]. Adding polysaccharides to suspensions of globular proteins induces depletion interactions which lead to an effective mutual attraction between the proteins [5]. Depletion interaction arises from the fact that a polymer molecule loses conformational entropy when located between neighboring colloidal particle surfaces. This gives rise to depletion of polymer from the region between neighboring protein particles. In the depleted region the partial osmotic pressure of the polymer molecules is smaller than in the bulk, which leads to an effective attraction between the colloidal particles.

In the present study we consider the interaction between EPS and (aggregated) whey protein colloids (AWCs). Both components are of practical and scientific relevance. The EPS used can be described as a random coil polymer with a low polydispersity [6]. The AWC particles are well-characterized and controlled in size and are representative of many other practical systems. In our EPS/whey protein mixtures, the polysaccharides in solution are much larger than the proteins. An overview of existing depletion theories, as given by Jenkins and Snowden [7], shows that the description of mixtures with relatively small polymer molecules and large spheres is well developed. This is not the case for systems with relatively large polymer molecules and small spheres as used in the present study.

The AWC-particles consist of aggregates of whey proteins, globular proteins with diameters in the range of 2-6 nm. Whey proteins constitute 20% of the proteins in bovine milk. They consist mainly of β -lactoglobulin (50% of the whey proteins), α -lactalbumin, bovine serum albumin (BSA) and immunoglobulins [8]. Upon heating whey proteins above 60°C, a common (required) treatment in the dairy and food industry, thiol/disulphide exchange reactions lead to the formation of intermolecular disulphide bonds of the whey proteins, which leads to aggregation [9].

It is known that mixing dextran with the whey protein BSA leads to phase separation [10]. Mixing native whey proteins with EPS did not lead to a phase separation. This is explained by

the fact that the reduction in the possible number of conformations of the polymer molecules in the neighborhood of the colloids decreases with decreasing colloid radius. The native whey proteins are thus too small to induce phase separation of mixtures with EPS.

We have also mixed the EPS with AWCs with a radius of about 30 nm, and these mixtures do exhibit a phase separation, even though the aggregates are still substantially smaller than the EPS (with a radius of gyration of 86 nm [6]). In this paper we consider the properties of such EPS/AWC mixtures. We first investigate equilibrium and transport properties in the one-phase region followed by the determination of the experimental phase diagram. This phase diagram is described by a recent mean-field theory by Schaink and Smit [11] for mixtures of small spheres in the presence of long polymers. Finally, we study phase separation kinetics in the unstable (two phase) region.

Theory

In this theoretical section we first describe the background of the scattering techniques which enable the characterization of the AWCs and of the attractions between the whey protein aggregates induced by EPS. Next, we briefly summarize a theory which gives a description of the phase boundary for small particles and large polymers. In the last section we shortly review theoretical descriptions on spinodal decomposition which will be used to describe the phase separation kinetics.

Static scattering

- Analysis of molar mass and radius of gyration

In a (static) light scattering experiment one measures the scattered intensity $I(Q)$ which is commonly normalized to give the Rayleigh ratio $R(Q)$. The scattered intensity is a function of the wavevector Q which equals $4\pi \cdot \sin(\theta/2)/\lambda$, where θ is the scattering angle and λ is the wavelength of the light in the medium. For polarized light, the scattered intensity as measured from a homodisperse colloidal suspension is proportional to the structure factor $S(Q)$ and the particle scattering form factor $P(Q)$ [12]:

$$R(Q) = K c M P(Q) S(Q) \quad 1$$

where c represents the particle mass concentration, M the molar mass of the particle and K is a material constant which depends on the optical contrast and the wavelength. Equation 1 is also valid for small-angle neutron scattering (SANS) for which K depends on the scattering

but as 'hard spheres' with a diameter σ_p towards the colloids. For $r < \sigma_c$, where σ_c is the colloid diameter, Vrij takes $U(r) = \infty$ and for $r > [\sigma_c + \sigma_p]$, $U(r) = 0$. In the range $\sigma_c < r < [\sigma_c + \sigma_p]$ Vrij derived for the potential [20]:

$$U(r) = -\frac{1}{6} \pi (\sigma_c + \sigma_p)^3 \left[1 - \frac{3r}{2(\sigma_c + \sigma_p)} + \frac{r^3}{2(\sigma_c + \sigma_p)^3} \right] \frac{c_p RT}{M} \quad 8$$

where the factor $c_p RT/M$ is just the osmotic pressure Π_p of the polymer solution, with polymer concentration c_p . Here, M is the molar mass of the polymer, and R and T have their usual meaning. For $\sigma_c > 2R_g$, the effective diameter σ_p approximately equals two times R_g . If the polymers become larger than the colloids, i.e. $2R_g > \sigma_c$ as in our case for AWCs and EPS, the effective depletion layer thickness becomes smaller: $\sigma_p < 2R_g$. Since the thermodynamic theories for depletion interaction of Vrij [20] and Lekkerkerker *et al.* [21] have been developed for $\sigma_c > \sigma_p$ these descriptions can not be applied to our system. Therefore we use the theory of Schaik and Smit [11] who developed a mean field theory which describes the depletion induced phase (meta-)stability of a suspension of relatively small spherical colloids and long polymer molecules. We shortly summarize the outline of their theory.

For a statistical mechanical approach it is convenient to work in the grand canonical ensemble [22,23]. In that framework the total free energy of a colloid-polymer mixture, $F_{\text{tot}}(\mu_c, \mu_p, \phi, \varphi_p, T)$, can be expressed as:

$$F_{\text{tot}}(\mu_c, \mu_p, \phi, \varphi_p, T) = F_c(\mu_c, \phi, T) + F_p(\mu_p, \varphi_p, T) \quad 9$$

where μ_c and μ_p are the thermodynamic potentials of colloid and polymer, respectively, φ_p is the polymer volume fraction (which equals c_p/ρ_p , with ρ_p the density of the polymer in the molten state) and F_c is the free energy of the hard spheres which can be approximated by the Carnahan-Starling equation of state [24]:

$$\frac{F_c}{N_c k_B T} = \frac{3}{2} \ln T + \ln \phi + \frac{4\phi - 3\phi^2}{(1-\phi)^2} \quad 10$$

where k_B is Boltzmann's constant, N_c the number of colloidal particles, each having a volume $\pi\sigma_c^3/6$ in a volume V and ϕ is the volume fraction of spheres ($=N_c\pi\sigma_c^3/6V$). The computation of the free energy F_p of the polymer is more difficult since the conformational entropy is a function of the distance from a colloidal sphere. Schaik and Smit expressed the contributions to F_p as a spatial integral of the local free energy density $f_p^{\text{tot}}(r)$:

$$F_p = \int f_p^{\text{tot}}(r) dr = \int (f_p^{\text{tr}}(r) + f_p^{\text{ex}}(r) + f_p^{\text{sg}}(r)) dr \quad 11$$

where $f_p^{\text{tr}}(r)$ is the translational entropy of the chains [25-27]:

$$f_p^{tr}(r) = k_B T \left(\frac{\phi_p(r)}{N_K} \left[\ln \left(\frac{\phi_p(r)}{N_K} \right) - 1 \right] \right) \quad 12$$

where $\phi_p(r)$ is the local volume fraction of polymer molecules and N_K is the number of Kuhn segments in a single chain and $f_p^{ex}(r)$ accounts for the excluded volume interactions between disconnected polymer segments [27]:

$$f_p^{ex}(r) = k_B T \left(\frac{1}{2} v \phi_p(r)^2 \right) \quad 13$$

where v is the polymer excluded volume which equals $1-2\chi$, where χ is the (polymer-solvent) Flory-Huggins parameter [27]. Finally, the term $f_p^{sg}(r)$ is the square gradient contribution which accounts for the restrictions on the possible chain conformations in the neighborhood of the spheres [25,26]:

$$f_p^{sg}(r) = k_B T \left(\frac{1}{24 \phi_p(r)} \left| \frac{d\phi_p(r)}{dr} \right|^2 \right) \quad 14$$

The integration in equation 11 has to be performed over the volume not occupied by the spheres. The determination of $\phi_p(r)$ and the subsequent integration is a complicated problem. Smit and Schaik [11] therefore introduced a cell model in order to simplify the system. The central assumption in the cell model is that the depletion profile of the polymer segments follows the surface of the nearest sphere. In a first approximation it is possible to treat the system as a set of N_c cells, where N_c represents the number of AWC particles. In this approximation the cells are assumed to have a spherical geometry with a volume $4\pi R_L^3/3$, where R_L is the radius of the spherical cell. All length scales are normalized with the Kuhn length l_k . The protein particle is centered in the cell. The cell thus consists of a sphere surrounded by a shell. The shell contains the polymer solution and includes the depletion layer. Within a single cell it is possible to calculate the polymer concentration profile $p(r)$, defined as $\phi_p(r)/\phi_p$, by minimizing the polymer free energy within the cell. It is assumed that the polymer segment density profiles of all cells are equal. Since $V = N_c 4\pi R_L^3/3$ and $V = N_c \pi \sigma_c^3/6\phi$, R_L equals $\sigma_c \phi^{-1/3}/2$. The protein particles are now treated as being isolated, which certainly is an approximation. Using geometrical arguments the spherical cells are corrected for sphere-cell and cell-cell correlations using hypothetical concentration layers in the cell. The macroscopic polymer volume fraction ϕ_p is finally expressed as:

$$\phi_p = \frac{3}{R_L^3} \int_{\sigma_c/2}^{R_L} \phi_p(r) r^2 \left\langle \frac{V_{free}(r)}{V_{shell}} \right\rangle dr + 3\phi_p(R_L) \frac{\langle V_{ov}(\sigma_c, R_L) \rangle}{4\pi(R_L^3 - (\sigma_c/2)^3)} \quad 15$$

where the first term on the right-hand side contains the term $\langle V_{free}(r)/V_{shell} \rangle$ which corrects for the mutual overlap of shells and the second term corrects for the overlap of spheres and shells

[11]. The term $\langle V_{\text{free}}(r)/V_{\text{shell}} \rangle$ contains the volume of the shells which do not overlap, $V_{\text{free}}(r)$, and the volume of the shell V_{shell} . The term $\langle V_{\text{ov}}(\sigma_c, R_L) \rangle$ is the averaged sphere-shell overlap volume. Finally, F_p can be written as:

$$F_p = 4\pi \int_{\sigma_c/2}^{R_L} f_p^{\text{tot}}(r) \left\langle \frac{V_{\text{free}}(r)}{V_{\text{shell}}} \right\rangle r^2 dr + f_p^{\text{tot}}(R_L) \langle V_{\text{ov}}(\sigma_c, R_L) \rangle \quad 16$$

which makes it possible to calculate F_p and hence F_{tot} and leads to solutions for F_{tot} as a function of ϕ and φ_p . From F_{tot} , the spinodal can be calculated from the following determinant [28]:

$$\begin{pmatrix} \frac{\partial^2 F_{\text{tot}}}{\partial \phi^2} \\ \frac{\partial^2 F_{\text{tot}}}{\partial \varphi_{\text{pol}}^2} \end{pmatrix}_{\varphi_{\text{pol}}} - \begin{pmatrix} \frac{\partial^2 F_{\text{tot}}}{\partial \phi \partial \varphi_{\text{pol}}} \end{pmatrix}_{\phi}^2 = 0 \quad 17$$

which will be used to compare with experimental phase lines in this study.

Phase separation kinetics

Strong attractions between colloids may induce phenomena like spinodal decomposition or fractal aggregation. Although seemingly quite different these processes are difficult to distinguish by scattering experiments. Recently, it has been shown that the evolution of the structure factor in time for diffusion-limited cluster aggregation (DLCA) behaves quite analogous as in the case of spinodal decomposition (SD) and that there are various close similarities between fractal aggregation and spinodal decomposition [29,30]. The processes can be characterized by determining the fractal dimension d_f of the aggregating clusters. The evolution of the scattered intensity during a spinodal decomposition obeys a scaling $I(Q) \sim Q^{-3}$ at high Q in the early stages [29,31]. For DLCA, $d_f = 1.75-1.80$ as found from 3D computer simulations of Jullien *et al.* [32], which agrees for instance with the experimental finding of Weitz and Oliveria [33] who found $d_f = 1.75$ for fractal aggregating gold sols. For fractal systems Teixeira [34] has shown that:

$$I(Q) \sim Q^{-d_f} \quad 18$$

for $a_{\text{low}} < 2\pi/Q < a_{\text{up}}$, where a_{low} and a_{up} refer to the upper and lower length scale limit in the system, respectively. Upon measuring the scattered intensity as a function of Q for demixing systems with AWC particles and EPS we found $d_f = 3$. Therefore our small-angle light scattering results will be compared with theory for spinodal decomposition.

Since the development of the theory for spinodal decomposition by Cahn and Hilliard [35] it turned out that a wide range of systems could be described with this mechanism. A theoretical discussion of spinodal decomposition of colloids in the initial and intermediate stages can be found in ref. [17]. After a quench into the two-phase region spontaneous

fluctuations in density are no longer stable with respect to a homogeneous distribution. The diffusion coefficient in a Fickian type of law then becomes negative, so that certain density fluctuations tend to grow in time. The evolution of density fluctuations can be divided into four stages: an initial, an intermediate, a transition and a final stage [17,36]. Siggia [37] only distinguishes two stages: an early (initial + intermediate) and a late (transition and final) stage. The theory of Cahn and Hilliard only applies to the initial and intermediate stages where the density waves have a small gradient. In the initial stage, in addition, the amplitude of density waves is small.

The Cahn-Hilliard theory predicts that during the early stage of the SD process there is a fastest growing density variation with a typical length scale $\Lambda=2\pi/Q_m$, with Q_m the wavevector where the scattered intensity has its maximum. In the initial stage the peak of the scattered intensity $I(Q)$ lies at a fixed Q_m value. The value of Q_m is affected by hydrodynamic interactions only in the intermediate stage (and later stages). Beyond the initial stage normalization of the $I(Q)$ curves can be used to investigate whether the data can be described as a universal mastercurve by plotting $I(Q)/I(Q_m)$ as a function of Q/Q_m . For spinodal decomposition in the final stage (off-critical conditions) Furakawa [36] proposed the following scaling relation:

$$\frac{I(Q)}{I(Q_m)} = \frac{3(Q/Q_m)^2}{2 + (Q/Q_m)^6} \quad 19$$

which we will compare with our results. In the final stage the temporal evolution of density inhomogenities can proceed through coalescence of droplets as described by Lifshitz and Slyzov [38]. Large clusters with size Λ coalesce with other clusters in a diffusion time $\tau \sim \Lambda^2/D$. By using the Stokes-Einstein equation $D=k_B T/(6\pi\eta_s\Lambda)$ the following differential equation for growth of the droplets can be derived:

$$\frac{d\Lambda^3(t)}{dt} \sim \frac{k_B T}{\eta_s} \quad 20$$

where η_s is the solvent (medium) viscosity. From equation 20 it follows that $Q_m \sim t^{-1/3}$. Siggia [37] later showed that for concentrated mixtures the coarsening kinetics is governed by hydrodynamics and the scaling changes to $Q_m \sim t^{-1}$. In the final stage Q_m reaches a minimum value and the scattering is then dominated by sharp interfaces which leads to a $I(Q) \sim Q^{-4}$ scaling, known as Porod behavior [39]. We will present experimental small-angle light scattering results of mixtures of AWC and EPS and compare the trends found in our experiment with the theoretical results above.

Methods and materials

Experimental techniques

- *Small-Angle Neutron Scattering (SANS)*

The SANS experiments were made at the Institute Max Von Laue-Paul Langevin (ILL) in Grenoble (France) using the D-22 spectrometer. Hellma QS quartz cells were used with a sample path length of 2 mm. For the required Q-range, we choose sample-detector distances of 14.4 and 18 m. The wavelength of the (cold) emitted neutrons was 1.0 nm with a width of 9%. The scattered intensity of EPS was negligible compared to the scattering of the whey protein aggregates; the intensity of the AWC suspensions was always more than 10 times the intensity of the EPS solutions. The EPS molecules themselves do thus not significantly contribute to the scattered intensity of a mixture of AWC aggregates and EPS.

- *Size exclusion chromatography-static light scattering (SEC-SLS)*

The heated AWC solutions were analyzed by using size exclusion chromatography (SEC). The equipment used consisted of two silica gel columns (Phenomenex TSK) in series as described by Hoffmann *et al.* [40]. The fractions were analyzed by static light scattering (SLS) with a Wyatt Technology DAWN apparatus, equipped with a 5 mW He-Ne laser ($\lambda_0 = 632.8$ nm).

- *Dynamic light scattering (DLS)*

Dynamic light scattering experiments were performed using a Spectra Physics 275 mW Ar laser with a wavelength of 514.5 nm. The sample cuvette housing is kept at a temperature of 25°C. The detected photons were processed by a digital ALV-5000 correlator to give the auto-correlation function from which the diffusion coefficient was calculated. We analyzed the data using a second-order cumulant fit.

- *Small-angle light scattering (SALS)*

In order to study spinodal decomposition small-angle light scattering experiments were performed using a Mastersizer X, Malvern Instruments Ltd, which contains detectors at low scattering angles. The cell was always cleaned intensively before a measurement was made. The scattered intensities given in the results section are the measured ones from the mixtures minus the scattered intensity of AWCs at the same concentration without EPS. At very low

wave vectors ($<0.2 \mu\text{m}^{-1}$) scattering of dust particles was unavoidable. Correction with the $I(Q)$ of the AWC solutions improved the accuracy in the low Q -range.

Material

- Exocellular polysaccharide

The EPS was produced on a pilot-plant scale at NIZO [6]. A *Lactococcus lactis* subsp. *cremoris* NIZO B40 was used to inoculate a whey permeate medium. After production EPS was isolated using a sequence of filtration steps [6]. This isolate was freeze-dried and used as such in this study. In a previous study [6] we determined various molecular parameters of B40 EPS. SEC-MALLS analysis of the polysaccharide in aqueous 0.10 M NaNO_3 solutions yielded a number-averaged molar mass of $(1.47 \pm 0.06) \cdot 10^3$ kg/mol. The radius of gyration (number-averaged) was found to be 86 ± 2 nm.

- Aggregated whey protein colloids (AWCs)

Whey protein isolate, produced by Davisco International Inc., USA, was purchased from Domo Food Ingredients, Beilen, The Netherlands. The isolate consisted of β -lactoglobulin (71%), α -lactalbumin (12%), bovine serum albumin (5%) and immunoglobulins (5%). The total amount of proteins in the powder is 93% and it further contains lactose (0.3%), ash (1.8%) and water (5%). The whey proteins (initial concentration was always 100 g/L) were heated for 2 hours at 68.5°C at pH 7.2 (no salt added). Between 30 and 60 minutes all native whey proteins were denatured, as determined by a method described earlier [9].

In order to prevent growth of micro-organisms during the experiments we added 0.02 % (w/w) sodium ethylmercurithiosalicylate ($\text{C}_2\text{H}_5\text{HgSC}_6\text{H}_4\text{COONa}$ - thiomersal, BDH Chemicals) to the mixtures. The protein mixtures containing thiomersal were physically and microbially stable for months.

For the SANS measurements 99.9% D_2O (Sigma) was used to dissolve the whey proteins and EPS. The pD of the D_2O mixtures was 7.1. Verheul and Roefs [41] investigated the heat-induced aggregation of β -lactoglobulin in D_2O compared to that in H_2O , which showed that the denaturation and aggregation mechanism is hardly affected by D_2O . The main effect is that the overall aggregation process is slowed down with D_2O and we have estimated (personal communication with S.P.F.M. Roefs) that 2.5 hours of heating in D_2O should give full denaturation and approximately the same particle size as obtained after heating for 2 hours in H_2O .

- Characterization of the AWC-aggregates

From the SEC-SLS analysis of the aggregates we obtained $R(Q)$ for the various fractions and from equation 2 we determined R_g and M of each fraction. It was found that the aggregates had a number-averaged radius of gyration R_g of 21 ± 2 nm. Since for a homogeneous sphere the radius of gyration is a factor $\sqrt{3/5}$ smaller than the sphere radius, we assume the AWC particles have a radius of 27 ± 3 nm. The (number-averaged) molar mass of the aggregates equals $3.6 \pm 0.1 \cdot 10^3$ kg/mol. By comparing the R_g 's and M 's of the various fractions we obtained $R_g \sim M^{0.33 \pm 0.01}$, which shows that the 'fractal dimension' within an aggregate is 3. The polydispersity expressed as the ratio M_w/M_n , with the weight (M_w) and number-averaged molar mass (M_n), equals 1.28 ± 0.03 .

Using DLS we found the hydrodynamic radius to be 33 ± 3 nm. Within experimental errors, the radii found from SEC-SLS and DLS agree. The radius shall be taken equal to 27 nm in the sequel. Next we measured the size of the aggregates in D_2O by DLS. These were prepared by heating for 2.5 hours at $68.5^\circ C$ in D_2O and we found a radius of 31 ± 3 nm which, within experimental error, is not different from the aggregates prepared in H_2O .

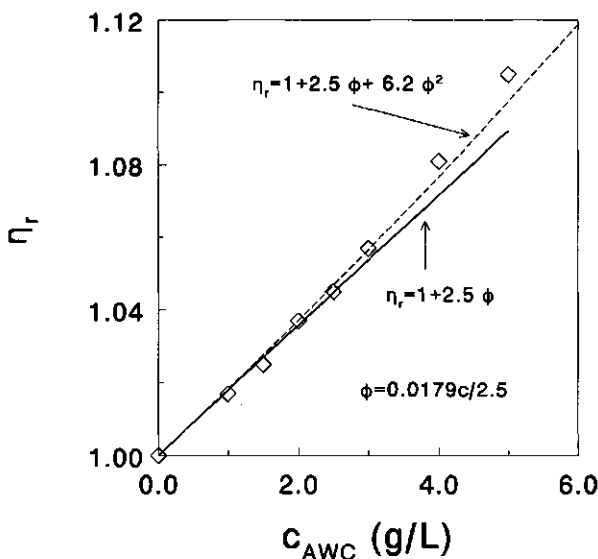


Figure 1 Relative viscosity as a function of the AWC concentration, c_{AWC} . Measurements are given by the data points and the curves represent predictions for hard sphere suspensions.

In Figure 1 we plot the relative viscosity as measured with an Ubbelohde capillary viscometer as a function of the whey protein aggregate concentration in the very dilute regime. For very dilute suspensions of colloidal particles we can use Einstein's expression: $\eta_r = 1 + 2.5\phi$, where η_r is the relative viscosity η/η_s , where η is the solution viscosity and η_s the viscosity of the continuous phase. We find for our data: $\eta_r = 1 + 0.0179c_{AWC}$ and thus $\phi = 0.0179c_{AWC}/2.5$. The voluminosity of the AWCs is therefore 7.2 mL/g. This makes it possible to convert the AWC concentration into a volume fraction. We have also inserted a curve which follows $\eta_r = 1 + 2.5\phi + 6.2\phi^2$ as derived by Batchelor [42], where the quadratic term accounts for two-particle interactions.

- AWC/EPS mixtures

EPS and AWC particles were mixed from stock solutions containing usually 5 g/L EPS and concentrated AWC solution. Sodium nitrate was used as salt and all mixtures were made such that the ionic strength was always set at 0.10 M.

Results and discussion

This results section is divided in three sub-sections. Firstly, the measurement of the depletion induced attractions will be considered, followed by a description of the experimental phase diagram as compared with theory. In the last part we will present measurements which allow an interpretation of the phase separation process.

Attractions

- Small-angle neutron scattering (SANS)

Using SANS we determined the scattered intensities of AWC solutions at three whey protein concentrations: 25, 30 and 40 g/L, respectively. At each AWC concentration we prepared a series of samples with varying EPS concentration. Indicative experimental results for 30 g/L AWC are plotted in Figure 2. The results are given as $I(Q)/I_0(Q)$ as a function of Q . The quantity $I_0(Q)$ refers to the scattered intensity of the whey protein aggregates (without EPS) and $I(Q)$ is the scattered intensity of the mixture of AWCs and EPS. The quantity $I(Q)/I_0(Q)$ has the property that any deviation from unity reflects the change of interactions between the proteins induced by the added EPS. Since ϕ and $P(Q)$ are constants for all measurements, and $I(Q) \sim \phi P(Q)S(Q)$, $I(Q)/I_0(Q)$ equals $S(Q)/S_0(Q)$ (where $S_0(Q)$ is the structure factor of AWC without EPS). From the plots in Figure 2 we observe an increase of

$I(Q)/I_0(Q)$ at small Q 's with increasing EPS concentration which indicates an increase of the structure factor with increasing polymer concentration.

We calculated $S(Q)/S_0(Q)$ from integral theory using the HNC closure (equations 3-5). In order to do this, we need to estimate the pair-interaction potential $U(r)$. Let us first evaluate the polymer segment density profile in the spherical cell model of Schaik and Smit [11]. Since the EPS can be regarded as a flexible polymer with $N_k \approx 150$ Kuhn segments and a Kuhn segment length l_k of 17 nm [6]. In the theory of Schaik and Smit the sphere radius is normalized with the Kuhn length. This means that the whey proteins, with a radius of 27 nm, have a normalized radius R/l_k of 1.6. We calculated the depletion interaction profile in the spherical cell for $\chi=0.50$, which gave (as will be shown later) the best results for the spinodal, for three volume fractions of AWCs. The computed profiles are plotted in Figure 3, where $p^2(r)$ is the segment concentration of polymer at a distance r relative to that at the radius of the spherical cells, R_L .

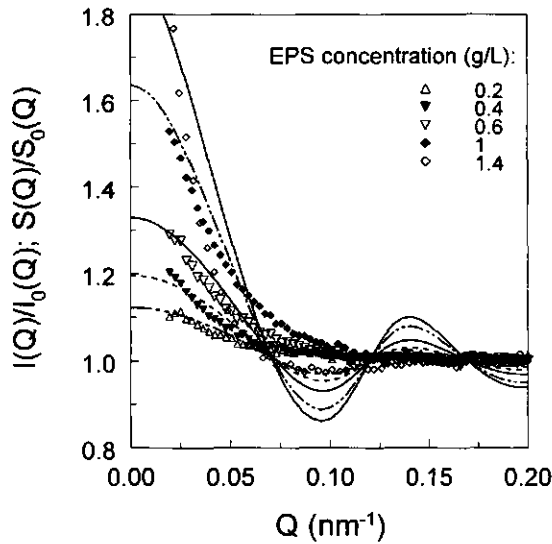


Figure 2 The relative scattered intensity $I(Q)/I_0(Q)$ as measured by SANS for 30 g/L AWC. Results are given for EPS concentrations of 0.2, 0.4, 0.6, 1.0 and 1.4 g/L. The curves are model predictions for the relative structure factor $S(Q)/S_0(Q)$ as obtained from the integral theories for the polymer concentrations corresponding to the experiments.

There is a strong effect of the volume fraction on the segment density profile near the particle surface: a higher volume fraction decreases the depletion layer thickness. From the theory of Schaik and Smit [11] it follows that the radius of the spherical cell R_c decreases with $\phi^{-1/3}$. According to mean-field theory of De Gennes [26] the effective depletion layer thickness δ corresponds to the value of r where $p(r)=\tanh(1)\approx 0.7616$. This expression allowed us to calculate the depletion layer thickness δ ($\approx \sigma_p/2$) from the profiles $p(r)$. For an AWC concentration of 30 g/L ($\phi=0.215$) the calculated depletion layer thickness in terms of δ/l_k is 0.51, corresponding to an effective layer thickness of 8.6 nm. This is much smaller than the radius of gyration (86 nm), which is usually taken as the depletion layer thickness for large spheres and small colloids. Physically it means that for particles which are sufficiently smaller than the polymer molecules the depletion interaction is less effective; the polymer molecule can still assume many conformations when placed near a small sphere.

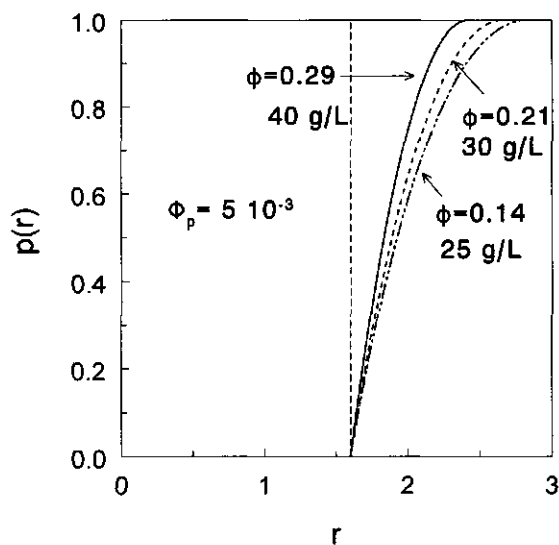


Figure 3 The function $p(r)$ as a function of the radius of the spherical cell for a sphere of $RI_k=1.6$, polymer volume fraction as indicated, and AWC concentrations of 25, 30 and 40 g/L. The corresponding hard sphere volume fraction is given in the plot.

In order to describe the curves in Figure 2 we need an expression for the interaction potential $U(r)$ and subsequently solve equations 3-5. We assume the colloids interact via a hard sphere interaction at contact (steep repulsion). For $r > \sigma_c$ we can not use the expression of Vrij (equation 8) since $2R_g > \sigma_c$. In a simple approximation we assume that $U(r)/k_B T$ is still proportional to c_p and that the shape is still the same. Therefore we propose:

$$\frac{U(r)}{k_B T} = -C_1 \left[1 - \frac{3r}{2(\sigma_c + 2\delta)} + \frac{r^3}{2(\sigma_c + 2\delta)^3} \right] c_p \quad 21$$

where C_1 is an unknown proportionality constant and the range of the attraction is now given by the depletion layer thickness evaluated from the Schaik-Smit theory. For 30 g/L AWC we thus use $\delta = 8.6$ nm. By using $U(r)/k_B T = \infty$ for $r < \sigma_c$, $U(r)/k_B T = 0$ for $r > (\sigma_c + \delta)$ (hard sphere approach) and equation 21 for $\sigma_c < r < (\sigma_c + \delta)$, evaluation of equations 3-5 yields $S(Q)$. We have determined C_1 as follows. Firstly, for each volume fraction of proteins we can calculate c_p at the spinodal from the theory of Schaik and Smit [11]. Secondly, we can calculate for which value of $U(r)/k_B T$ the structure factor at zero wavevector $S(Q=0)$ diverges at the spinodal. Then we have both $U(r)/k_B T$ and c_p at the spinodal, from which C_1 can be calculated using equation 21.

The $S(Q)/S_0(Q)$ values obtained in this way are plotted in Figure 2 for corresponding EPS concentrations and it is shown that theory and experiment give the same quantitative description of the trends at low Q . The increase of $S(Q)/S_0(Q)$ at low Q 's is due to effective attractions and the deviation from unity increases with increasing polymer concentration. It follows that upon increasing the EPS concentration the whey protein aggregates become effectively more attractive, as described by the applied depletion interaction model. At $Q > 0.07$ nm⁻¹ the theoretical curves exhibit oscillations while the experimental results do not. This can be explained by a strong damping of both $I(Q)$ and $I_0(Q)$ due to polydispersity in both the AWC and EPS particle size and the neutron wavelength. The effect of size polydispersity is illustrated in the Appendix.

In Figure 4 we plot the inverse of the measured scattered intensities times the form factor $P(Q)$ as a function of Q^2 in the low Q -range (Ornstein-Zernike plot) for various EPS concentrations and (as a representative) AWC concentrations of 25 g/L. According to equation 1, $S(Q)^{-1}$ is proportional to the inverse of the scattered intensity $R(Q)$ ($\sim I(Q)$) multiplied by $P(Q)$, which was taken as $P(Q) = \exp(-Q^2 R_g^2/3)$, using $R_g = 21$ nm. It is clear from Figure 4 that $P(Q)/I(Q)$ ($\sim S(Q)^{-1}$) depends approximately linearly on Q^2 for $Q^2 < 0.0015$ nm⁻². According to equation 6 in the form $S(Q)^{-1} = A(\xi^{-2} + Q^2)$, the ratio of the intercept and the slope gives ξ^{-2} , hence the correlation length ξ . In this way we calculated ξ values for $c_{\text{AWC}} = 25, 30$ and 40 g/L as a function of the EPS concentration and the results, given as ξ^{-1} as a function of c_p , are plotted in Figure 5. Extrapolation to $\xi^{-1} = 0$ yields the spinodal which was determined from the fit in Figure 5 as 3.9, 3.0 and 2.5 g/L EPS, respectively.

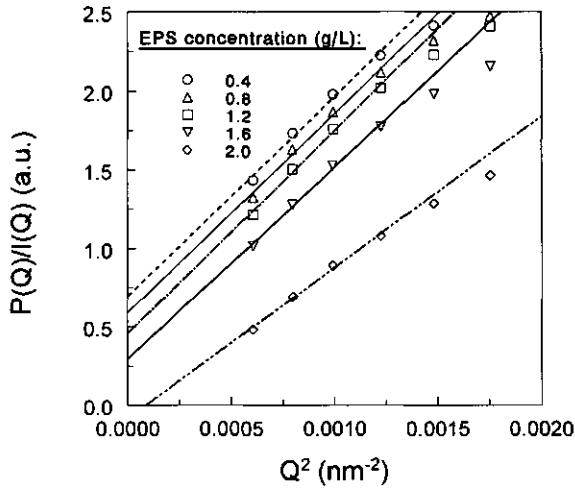


Figure 4 Ornstein-Zernike plots from SANS measurements for 25 g/L AWC at varying EPS concentrations as indicated. The curves are best fits to equation 6 in the range $Q^2 < 0.0015 \text{ nm}^{-2}$.

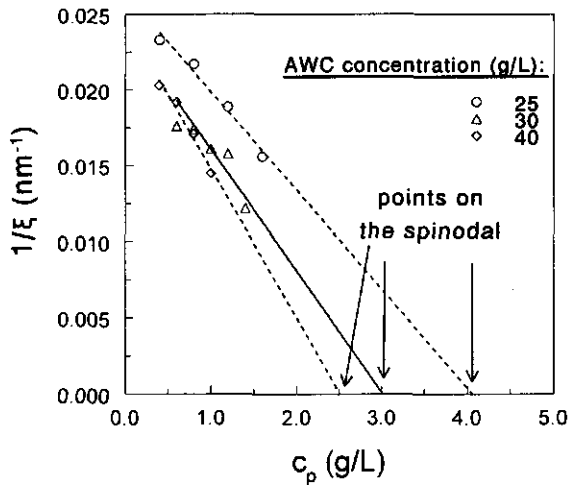


Figure 5 The inverse of the correlation length ξ determined from Ornstein-Zernike plots as a function of the EPS concentration for three AWC concentrations as indicated in the Figure. Drawn curves are linear fits to the data points.

- Dynamic light scattering

We measured the diffusion coefficients of the AWC particles as a function of Q in the range $8 < Q < 30 \mu\text{m}^{-1}$ at various EPS concentrations. Results are presented for 7.5 and 15 g/L AWC in Figures 6 (a) and (b), respectively. Upon increasing the EPS concentration the diffusion coefficient decreases, especially at low Q . Slowing down of collective diffusion is clearly observed. On the spinodal there is no driving force to oppose very small concentration gradients and the collective diffusion coefficient goes to zero at $Q=0$.

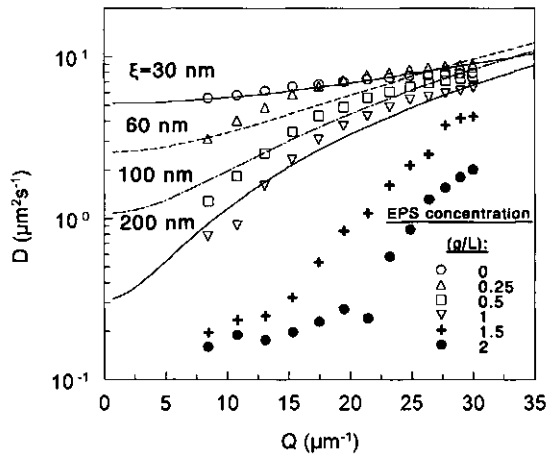


Figure 6 (a) Diffusion coefficients for 7.5 g/L AWC as a function of Q . The various EPS concentrations are indicated in the plots. The curves were calculated from equation 7 and the correlation lengths which give a good description of the data are indicated in the Figures.

Using equation 7 we calculated the effect of increasing the correlation length on $D(Q)$ and we have plotted theoretical curves from the model calculations with fit-parameters Σ and ξ in Figure 6 (a) and (b). The values from the fits for the correlation lengths are given in the plots. The value of Σ decreased weakly with increasing EPS concentration. The results for 1.5 and 2.0 g/L EPS are affected by multiple scattering and could therefore not be fitted to the theoretical prediction of equation 7. The results show that adding EPS increases the correlation length of the AWC particles due to depletion induced attractions as also followed from the SANS results. The qualitative correspondence as presented in Figure 6 (a) and (b) is satisfactory which shows that both equilibrium properties such as $S(Q)$ as well as transport properties are affected by changing the EPS concentration in suspensions of globular proteins.

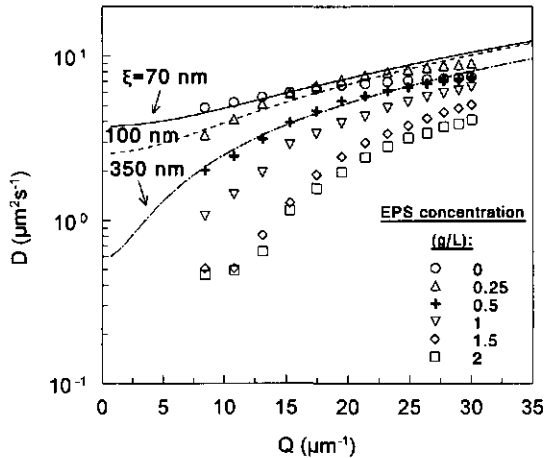


Figure 6 (b) As 6 (a) for 15 g/L AWC.

Above 15 g/L AWC the system became too turbid for a reliable measurement of the diffusion coefficient of AWC particles due to multiple scattering.

Phase diagram

The experimental data given in the preceding section concern mixtures in the one-phase region. Upon increasing either the EPS or the AWC concentration phase separation will occur when the phase boundary is crossed. The observed phase diagram is presented in Figure 7. The full line is drawn to guide the eye. Stable mixtures are indicated by the open circles. In the unstable region various types of coexisting phases can be observed as indicated in Figure 7. Firstly, just above the phase boundary we recognized a two-phase system (filled circles) consisting of an upper phase concentrated in EPS and a lower phase concentrated in AWCs, the latter being viscous when the initial concentration was 30 g/L or higher. The interface was always very sharp. Secondly, sometimes a third phase was formed (triangles) between the two phases mentioned above. This phase was rather turbid and seemed to arise from whey proteins which sediment from the upper phase. Possibly, size fractionation of AWC occurs. Thirdly, the lower phase, containing most of the AWCs is sometimes gel-like (diamonds). This is not surprising since aggregating whey proteins are initially somewhat mutually attractive, which enhances gelation (for very short-ranged attractions).

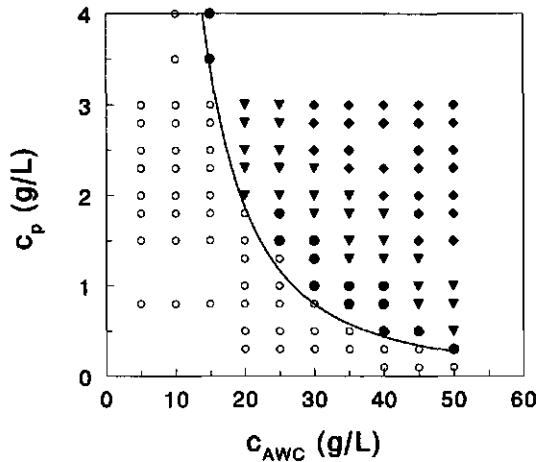


Figure 7 Phase diagram as obtained from visual observation. The polymer concentration is given as a function of the AWC concentration. The drawn line is only a guide to the eye. Open circles refer to stable mixtures. Closed circles are two-phase systems, triangles two-phase systems with a third turbid middle 'phase' and the diamonds refer to three-phase systems where one 'phase' is a gel.

We calculated the total free energy of the mixture F_{tot} , as defined in equation 9, from the Schaink-Smit theory [11] and applied equation 17 for calculating the spinodal. As explained before we used $\sigma_c=3.2$ (corresponding to 54 nm) and $N_K=150$ in the calculations. The results matched best if $\chi=0.5$ was used in the calculations, although the χ -dependence of the spinodal is weak. For lower χ -values (or better solvent quality) the spinodal curve shifts to higher polymer concentrations. The theoretical curve for $\chi=0.5$ is plotted in Figure 8 in terms of the polymer volume fraction ϕ_p and the AWC volume fraction ϕ . In Figure 8 we have replotted the experimental data, as well as the experimental phase line from the phase diagram given in Figure 7. The whey protein concentrations were converted to ϕ values by using $\phi=0.0179c_{AWC}/2.5$. The polymer volume fraction ϕ_p was calculated from c_p/ρ_p , where ρ_p is the segment density and was taken as 1000 kg/m^3 which is a common value for polysaccharides [43]. The shape of the curve as well as the values of the calculated spinodal and the experimental phase boundary (the binodal) correspond satisfactorily.

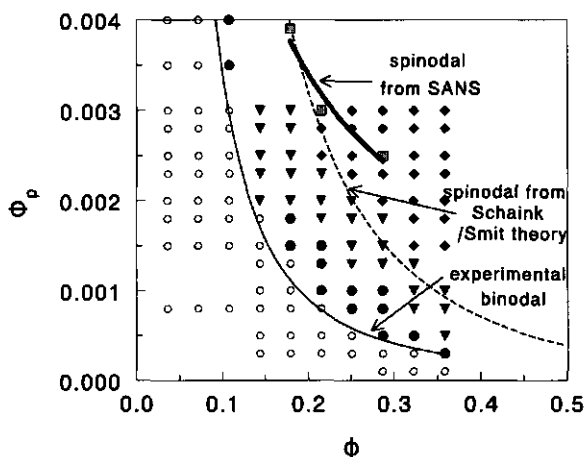


Figure 8 Phase diagram with data points and (full) line to guide the eye as in Figure 7. The symbols ϕ_p and ϕ are the volume fractions of polymer and protein aggregates, respectively. The dotted curve is the prediction from the theory of Schaink and Smit [11] and the full thick line is the spinodal as determined from SANS (gray squares), see Figure 5.

Note that the model of Smit and Schaink [11] was developed for monodisperse polymers and spheres and our EPS and AWC particles are polydisperse, so that no quantitative agreement can be expected, and in particular no critical point can be determined by combining the experimental binodal and the theoretical spinodal.

In Figure 8 we also added the experimentally determined spinodal points from the SANS measurements (gray squares), using the criterion $\xi^{-1}=0$ (see Figure 5). These data are in reasonable correspondence with the curve from the theory of Schaink and Smit which shows that SANS is a good tool to measure attractions and to predict the spinodal from measurements in the one-phase region.

Phase separation kinetics

In the unstable region the mixtures phase separate and the scattered intensity of several of such unstable mixtures was studied by small-angle light scattering (SALS). For several samples (far above the phase line) the transmission was too low to neglect multiple scattering. At very high AWC concentration (>35 g/L) the transmission was also too low to perform accurate measurements for all mixtures. Therefore our attainable experimental range of AWC concentrations is between the phase boundary and 35 g/L.

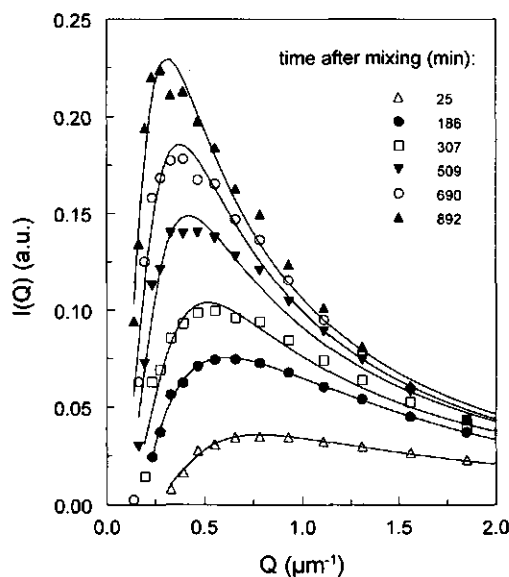


Figure 9 (a) Scattered intensity $I(Q)$ as a function of the wavevector Q measured at various time intervals after mixing EPS and AWC particles. The initial mixture contained 30 g/L AWC and 1.5 g/L EPS. Curves are drawn to guide the eye.

In Figure 9 (a) the time evolution of the scattered intensity as a function of the wavevector is given for a mixture of 30 g/L AWC particles and 1.5 g/L EPS. This system is representative for the evolution of the scattered intensity of the mixtures measured in the unstable region. It is evident that the overall value of the scattered intensity increases in time. All curves go through a maximum in the scattered intensity as a function of Q . The first recorded value of Q_m , the

value of Q where $I(Q)$ goes through a maximum, corresponds to a characteristic length scale (the fastest growing density variation has a typical length scale $\Lambda=2\pi/Q_m$) Λ of $\sim 9 \mu\text{m}$. The large detected sizes agree with the visual observation that unstable mixtures became very turbid. The value of Q_m decreases with time and is independent of time only in the initial stage [17], which stage thus occurs on time scales which are outside our experimental time window. Such a time-dependent behavior as we observe is common to spinodally decomposing systems, such as gelatin/dextran mixtures [44], binary liquid mixtures [45], adhesive hard sphere suspensions [46], polymer mixtures [47], and unstable suspensions of micelles [48].

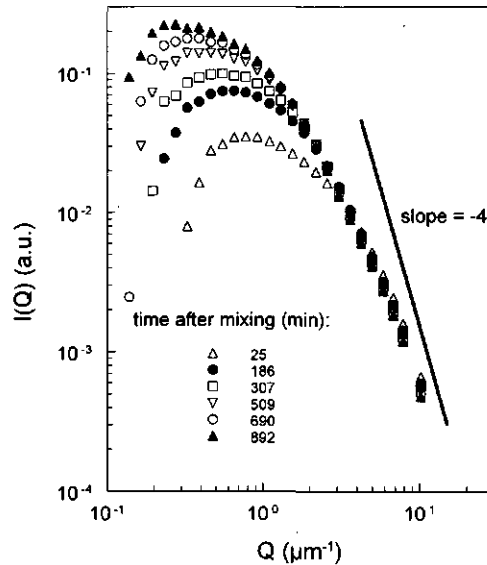


Figure 9 (b) Same results as in Figure 9 (a) but plotted logarithmically and also for the higher Q -range. The straight line corresponds to Porod behavior $I(Q)\sim Q^{-4}$.

In Figure 9 (b) the scattered intensity is plotted as a function of Q on a log-log scale. As can be seen in Figure 9 (b), the slope of $\ln\{I(Q)\}$ versus $\ln\{Q\}$ at large Q -values approaches asymptotically -4 , as expected for sharp interfaces [39]. We are thus not dealing with aggregation, in which case the slope is equal to the fractal dimension of the aggregates, with an expected slope around -2 [32].

From the maximum of the curves plotted in Figure 9 (a) we determined the values of Q_m as a function of time and plotted the characteristic length scale $\Lambda (=2\pi/Q_m)$ in Figure 10 as a function of time. For the mixtures investigated the exponent generally varied between 0.3 and 0.6. Verhaegh *et al.* [49] found, for a spinodal decomposition (SD) of unstable mixtures of silica spheres (coated with stearyl alcohol) and PDMS as polymers, an exponent of $1/3$ in the earlier stages and a crossover to 1 in the late stage. Their results agree with theoretical predictions of Lifshitz and Slyozov [38] ($1/3$) for the early stage and Siggia [37] (1) for the late stage. Our results in Figure 10 seem to agree with these theoretical results.

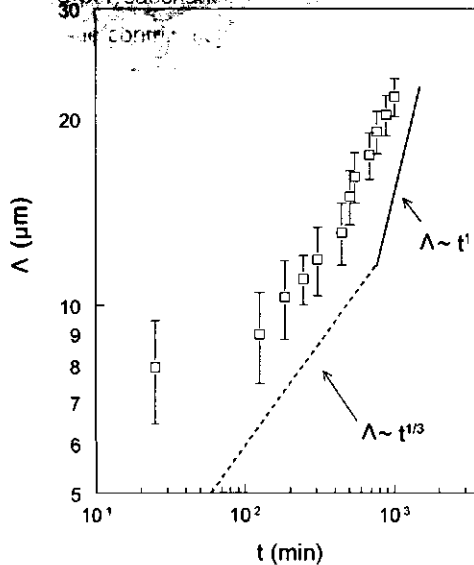


Figure 10 Position of the typical length scale Λ as a function of time after mixing EPS and AWC for the results presented in Figure 9 (a). Drawn curves represent the theoretical scaling relations $\Lambda \sim t^{1/3}$ and $\Lambda \sim t$.

It is known that rescaling the $I(Q)$ versus Q curves leads to a master curve for systems which exhibit SD. In Figure 11 we plot $I(Q)/I(Q_m)$, where $I(Q_m)$ is the maximum scattered intensity, as a function of Q/Q_m and we find that within experimental error the data collapse to a single master curve.

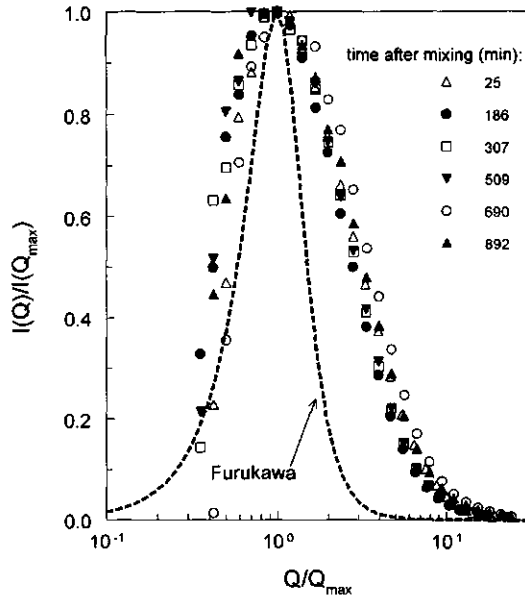


Figure 11 Normalized scattered intensity $I(Q)/I(Q_m)$ as a function of the normalized wavevector Q/Q_m for the results given in Figure 9 (a).

The dotted curve added in Figure 11 is the prediction of Furukawa [36] for off-critical behavior. The Furukawa prediction differs from the experimental data, especially at high Q . The same deviation was found by Rouw *et al.* [46] for an adhesive hard sphere suspension which demixed through SD. The difference might be due to polydispersity which tends to spread out the scattered intensity over a wider Q -range.

Conclusions

Mixing aggregated whey protein colloids (AWCs) with exocellular polysaccharides leads to a segregative interaction. Effective attractions between the protein colloids can be probed by small-angle neutron scattering (SANS) and dynamic light scattering (DLS) experiments. The SANS results could be quantitatively described by a depletion interaction model and the results from DLS could be described qualitatively. Ornstein-Zernike plots allowed a calculation of the correlation length of the AWC particles. From these correlation lengths the spinodal was calculated for three whey protein concentrations; this spinodal lies above the binodal as determined by visual observation, but is within the same order of magnitude.

The spinodal was also calculated from a recently developed mean-field theory. The calculated spinodal and the shape of the curve of the theoretical prediction are consistent with the observed phase diagram. The spinodal as determined from SANS lies in between the experimental binodal and the theoretical prediction for the spinodal.

Small-angle light scattering experiments were performed to detect the temporal evolution of the scattered intensity of mixtures in the unstable region. The results showed that the phase separation can be described as a spinodal decomposition on the basis of scaling arguments.

Appendix

The calculated curves in Figure 2 give a good description of the experimental data in the low Q range, but for higher values of ($Q > 0.07 \text{ nm}^{-1}$) the theoretical predictions exhibit oscillations around unity whereas the experimental data converge to unity without showing oscillations. This difference is due to polydispersity in size of the AWC particles, the EPSs and polydispersity in neutron wavelength. It is beyond the scope of this study to extend the theory in order to account for polydispersity in size of the particles and of the neutron wavelength. However, use can be made of the model developed by Robertus *et al.* [50] for scattering of polydisperse adhesive hard spheres. In Figure A1 we plot the calculated results for $S(Q)/S_0(Q)$ for a suspension with monodisperse colloids with a volume fraction of 0.2.

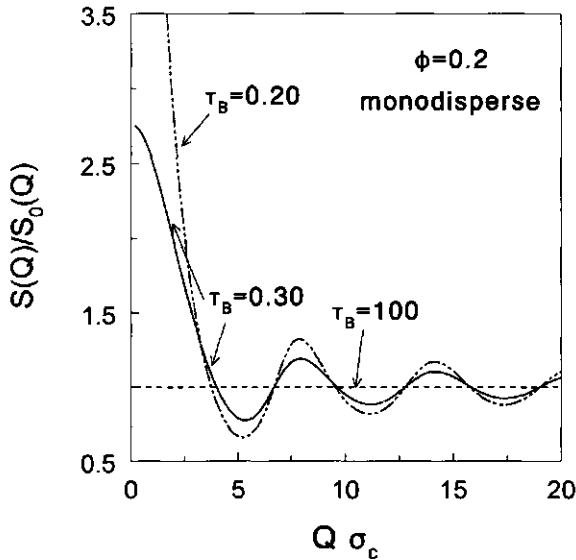


Figure A1 The relative structure factor $S(Q)/S_0(Q)$ as a function of $Q\sigma_c$ for monodisperse adhesive hard spheres with varying stickiness.

Here $S(Q)$ is the structure factor of an adhesive hard sphere suspension with a certain adhesiveness, expressed by the Baxter parameter τ_B [51,52] and $S_0(Q)$ is the structure factor of a hard sphere suspension. The results are given for three values of the Baxter parameter: $\tau_B=100, 0.30$ and 0.20 , corresponding to an increasing effective attraction. The oscillations are clearly visible over the plotted Q -range. In Figure A2 the results are plotted for colloidal particles which have a dispersion in size according to a Schulz-Flory distribution with a standard deviation of 20% for the same volume fraction and adhesiveness as in Figure A1. Although at low Q (below $Q\sigma_c \approx 5$) the results are almost identical, at higher Q the oscillations in the relative structure factor $S(Q)/S_0(Q)$ have dampened strongly which illustrates that the difference between experiment and theory at high Q is probably due to polydispersity.

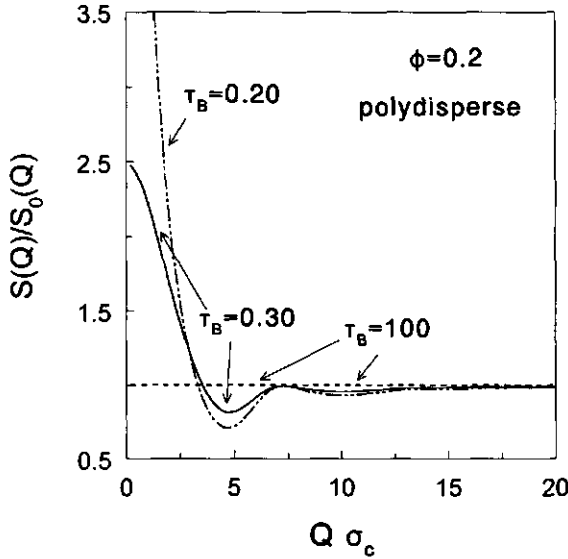


Figure A2 As Figure A1 for particles with a Schulz-Flory size distribution with a standard deviation of 20%.

Acknowledgment

Dominique Ginapé and Alexandra Le Roy are thanked for performing many experiments. Jan van Riel, NIZO food research, is thanked for performing the SEC-MALLS measurements. The help of and discussions with Dr. C. Holt (Hannah research institute, UK) and Dr. P.A. Timmins (ILL, Grenoble, France) concerning the SANS experiments are highly appreciated. Dr. H.M. Schalk, University of Twente, Rheology Group, is thanked for useful discussions and providing us his computer program which made possible the mean-field calculations. We thank Drs P. van der Schoot (Van't Hoff laboratory, Utrecht University), P.J.J.M. van Mil, S.P.F.M. Roefs, E. ten Grotenhuis, and R.H. Tromp (NIZO food research) for useful discussions.

References

- [1] Cerning, J., *FEMS Microbiol. Rev.*, **87** (1990) 113.
- [2] Abbad Andaloussi, S., Talbaoui, H., Marczak, R., Banally, R., *Appl. Microbiol. Biotechnol.* **43** (1995) 995.
- [3] Marle, M.E. van, PhD thesis Twente University, The Netherlands, 1998.
- [4] Grinberg, V.Ya., Tolstoguzov, V.B., *Food Hydrocoll.* **11** (1997) 145.
- [5] Tuinier, R., ten Grotenhuis, E., Holt, C., Timmins, P.A., de Kruif, C.G., *Phys. Rev. E*, in press; Chapter 6.
- [6] Tuinier, R., Zoon, P., Olieman, C., Cohen Stuart, M.,A., Fler, G.J., de Kruif, C.G., *Biopolymers* **49** (1999) 1; Chapter 2 of this thesis.
- [7] Jenkins, P., Snowden, M., *Adv. Colloid Interface Sci.* **68** (1996) 57.
- [8] Fox, P.F., In: 'Developments in Dairy Chemistry, 4. Functional Milk Proteins,' Fox, P.F. Ed., Elsevier Publ. London, 1989.
- [9] Hoffmann, M.A.M., Roefs, S.P.F.M., Verheul, M., Van Mil, P.J.J.M., De Kruif, C.G., *J. Dairy Res.* **63** (1996) 423.
- [10] Smit, J.A.M., Schaink, H.M., *Ind. Proteins* **2** (1995) 8.
- [11] Schaink, H.M., Smit, J.A.M., *J. Chem. Phys.*, **107** (1997) 1004.
- [12] Kerker, M., 'Scattering of light and other electromagnetic radiation,' Academic Press, New York, 1969.
- [13] McQuarrie, D.A., 'Statistical Mechanics,' Harper & Row, New York, 1976.
- [14] Ornstein, L.S., Zernike, F., *Proc. Acad. Sci.*, **17** (1914) 793.
- [15] van Leeuwen, J.M.J., Groeneveld, J., de Boer, J., *Physica* **25** (1959) 792.
- [16] Gillan, M.J., *Mol. Phys.*, **38** (1979) 1781.
- [17] Dhont, J.K.G., 'An Introduction to Dynamics of Colloids,' Elsevier Science, Amsterdam, 1996.
- [18] Kawasaki, K., *Ann. Phys.* **61** (1970) 1.
- [19] Asakura, S., Oosawa, F., *J. Chem. Phys.* **22** (1954) 1255.
- [20] Vrij, A., *Pure & Appl. Chem.*, **48** (1976) 471.
- [21] Lekkerkerker, H.N.W., Poon, W.C.K., Pusey, P.N., Stroobants, A., Warren, P.B., *Europhys. Lett.* **20** (1992) 559.
- [22] Lekkerkerker, H.N.W., *Colloids Surf.* **51** (1990) 419.
- [23] Meijer, E.J., Frenkel, D., *Phys. Rev. Lett.*, **67** (1991) 1110.
- [24] Carnahan, N.F., Starling, K.E. *J. Chem. Phys.*, **53** (1970) 600.
- [25] Grosberg, A.Y., Khoklov, A.R., 'Statistical Mechanics of Macromolecules,' AIP, New York, 1994.
- [26] De Gennes, P.G., 'Scaling Concepts in Polymer Physics,' Cornell University Press, Ithaca, 1979.
- [27] Flory, P.J., 'Principles of Polymer Chemistry,' Cornell University Press, New York, 1953.

- [28] Press, W.H., Flannery, S.A., Teukolsky, S.A., Vetterling, W.T., 'Numerical Recipes,' Cambridge University Press, Cambridge, 1987.
- [29] Ramirez-Santiago, G., González, A.E., *Physica A* **236** (1997) 75.
- [30] Poon, W.C.K., Haw, M.D., *Adv. Colloid Interface Sci.* **73** (1997) 71.
- [31] Carpineti, M., Giglio, M., *Phys. Rev. Lett.*, **68** (1992) 3327.
- [32] Jullien, R., Kolb, M., Botet, R., *J. Physique Lett.*, **51** (1984) 211.
- [33] Weitz, D.A., Oliveira, M., *Phys. Rev. Lett.*, **52** (1984) 1433.
- [34] Teixeira, *J. Appl. Cryst.*, **21** (1988) 781.
- [35] Cahn, J.W., Hilliard, J.E., *J. Chem. Phys.* **28** (1958) 258; *J. Chem. Phys.* **31** (1959) 688.
- [36] Furukawa, H., *Physica A*, **123** (1984) 497.
- [37] Siggia, E.D., *Phys. Rev. A*, **20** (1979) 595.
- [38] Lifshitz, I., Slyuzov, V.V., *J. Phys. Chem. Solids* **19** (1961) 35.
- [39] Porod, G., in: 'Small-Angle X-ray Scattering,' Glatter, O., Kratky, O., (Eds.) Academic Press, London, 1982.
- [40] Hoffmann, M.A.M., Sala, G., Olieman, C., De Kruijff, C.G., *J. Agric. Food Chem.* **45** (1997) 2949.
- [41] Verheul, M., Roefs, S.P.F.M., *FEBS Letters*, **421** (1998) 273.
- [42] Batchelor, *J. Fluid Mech.*, **52** (1972) 245.
- [43] Brandrup, J., Immergut, E.H., 'Polymer Handbook,' Wiley, 1989.
- [44] Tromp, R.H., Rennie, A.R., Jones, R.A.L., *Macromolecules*, **28** (1995) 4129.
- [45] Huang, J.S., Goldberg, W.I., Bjerkaas, A.W., *Phys. Rev. Lett.* **32** (1974) 921.
- [46] Rouw, P., Woutersen, A.T.J.M., Ackerson, B.J., De Kruijff, C.G., *Physica A*, **156** (1989) 876.
- [47] Bates, F.S., Wiltzius, P., *J. Chem. Phys.* **91** (1989) 3258.
- [48] Wilcoxon, J.P., Martin, J.E., Odinek, J., *J. Non-Cryst. Solids* **172** (1994) 1142.
- [49] Verhaegh, N.A.M., van Duijneveldt, J.S., Dhont, J.K.G., Lekkerkerker, H.N.W., *J. Chem. Phys.* **102** (1996) 409.
- [50] Robertus, C., Philipse J., Joosten, J.G.H., Levine, Y.K., *J. Chem. Phys.* **90** (1989) 4482.
- [51] Baxter, R.J., *J. Chem. Phys.* **49** (1968) 2770.
- [52] Penders, M.H.G.M., Vrij, A., *J. Chem. Phys.*, **93** (1990) 3704.

6

Depletion interaction of casein micelles and an exocellular polysaccharide

Abstract

Casein micelles become mutually attractive when an exocellular polysaccharide produced by *Lactococcus lactis* subsp. *cremoris* NIZO B40 (hereafter called EPS) is added to skim milk. The attraction can be explained as a depletion interaction between the casein micelles induced by the non-adsorbing EPS. We used three scattering techniques (small-angle neutron scattering, turbidity measurements and dynamic light scattering) to measure the attraction. In order to connect the theory of depletion interaction with experiment we calculated structure factors of hard spheres interacting by a depletion pair potential. Theoretical predictions and all the experiments showed that casein micelles became more attractive upon increasing the EPS concentration.

Introduction

There is a significant interest in the production of exocellular polysaccharides (EPSs) by food grade micro-organisms [1]. A familiar example is the *'in-situ'* production of EPSs by lactic acid bacteria in products such as yogurt and viilli [2]. The EPS seems to influence the rheological properties of these products and is responsible for the thread-like pouring behavior which is also referred to as 'long behavior' (see van Marle [3]).

Much attention has been given to the analysis of the chemical structure of the monomeric units of EPSs [4-6]. Previously, we characterized various properties of an EPS produced by *Lactococcus lactis* subsp. *cremoris* strain NIZO B40 [7]. This EPS has a number-averaged molar mass (M_n) of $1.47 \cdot 10^6$ g/mol, a number-averaged radius of gyration of 86 nm [7] and a polydispersity index M_w/M_n of 1.13; here M_w is the weight-averaged molar mass. This polysaccharide has interesting thickening capacities in comparison with other polysaccharides and is a common ingredient of 'health foods'.

In a dairy product like yogurt containing both polysaccharides and proteins, both biopolymers contribute to the structural and textural properties of food products by their thickening properties, gel formation and water-binding capacity. When there are significant interactions between polysaccharide and protein the ternary mixture is not ideal [8].

Therefore we have studied the effect of added EPS on the physical properties of a (model) dairy product. As a model system we chose low-heat skim milk, prepared from reconstituted skim milk powder, since this protein dispersion is simpler than commercial dairy products. From a colloid physics point of view skim milk can be considered as a dispersion of casein micelles (about 100 nm radius and a volume fraction $\phi \approx 0.1$) in a continuous phase containing water, salts, lactose and small (< 5 nm) globular proteins. Previous work has shown that casein micelles in such a system behave effectively as hard spheres [9].

From previous work [8,10,11] it follows that incompatibility is a general phenomenon in protein-polysaccharide solutions. This originates from the fact that saccharide-amino acid contacts are usually energetically unfavorable compared with the interaction with the solvent [8]. A repulsive polysaccharide-protein interaction leads to an attractive interaction between the globular proteins commonly referred to as depletion interaction. In the case of protein particles, such as casein micelles in milk, a depletion layer is present when a polysaccharide does not adsorb onto the casein micelle. The physics of depletion interactions can be understood as follows. On mixing colloidal particles with swollen polymer molecules, the centers of mass of these molecules are excluded from a zone of liquid adjacent to the surface of the rigid object. This zone has a thickness equal to an average effective radius of the polymer molecule. In the depletion layer the osmotic pressure (Π_p) due to the polymer is

smaller than in the bulk due to a lower polymer segment concentration in that layer. Brownian motion of the casein micelles occasionally causes overlap of two depletion layers. This overlap volume (V_{overlap}) of two depleted layers increases the bulk volume available to the polymer and thereby decreases the free energy of the system by an amount $\Pi_p \cdot V_{\text{overlap}}$. The result is that the colloidal particles tend to stick together. One may say they are pushed together by the unbalanced osmotic pressure difference. Asakura and Oosawa [12] were the first to describe the origin of the depletion interaction between colloidal particles and non-adsorbing polymers. They pointed out that the attractive force between the particles is proportional to the osmotic pressure of the polymer solution.

Upon increasing the attraction between the particles, a phase separation into a colloidal gas and a colloidal liquid phase may occur [13,14]. Making colloidal particles attractive does not only change the phase behavior but also affects transport properties such as diffusion, sedimentation and rheology of the suspension [15].

We have used various scattering methods in order to determine the strength of the attractions between the casein micelles in the presence of EPS. In the following section we first discuss theoretical approaches which were used to interpret the experimental results. The materials and experimental techniques used are explained subsequently followed by the results and discussion.

Theory

Depletion interaction theory

Vrij [16] developed a theory which allows a calculation of the attractive potential between two hard spheres as induced by the presence of non-adsorbing polymer molecules. The polymer molecules, with an effective diameter σ_p (twice the depletion layer thickness Δ) are mutually freely permeable (θ -solvent) but are hard spheres for the colloids. The approach of Vrij is only valid for polymer molecules which are smaller than the colloidal spheres since it is tacitly assumed that the center of mass of a polymer molecule will not approach a sphere to a distance smaller than Δ in order to avoid a loss of conformational entropy. For polymer molecules that are much larger than the colloidal spheres there is still an entropy loss but this is substantially lower than that predicted by the Vrij theory. The theory is thus only valid for relatively large spheres. Vrij [16] assumed that the attractive interparticle potential between two spherical colloidal particles with diameter σ_c , which behave as hard spheres towards one another, equals $-\Pi_p V_{\text{overlap}}$. In the range $\sigma_c < r < (\sigma_c + \sigma_p)$ the interaction potential then equals:

$$U(r) = -\frac{1}{6} \pi (\sigma_c + \sigma_p)^3 \left[1 - \frac{3r}{2(\sigma_c + \sigma_p)} + \frac{r^3}{2(\sigma_c + \sigma_p)^3} \right] \frac{c_p RT}{M} \quad 1$$

where r is the distance between the centers of the colloidal spheres and $c_p RT/M$ represents the ideal osmotic pressure Π_p of a polymer solution with concentration c_p .

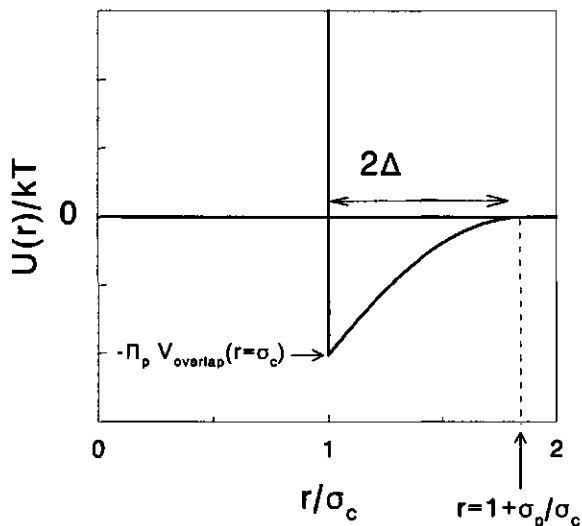


Figure 1 (a) Interaction potential profile for depletion interaction following Vrij's theory (equation 1).

We denote the minimum of the interaction potential at $r=\sigma_c$, $U(\sigma_c)$, as U_0 , which can be expressed as:

$$U_0 = -\frac{1}{6} \pi (\sigma_c + \sigma_p)^3 \left[1 - \frac{3}{2(1+\zeta)} + \frac{1}{2(1+\zeta)^3} \right] \frac{c_p RT}{M} \quad 2$$

where $\zeta = \sigma_p/\sigma_c$. The radius of gyration of the polymer molecules R_g is a good measure for the depletion layer thickness $\Delta (= \sigma_p/2)$. The depletion interaction potential $U(r) = -\Pi_p V_{\text{overlap}}(r)$ is schematically drawn in Figure 1 (a) for $\zeta=0.86$ as in the present study.

Adhesive hard sphere model

When EPS is added to skim milk the casein micelles experience an effective attraction. A simple approach then is to use the adhesive hard sphere (AHS) model as introduced by Baxter [17]. Although this approach is less elegant than the Vrij theory, we will introduce it in order to study transport properties. In that way we can make a connection between dynamic light scattering (DLS) experiments and the attraction between colloidal particles, as will be shown.

For attractive spheres, Baxter [17] introduced for mathematical reasons a square well potential with an infinitely narrow width ($\lim \delta \rightarrow 0$, where δ is the range of the attraction) which is described in the following equation:

$$\frac{U(r)}{k_B T} = \begin{matrix} +\infty & 0 < r < \sigma_c, \\ \ln[12\tau_B\delta / (\sigma_c + \delta)] & \sigma_c \leq r \leq (\sigma_c + \delta), \\ 0 & r > (\sigma_c + \delta), \end{matrix} \quad 3$$

where τ_B is the Baxter parameter, which is allowed to take values $0 < \tau_B < \infty$ and the inverse of τ_B reflects the strength of the attractive force (adhesiveness) between the spheres. The product $\tau_B\delta$ remains finite. A sketch of the AHS interaction potential is given in Figure 1 (b).

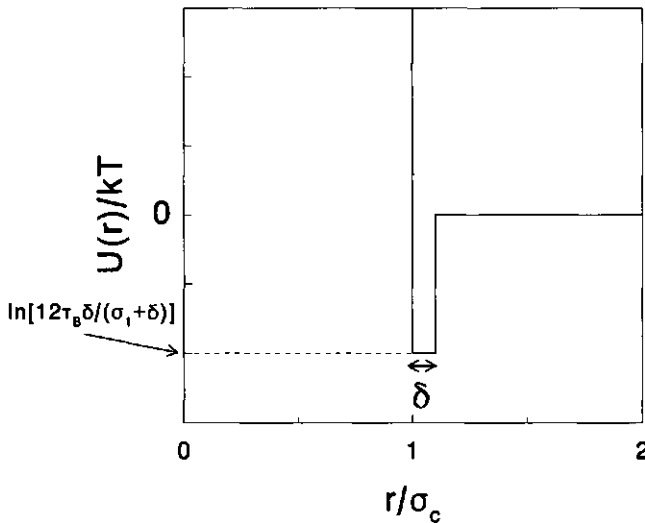


Figure 1 (b) Interaction potential for the adhesive hard sphere model (AHS) according to equation 3.

It should be remarked here that the attractive potential induced by the EPS is certainly not short-range. The range of the potential, its width, is of the order of the radius of gyration of EPS. Nevertheless we apply the Baxter model since it provides a simple theoretical framework which allows us to relate interaction strength to dynamic light scattering. In experimental techniques like osmotic pressure and scattering measurements one measures the second virial coefficient B_2 . In fact B_2 is simply related to τ_B by [18]:

$$B_2 = 4 - \frac{1}{\tau_B} \quad 4$$

Hence, the Baxter parameter can easily be obtained via B_2 and it has been shown that the Baxter parameter τ_B can be determined experimentally by dynamic light scattering [15] as will be discussed in the next section.

Scattering techniques

- Dynamic light scattering (DLS)

With this technique the short-time self-diffusion coefficients can be measured, in our case of casein micelles as a function of the EPS concentration. Self-diffusion is related to the dynamics of a single particle in a system with a homogeneous density. In dilute colloidal suspensions containing spherical particles, the hydrodynamic radius of the diffusing sphere a_H can be calculated from the short time self-diffusion coefficient D_s through the Stokes-Einstein equation:

$$D_s = \frac{k_B T}{6\pi\eta_s a_H} \quad 5$$

where η_s is the solvent viscosity. The parameter D_s depends on the particle volume fraction ϕ :

$$\frac{D_s}{D_0} = 1 - k_1\phi \quad 6$$

Here D_0 is the diffusion coefficient at infinite dilution and k_1 has a positive value. For a suspension of colloidal hard spheres Batchelor [19] and Felderhof [20] calculated the coefficient k_1 assuming that the diffusing particle is surrounded by non-adhesive Brownian hard spheres with fixed positions. They found $k_1=1.832$ [20]. When the particles become adhesive, the probability of two particles being near one another is larger than for hard spheres, which leads to a stronger hydrodynamic interaction and friction. The equivalent Stokes radius appears to be increased. Cichocki and Felderhof [21] extended the equations of motions of Felderhof [20] to those for adhesive spheres and their result for the diffusion coefficient is:

$$\frac{D_s}{D_0} = 1 - \left(1.832 + \frac{0.295}{\tau_B}\right)\phi \quad 7$$

which shows that D_s decreases with increasing adhesiveness (τ_B becoming smaller). By measuring D_s , equation 7 allows a calculation of τ_B for adhesive hard spheres. In a colloidal suspension of skim milk with casein micelles Π_p is larger at higher EPS concentration. This means that at higher EPS concentration the adhesiveness increases when the concentration of non-adsorbing EPS increases.

- Small-angle neutron scattering (SANS)

Neutrons can be regarded as electromagnetic waves and therefore neutron scattering is described here by the Rayleigh-Gans-Debye theory [22]. In a small-angle neutron scattering (SANS) experiment the normalized scattering intensity is then given by the Rayleigh ratio $R(Q)$, which depends on the wave vector Q which is defined as $4\pi n \sin(\theta/2)/\lambda_0$, where n is the refractive index, θ is the angle at which the scattered intensity is detected and λ_0 is the wavelength in vacuo. For homodisperse sols $R(Q)$ is related to the structure factor $S(Q)$ and the scattering particle form factor $P(Q)$ by [22]:

$$R(Q) = K c M P(Q) S(Q) \quad 8$$

where c represents the particle concentration, M the molar mass of the particle and K is a material constant which for SANS depends on the difference between the scattering length densities of particle and solvent. For colloidal spheres, the scattering form factor reads:

$$P(Q) = \left\{ 3 \left(\frac{\sin(Qa) - Qa \cos(Qa)}{(Qa)^3} \right) \right\}^2 \quad 9$$

with the sphere radius $a = \sigma_p/2$.

Upon adding non-adsorbing but 'invisible', i.e. with negligible contribution to the scattering, polymer molecules to a colloidal suspension, the scattering intensity will change. This originates from the fact that the structure of a colloidal suspension, which is measured via $S(Q)$, is strongly affected by the interactions between colloidal particles.

In the limit $Q=0$, the structure factor is related to the isothermal osmotic compressibility $\partial\rho/\partial\Pi_c$ by:

$$S(Q=0) = k_B T \frac{\partial\rho}{\partial\Pi_c} \quad 10$$

Here $\rho (=6\phi/\pi\sigma_c)$ is the number density and Π_c is the osmotic pressure of the colloidal particles. For attractive particles $\partial\Pi_c/\partial\rho$ is smaller than for hard spheres and when $\partial\Pi_c/\partial\rho < 0$ the system

spontaneously phase separates. At the spinodal the compressibility is infinite, the system shows critical opalescence, and $S^{-1}(Q=0) = 0$. This illustrates that $S(Q)$ is indicative of the stability of colloidal suspensions. Physically, this can be understood since $S(Q)$ is the Fourier transform of the radial distribution function $g(r)$ of the particles:

$$S(Q) = 1 + 4\pi\rho \int_0^{\infty} r^2 (g(r) - 1) \frac{\sin(Qr)}{Qr} dr \quad 11$$

where r is the distance from the center of a probe particle to the center of any random particle. The radial distribution function $g(r)$ reflects the probability of finding a particle at a distance r from the center of another particle. It is obvious that $g(r)$ changes when either the particle concentration or the particle interactions are changed. The radial distribution function is expressed in direct and indirect contributions by the Ornstein-Zernike equation (OZE) [18,23]:

$$h(r) = c(r) + \rho \int c(r_{13}) h(r_{23}) dr_3 \quad 12$$

where $c(r)$ is the direct correlation function and $h(r) = g(r) - 1$ the total correlation function. The total correlation function is the sum of the direct correlation of particle 1 with particle 2 and an indirect correlation between 1 on 2 in which all other particles are involved. The total and direct correlation functions can be calculated if an appropriate closure relation is used.

For adhesive hard spheres, interacting via a Baxter potential, Menon *et al.* [24] solved the Ornstein-Zernike relation using the Percus-Yevick closure [25]. The $S(Q)$ obtained from the model of Menon *et al.* [24] closely matches the results of Kranendonk and Frenkel [26] who used computer simulations to calculate $S(Q)$ s of suspensions containing adhesive hard spheres.

We are interested in expressions for $S(Q)$ for colloidal suspensions with added non-adsorbing polymer. For any interaction potential Gillan [27] developed a solution procedure of the OZE with the hypernetted chain (HNC) closure [18,28,29] defined by:

$$c(r) = h(r) - \ln(g(r) - U(r)/k_B T) \quad 13$$

Gillan's method combines the Picard method and the Newton-Raphson technique [27]. We apply the interaction potential profile suggested by Vrij [16] to equations 12 and 13 and calculate $S(Q)$.

- Turbidity measurement

The turbidity (τ) reflects the attenuation of a light beam by scattering when it passes through a sample. It is related to the transmission t by the Lambert-Beer relation:

$$\tau = \frac{1}{b} \ln \left[\frac{1}{t} \right] \quad 14$$

where b is the path length through the sample. If absorption of radiation can be neglected, so that all the reduction of the measured transmission is caused by scattering, a simple conservation law relates scattering and turbidity:

$$\tau(\lambda_0) = 2\pi \int_0^\pi R(Q) \sin(\theta) d\theta \quad 15$$

or upon substituting equation 8 and $Q=4\pi n \sin(\theta/2)/\lambda_0$:

$$\tau(\lambda_0) = 8\pi K c M \int_0^{4\pi n/\lambda_0} P(Q) S(Q) \left\{ 1 + \left(1 - 2Q^2 \left(\frac{\lambda_0}{4\pi n} \right)^2 \right)^2 \right\} Q \left(\frac{\lambda_0}{4\pi n} \right)^2 dQ \quad 16$$

Since we can calculate $S(Q)$ as shown in the previous section and take equation 9 for $P(Q)$ we can calculate the turbidity from equation 16.

Experimental methods

Material

EPS was produced on a pilot-plant scale at NIZO [7]. A *Lactococcus lactis* subsp. *cremoris* NIZO B40 was used to inoculate a whey permeate medium. After production EPS was isolated using various filtration steps [7]. This isolate was freeze-dried and used as such in this study.

Reconstituted skim milk was prepared by mixing 10.45 grams of skim milk powder in 100 grams of demineralized water at 40°C. The suspension was stirred and kept at this temperature for 45 minutes. Afterwards, the milk was centrifuged at 10⁴ r.p.m for 20 minutes in order to remove the small amount of undissolved milk powder left in the solution. Measurements of the relative viscosity as a function of the casein micelle concentration by Jeurnink and De Kruif [30] showed that casein micelles can be considered as hard spheres and have a volume fraction of 0.130 in (low-heat) skim milk. Skim milk permeate (i.e. the 'solvent' of the casein micelles) was prepared from skim milk by a membrane filtration process. An Amicon hollow-cartridge HIMPO 1-43 membrane with a cut-off of 0.1 μm was used. The pH of the permeate was the same as that of the skim milk (6.60 ± 0.10). The mixtures were prepared by dissolving EPS in permeate and mixing this EPS-skim milk permeate solution with skim milk. All mixtures were studied at 298 K.

For the SANS measurements 99.9% D₂O (Sigma) was used to dissolve skim milk powder and EPS. The 'pH', as measured with a pH meter, of the D₂O mixtures was 6.75. D₂O skim milk permeate was prepared from the D₂O milk by ultracentrifugation.

In order to prevent growth of micro-organisms during the experiments we added 0.02 % (w/w) sodium ethylmercurithiosalicylate (C₂H₅HgSC₆H₄COONa - thiomersal, BDH Chemicals) to the mixtures which prevented any bacterial growth and subsequent pH changes. In the absence of EPS, skim milk and permeate containing thiomersal were stable for months.

Scattering techniques

- Dynamic Light Scattering (DLS)

Dynamic light scattering experiments were performed to determine the diffusion coefficients of the casein micelles with Malvern Hi-C particle size analysis equipment, which operates in a back-scattering mode. Under these conditions the scattering vector has its maximum value at the given wavelength. At this Q-value $Q\sigma_c \gg 1$ which means that self-diffusion will dominate collective diffusion for our set-up. Measurements were made at 298 K.

- Small-Angle Neutron Scattering (SANS)

The SANS experiments were performed by using cold thermal neutrons emitted from the core of the high-flux nuclear reactor at the Institute Max Von Laue- Paul Langevin in Grenoble (France) using the D-11 spectrometer, as described by Ibel [31]. Hellma QS quartz cells were used with a sample path length of 2 mm. For this small path length multiple scattering is negligible at a volume fraction of 0.12 as studied. All samples were mixed thoroughly before measuring. For casein micelles, the S(Q) peak, as calculated for a diameter of 200 nm, lies around $Q=0.031 \text{ nm}^{-1}$. Therefore, we performed measurements in the Q-range $0.01 < Q < 0.08 \text{ nm}^{-1}$. In order to obtain the desired Q-range, a sample-detector distance of 35.7 m was chosen. The mean wavelength of the emitted neutrons was 1.0 nm with a width at half height of 9%.

- Turbidity measurement

The experiments were made with a Hitachi (model U-1100) single beam spectrophotometer and the samples were measured in quartz glass cuvettes (Hellma, type 110 QS). Cuvettes with a path length of 2 mm were chosen to enable accurate measurement of the transmission. The light source of the spectrophotometer produces a wide range of radiation. The required wavelength can be selected by a prism or grating monochromator. The beam is split, and the beams are led to the sample cell and the

reference cell (containing only permeate), respectively. The transmissions were measured by recording the intensities of sample (skim milk with or without EPS) and permeate. To eliminate the effect of aggregated particles which may blur the results, the mixtures were filtered (pore size 5 μm) before use.

Results and discussion

Self-diffusion

The diffusion coefficient of the casein micelles in milk and several solutions of milk diluted with permeate was measured in order to check whether the casein micelles behave as hard spheres. In Figure 2 the self-diffusion coefficient (D_s) is shown as a function of the volume fraction of the casein micelles in permeate. This self-diffusion coefficient depends linearly on the volume fraction. By extrapolation to $\phi=0$, a value of $2.09 \cdot 10^{-12} \text{ m}^2 \cdot \text{s}^{-1}$ was found for D_0 . According to equation 5 this gives a hydrodynamic radius (a z-average) of the casein micelles of 117 nm which is consistent with literature values [32,33] and with the distribution of casein micelles in skim milk from which a number-averaged radius of 100 nm follows [34]. The volume fraction dependence in permeate can be described with equation 6, with $k_1=2.0$, which is in reasonable agreement with the theoretical value of 1.83 for hard spheres.

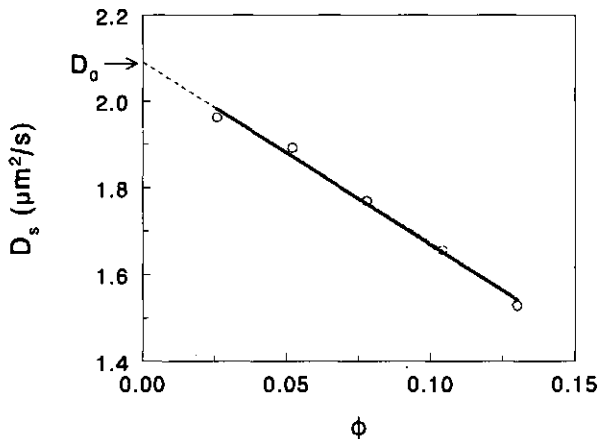


Figure 2 The self-diffusion coefficient of casein micelles as a function of their volume fraction.

The self-diffusion of the casein micelles was measured as a function of the EPS concentration. For $\phi=0.11$ a representative result is plotted in Figure 3. The plotted curve was calculated from equation 7, using the following expression for the Baxter parameter τ_B :

$$\tau_B = \frac{\delta + \sigma_c}{12\delta} \exp\left(-\frac{V_{\text{overlap}}^{\text{av}} c_p}{m}\right) \quad 17$$

where $m = M/N_{\text{AV}}$ is the mass of a polymer molecule. This equation follows from combining equations 1 and 3 and indicates how the attraction depends on the EPS concentration. In order to compare the depletion interaction potential with the Baxter potential the overlap volume is taken as 'an average' value and does not depend on r anymore. The terms $(\delta + \sigma_c)/12\delta$ and $V_{\text{overlap}}^{\text{av}}/m$ were used as fitting parameters. Equation 17 describes the measured data up to 0.8 g/L. For the two highest EPS concentrations demixing was observed during the experiment and the diffusion coefficients of these samples were not fitted.

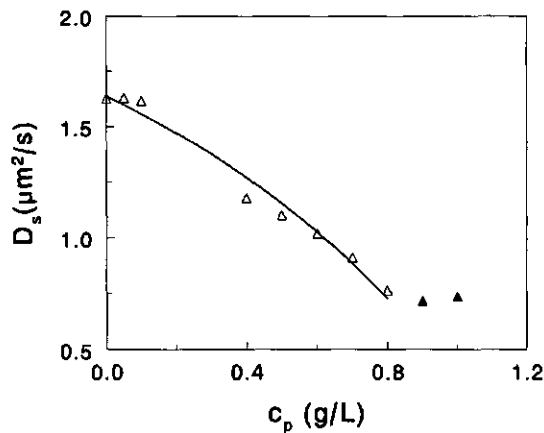


Figure 3 Self-diffusion coefficients measured in diluted skim milk ($\phi=0.11$) as a function of the EPS concentration. Data points are given by the open triangles. The filled triangles represent samples within the two-phase region. The drawn curve was computed from equations 7 and 17.

It follows from Figure 3 that increasing the EPS concentration gives a decrease in the self diffusion coefficient which corresponds to a lower Baxter parameter and thus more attraction between the casein micelles. The Baxter result can be applied for short range attraction. It appears here that a qualitatively correct interpretation of the data can be given. At very low

EPS concentrations there is hardly any effect on the diffusion coefficient. If EPS adsorbed onto the casein micelles a thick layer (of order 80-90 nm, which is the radius of gyration) would form which would strongly decrease the diffusion coefficient of the casein micelles: their hydrodynamic size would increase by a factor of about 1.7. The independence of D_s on c_p at very low concentrations indicates that indeed EPS does not adsorb on the casein micelles.

Structure factors

In this section we compare SANS measurements with model calculations of structure factors as obtained from the theories given in the theoretical sections. We have calculated $S(Q)$ from equations 11-13, where we used Vrij's depletion interaction potential [16].

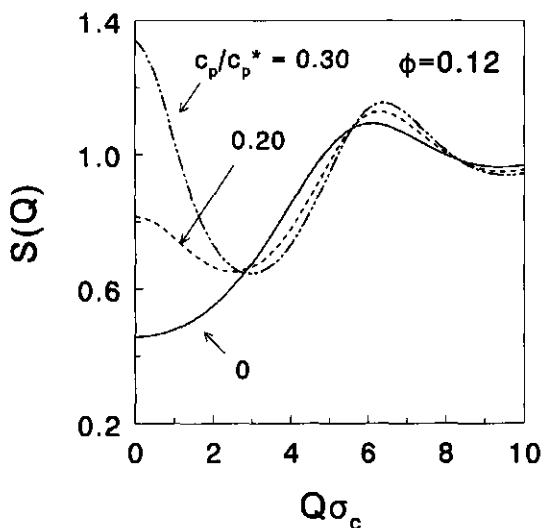


Figure 4 The structure factor of hard sphere suspensions ($\phi=0.12$) as a function of $Q\sigma_c$ for depletion interacting hard spheres with $\sigma_p/\sigma_c=0.86$, as calculated using equations 11-13. Results are given for polymer concentrations of $c_p/c_p^*=0, 0.2$ and 0.3 .

The $S(Q)$ profiles were calculated for a monodisperse suspension with a volume fraction of 0.12 without polymer molecules ($c_p=0$) and in the presence of non-adsorbing polymer molecules ($\sigma_p=176$ nm) at two concentrations $0.2c_p^*$ and $0.3c_p^*$, where $c_p^*=3M/(4\pi R_g^3 N_{AV})$ is the coil overlap concentration; it equals 0.9 ± 0.1 g/L for EPS in a 0.10 M NaNO_3 aqueous solution. The results for $S(Q)$ are plotted in Figure 4. At $Q\sigma_c=2\pi$ we recover the characteristic first peak for the hard sphere suspension. Upon adding polymers the shape of the $S(Q)$ curve has significantly changed. At low Q , $S(Q)$ increases with increasing c_p , which corresponds to the fact that the system becomes less stable when the particles attract one another more strongly (for $1/S(Q=0)=0$ spinodal decomposition is found).

From an experimental point of view it is convenient to normalize the structure factor. We have calculated $S(Q)/S_0(Q)$ for AHS and colloidal depletion interacting particles. We define $S_0(Q)$ as the structure factor of the hard sphere suspension and take $S(Q)$ as the structure factor of the same suspension including attraction either by the AHS model or by depletion interaction.

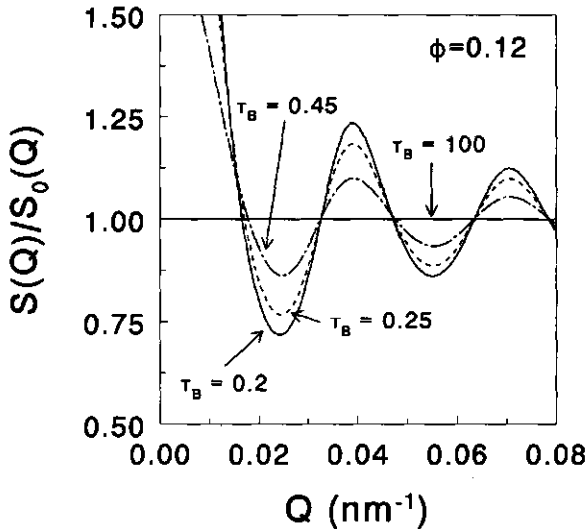


Figure 5 (a) Normalized structure factor as a function of Q for monodisperse particles with a diameter of 200 nm for adhesive hard spheres for values of the Baxter parameter as indicated.

Results for calculated $S(Q)/S_0(Q)$ as a function of Q are given for colloidal particles with a diameter of 200 nm (casein micelles) in Figure 5 (a) (adhesive hard spheres) and b (depletion interaction). The results for both theoretical models are rather similar showing that depletion interaction can be regarded as an effective attraction between the casein micelles. It is remarkable that for the broader depletion potential the oscillations are 'dampened' more strongly and are of a 'shorter' wavelength. Since the depletion interaction calculations given in Figure 5 (b) are closer to the real system we will compare these results with the experimental SANS results. For polydisperse systems the oscillations are progressively dampened with increasing Q and only approximately the first minimum will still be visible. These polydispersity effects hardly affect $S(Q)$ in the low Q -range [35].

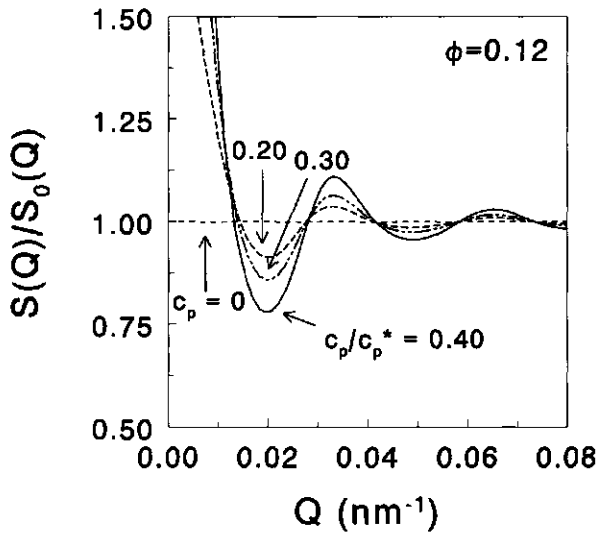


Figure 5 (b) Normalized structure factor as a function of Q for monodisperse particles with a diameter of 200 nm for depletion interacting hard spheres at polymer concentrations as indicated.

The scattering intensities were measured for skim milk in D_2O as well as for mixtures of EPS and skim milk in D_2O . The volume fraction of casein micelles was $\phi=0.12$. The scattered intensity is plotted as a function of the wavevector in Figure 6 for various EPS concentrations. By increasing the EPS concentration the scattering intensity decreased in the measured Q range. We have normalized the measured intensities $I(Q)$ with the intensity of skim milk without EPS, $I_0(Q)$.

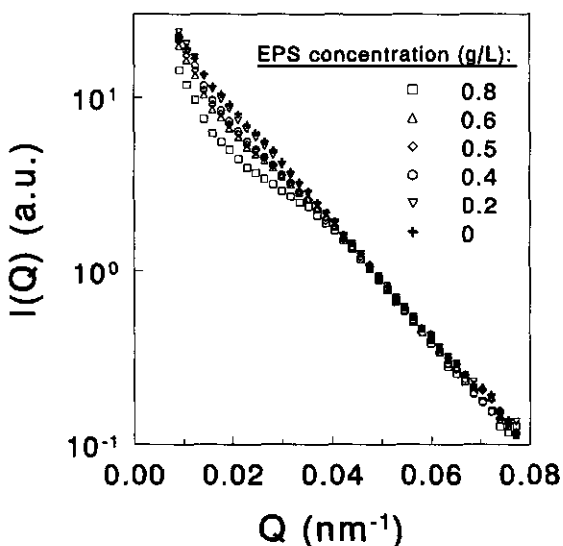


Figure 6 The scattering intensity $I(Q)$ of skim milk-EPS mixtures as a function of Q as measured by SANS. The measured data are in a range from 0 to 0.8 g/L EPS) are divided by the scattering intensity of the suspension ($\phi=0.12$) in the absence of EPS.

In Figure 7 the normalized scattered intensities $I(Q)/I_0(Q)$ are given as a function of Q for four EPS concentrations. We assume that the form factor of the casein micelles is not changed. Therefore changes in the scattered intensity are attributed to a change in $S(Q)$ and $I(Q) \sim S(Q)$. Then equation 8 can be rewritten as:

$$\frac{I(Q)}{I_0(Q)} = \frac{S(Q)}{S_0(Q)}$$

where $S_0(Q)$ is the structure factor of the suspension of casein micelles and $S(Q)$ represents the structure factor of the same suspension when EPS is added. From Figure 7 it follows that $I(Q)/I_0(Q)$ has a minimum at $Q=0.02 \text{ nm}^{-1}$. From Figure 5 (b) follows that $S(Q)/S_0(Q)$ is smaller than unity between $Q=0.013$ and 0.029 nm^{-1} and also goes through a minimum at $Q=0.02 \text{ nm}^{-1}$.

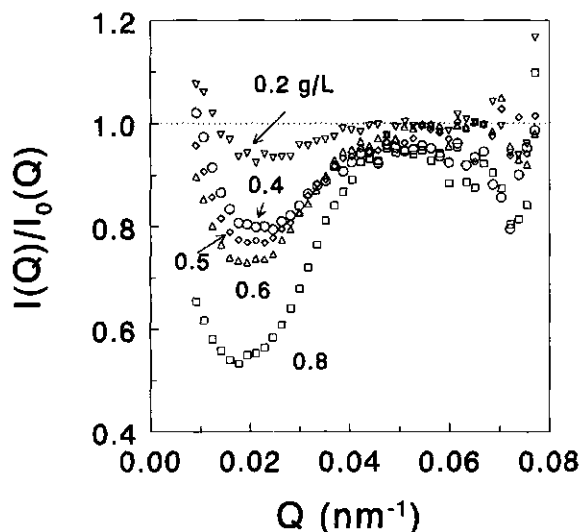


Figure 7 The normalized scattering intensity $I(Q)/I_0(Q)$ of skim milk-EPS mixtures as a function of Q as measured by SANS. The measurements (in a range from 0.2 to 0.8 g/L EPS) are divided by the scattered intensity of the suspension ($\phi=0.12$) in the absence of EPS.

It is true that the experimental convex curve as given in Figure 7 is wider than the theoretical one in Figure 5 (b). We think that this is mainly due to distribution in both micelle size and wavelength spread and divergence of the neutron beam, leading to a smearing out of the first $S(Q)$ peak.

The next step is a quantitative comparison between attractions as measured experimentally, presented in Figure 7, and the prediction of the theory of Vrij. Therefore we calculated values for U_0 which gave the best correspondence of $S(Q)/S_0(Q)$ with the minimum of the $I(Q)/I_0(Q)$ curves. These U_0 -values are plotted as a function of the experimental polymer concentration in Figure 8.

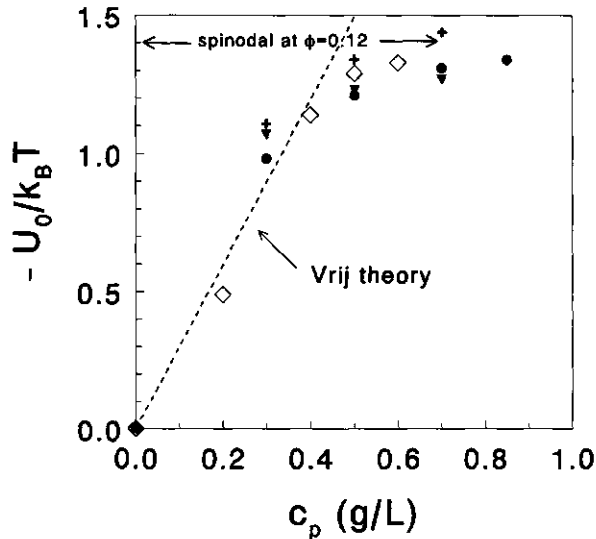


Figure 8 The minimum of the interaction potential profile $U_0/k_B T$ as a function of the EPS concentration c_p as calculated from the SANS measurements (open diamonds) and turbidity measurements (crosses for $\phi=0.06$, filled triangles for $\phi=0.08$ and filled circles for $\phi=0.10$).

The prediction from the theory of Vrij as given by equation 1 as a straight dotted curve. It is seen that the experimental data do not follow the straight curve as predicted by the Vrij theory and that there is some discrepancy between the absolute values. This is probably due to the fact that the Vrij theory considers the chains as ideal and only applies for monodisperse polymers and spheres. The increase of U_0 with c_p as found experimentally has the shape of a saturation process; just before the spinodal is reached the increase in U_0 as a function of c_p is very small. Ye *et al.* [36] also calculated U_0 as a function of c_p from SANS for a depletion interacting colloidal dispersion and found the same shape of the $U_0(c_p)$ -curve. The position of the theoretical phase boundary expressed as $U_0/k_B T$ is given by the arrow. From the experimental data we estimated the limiting polymer concentration as being 0.4-0.6 g/L, which corresponds with visual observation [37]. We conclude that experiment and theory are quite consistent for such a practical system. Information on the structure of a colloidal suspension can also be obtained from turbidity measurements as presented in the following section.

Turbidity

First, we measured the transmission of permeate (with EPS) and found that EPS did not significantly affect the transmission in the range 400-750 nm over the relevant EPS concentrations. In this wavelength range absorption of photon energy can be considered absent in our system. Next, we measured the transmission of skim milk with various amounts of EPS. Adding EPS significantly increased the turbidity of skim milk suspensions at wavelengths larger than 500 nm, which was attributed to a depletion interaction between the casein micelles induced by the EPS.

The effect can be visualized clearly by dividing the turbidity of the mixture of EPS and casein micelles by the turbidity of skim milk (only casein micelles). Any deviation from 1 should originate from interactions since the EPSs have a negligible scattering relative to the casein micelles. The turbidity of skim milk is indicated by the symbol τ_0 .

Theoretical predictions were obtained from the Vrij theory by calculating the structure factor as before and integrating the resulting $S(Q)$ by applying equation 16. In Figure 9 the theoretical results (curves) of the turbidity are plotted as a function of λ^{-2} as calculated from equation 16 for $\phi=0.10$, $\sigma_c=200$ nm and $\zeta=0.86$. The refractive index of skim milk permeate at 25°C was taken as 1.3475 [38] which is hardly affected by the EPS present and is close to the value for the refractive index of water at 25°C. We chose for λ^{-2} as variable since expansion of τ leads to a first-order λ^{-2} -dependence [39]. For high values of λ^{-2} (corresponding to integration of $P(Q)S(Q)$ from 0 to high Q^2) τ/τ_0 approaches unity while for lower λ^{-2} values there is a characteristic upswing of τ/τ_0 . This upswing originates from an increase of the structure factor. The upswing is stronger for higher polymer concentrations (more attraction). The line given for $c_p=0.38$ g/L is just below the theoretical spinodal.

The turbidity was measured as a function of wavelength at four EPS concentrations, 0.3, 0.5, 0.7 and 0.85 g/L for $\phi=0.06$, 0.08 and 0.10. The results for $\phi=0.10$ are given in Figure 9. The experimental data qualitatively correspond very well to the theoretical predictions. The agreement is especially good in the range of the upswing at low λ^{-2} .

At high λ^{-2} values the experimental results for the various EPS concentrations seem to approach unity more rapidly (at lower λ^{-2} values) than the theoretical curves predict. This can be explained by a polydispersity effect [35]. Polydispersity gives rise to a dampened $S(Q)$ becoming unity for small wavelengths which explains a faster decrease to unity of the experimental τ/τ_0 with decreasing wavelength. In general both experiment and theory show that upon increasing the EPS concentration the turbidity increases at long wavelengths which corresponds to a stronger attraction between the casein micelles.

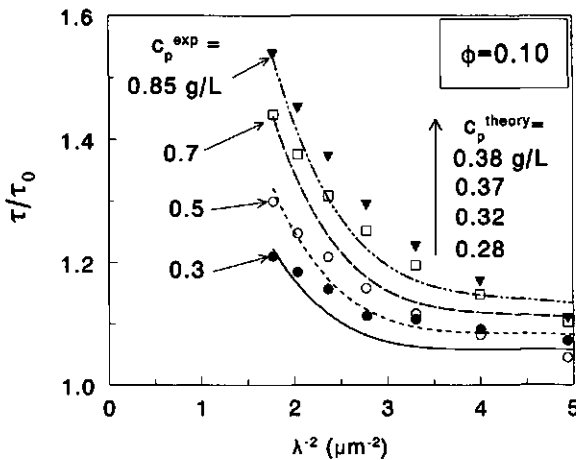


Figure 9 Measured turbidities of skim milk with a volume fraction of micelles $\phi=0.10$ as a function of the inverse wavelength for various concentrations of EPS as indicated (c_p^{exp}). Best theoretical predictions of the Vrij model are given as (dashed) lines and the polymer concentrations are indicated by c_p^{theory} (increasing from bottom to top).

Quantitatively, the experimental and theoretical polymer concentrations have the same order of magnitude but differ by approximately a factor 2. This is due to polydispersity of casein micelles, EPS and wavelength and due to the limitations of the Vrij theory which applies only for ideal chains and does not take into account higher order terms in the osmotic pressure of the polymer solution.

The same turbidity experiments were done for $\phi=0.06$ and 0.08 with varying EPS concentrations. The main trends are the same as in Figure 9. From the comparison with the model calculations we obtained the results given in Figure 8 together with the SANS data. It follows that the depth of the potential well U_0 increases with increasing EPS concentration and is quantitatively consistent with results from the SANS measurements.

Conclusions

Dynamic light scattering experiments, small-angle neutron scattering and turbidity measurements showed that the casein micelles become attractive upon adding EPS. The attraction can be attributed to depletion interaction. The self-diffusion coefficients obtained from DLS can be interpreted by the adhesive sphere model. The attraction found by SANS and turbidity measurements can be described by the structure factors calculated from a theory based on the depletion interaction potential as described by the Vrij model. These findings show that mixing certain biopolymers together strongly affects the properties of the system and the calculation of the attraction can be used to get an idea of the resulting structure and consistency. The attractions not only affect the phase behavior but also the equilibrium and transport properties, such as the self-diffusion and the viscosity.

Acknowledgment

Blandine Oudin and the late Cyril Renaud are thanked for performing self-diffusion and turbidity experiments, respectively, and for their pleasant co-operation.

References

- [1] Sandford, P.A, Cottrell, I.W., Pettiitt, D.J., *Pure Appl. Chem.* **56** (1984) 879.
- [2] Cerning, J., *FEMS Microbiol. Rev.*, **87** (1990) 113.
- [3] Marle, M.E. van, PhD Thesis Twente University, The Netherlands, 1998.
- [4] Gruter, M., Leeftang, B.R., Kuiper, J., Kamerling, J.P., Vliegthart, J.F.G., *Carbohydr. Res.* **231** (1992) 273.
- [5] Osman, S.F., Fett, W.F., Dudley, R.L., *Carbohydr. Res.* **265** (1994) 319.
- [6] Robijn, G.W., van den Berg, D.J.C., Haas, H., Kamerling, J.P., Vliegthart, J.F.G., *Carbohydr. Res.* **276** (1995) 117.
- [7] Tuinier, R., Zoon, P., Olieman, C., Cohen Stuart, M.,A., Fler, G.J., de Kruij, C.G., *Biopolymers* **49** (1999) 1.
- [8] Grinberg, V.Ya., Tolstoguzov, V.B., *Food Hydrocoll.* **11** (1997) 145.
- [9] De Kruij, C.G., *Langmuir* **8** (1992) 2932.
- [10] Semenova, M.G., Pavloskaya, G.E., Tolstoguzov, V.B., *Food Hydrocoll.* **4** (1991) 469.
- [11] Kasapis, S., Morris, E.R., Norton, I., Clark, A.H., *Carbohydr. Pol.* **21** (1993) 243, *Carbohydr. Pol.* **21** (1993) 249, *Carbohydr. Pol.* **21**(1993) 261, *Carbohydr. Pol.* **21** (1993) 269.
- [12] Asakura, S., Oosawa, F., *J. Chem. Phys.* **22** (1954) 1255; *J. Polymer Sci.* **33** (1958) 183.

- [13] M. Baus, L.F.Rull, J-P.Ryckaert (Eds.), In: *Observation and Simulation of Phase Transitions in Complex Fluids*, Kluwer, Dordrecht, 1995.
- [14] Lekkerkerker, H.N.W., Poon, W.C.K., Pusey, P.N., Stroobants, A., Warren, P.B., *Europhys.Lett.* **20** (1992) 559.
- [15] De Kruijff, C.G., Jansen, J.W., Vrij, A., 'Symp. *Complex fluids*,' p.315, 1985.
- [16] Vrij, A., *Pure & Appl. Chem.* **48** (1976) 471.
- [17] Baxter, R.J., *J. Chem. Phys.* **49** (1968) 2770.
- [18] McQuarrie, D.A., *Statistical Mechanics*, Harper & Row, New York, 1976.
- [19] Batchelor, G.K., *J. Fluid Mech.* **74** (1976) 1.
- [20] Felderhof, B.U., *J. Phys. A* **11** (1978) 929.
- [21] Cichocki, B., Felderhof, B.U., *J. Chem. Phys.* **93** (1990) 442.
- [22] Kerker, M., 'Scattering of light and other electromagnetic radiation', Academic Press, New York, 1969.
- [23] Ornstein, L.S., Zernike, F., *Proc. Koninkl. Nederland Akad. Wetenschap, Amsterdam*, **17** (1914) 793.
- [24] Menon, S. V. G., Manohar, C., Srinivasa Rao, K., *J. Chem. Phys.*, **95** (1991) 9186.
- [25] Percus, J.K., Yevick, G.J., *Phys. Rev.* **110** (1958) 1.
- [26] Kranendonk, W.G.T., Frenkel, D., *J. Chem. Phys.*, **64** (1988) 403.
- [27] Gillan, M.J., *Mol. Phys.*, **38** (1979) 1781.
- [28] van Leeuwen, J.M.J., Groeneveld, J., de Boer, J., *Physica* **25** (1959) 792.
- [29] Morita, T., Hiriokem, K., *Prog. Theor. Phys.* **23** (1960) 1003.
- [30] Jeurnink, Th.J.M., De Kruijff, C.G., *J. Dairy Res.* **60** (1993) 139.
- [31] Ibel, K., *J. Appl. Cryst.* **9** (1976) 296.
- [32] Bauer, R., Hansen, M., Ogendal, L., Lomholt, S.B., Qvist, K.B., *J. Chem. Phys.* **103** (1995) 2725.
- [33] Hansen, S., Bauer, R., Lomholt, S.B., Quist, K.B., Pedersen, J.S., Mortensen, K., *Eur. Biophys. J.* **24** (1996) 143.
- [34] De Kruijff, C.G., *J. Dairy Sci.*, **81** (1998) 3019.
- [35] Frenkel, D., Vos, R.J., De Kruijff, C.G., and Vrij, A. *J. Chem. Phys.*, **84** (1986) 4625.
- [36] Ye, X., Narayanan, T., Tong, P., Huang, J.S., *Phys. Rev. Lett.* **76** (1996) 4640.
- [37] Chapter 7 of this thesis.
- [38] Walstra, P., Jenness, R., In: 'Dairy Chemistry and Physics,' Wiley, New York, 1984.
- [39] Penders, M.H.G.M., Vrij, A., *J. Chem. Phys.*, **93** (1990) 3704.

Phase behavior of casein micelles/exocellular polysaccharide mixtures; experiment and theory

Abstract

Dispersions of casein micelles and an exocellular polysaccharide (EPS), obtained from *Lactococcus lactis* subsp. *cremoris* NIZO B40 EPS, show a phase separation. The phase separation is of the colloidal gas-liquid type. We have determined a phase diagram that describes the separation of skim milk with EPS into a casein-micelle rich phase and an EPS rich phase. We compare the phase diagram with those calculated from theories developed by Vrij, and by Lekkerkerker and co-workers, showing that the experimental phase boundary can be predicted quite well. From dynamic light scattering measurements of the self-diffusion of the casein micelles in the presence of EPS the spinodal could be located and it corresponds with the experimental phase boundary.

Introduction

Solutions containing both proteins and polysaccharides may exhibit phase separation. This was first reported in 1896 by Beijerinck, who observed a phase separation after mixing aqueous solutions of gelatin and starch [1]. Milk proteins and polysaccharides also exhibit incompatibility, as was reported for example by Tolstoguzov [2,3] and Antonov *et al.* [4]. During the production process of dairy products polysaccharides and proteinaceous particles are often combined. Mixing proteins and polysaccharides also takes place during the fermentation process where exocellular polysaccharides (EPSs) by lactic acid bacteria are produced '*in-situ*' in products such as yogurt. In yogurt the EPS seems to play an important role and is responsible for the thread-like pouring behavior of some types of yogurt. Previously, we have characterized physical properties of an EPS produced by *Lactococcus lactis* subsp. *cremoris* strain NIZO B40, which has a number-averaged molar mass of $1.47 \cdot 10^6$ g/mol and a number-averaged radius of gyration of 86 nm, and has a small polydispersity [5].

Low-heat skim milk was chosen as milk protein system. Skim milk can be regarded as a 10 % (v/v) suspension of casein micelles, which are association colloids with a diameter of 200 nm, in an aqueous (continuous) phase containing other but very small (< 5 nm) components (salts, lactose and whey proteins). Casein micelles can be considered as hard spheres as follows from diffusion [6] and rheology measurements [7].

B40 EPS, when added to skim milk above a certain concentration, induces phase separation, as will be shown. When the continuous phase of skim milk is mixed with B40 EPS (further denoted as EPS) nothing happens. This indicates that the interactions between casein micelles and EPS are responsible for the observed phenomena.

The phase separation is caused by the so-called depletion type of interaction and is also referred to as depletion flocculation. A better term would be segregative behavior. An early experimental observation of phase separation driven by depletion interaction was reported by Traube [8], who investigated the effect of adding polymer molecules on creaming of natural rubber. About ten years later the depletion phenomenon was used in practice for the concentration of natural latex by plant polysaccharides, as described by Vester [9]. Asakura and Oosawa [10] gave a theoretical expression for the depletion interactions between two flat plates. Vrij [11] developed a thermodynamic model for the depletion in a mixture of colloidal spherical particles and non-adsorbing polymer molecules. De Hek and Vrij [12] observed phase separation in mixtures of colloidal silica spheres and polystyrene polymers, and the theory of Vrij [11] reasonably predicts the limiting polymer concentration for this system. Lekkerkerker [13] also developed a more sophisticated theory for depletion interaction using a

different thermodynamic route. More recently, Lekkerkerker *et al.* [14] and Poon and Pusey [15] extended and refined this theoretical description.

In this paper it is shown that EPSs do not adsorb onto casein micelles and induces depletion flocculation in skim milk. We will compare two theoretical methods which allow the calculation of the phase line. An instability condition for a simpler adhesive hard sphere model will also be given in order to locate a phase boundary from dynamic light scattering measurements. In this paper we show that phase diagrams calculated from depletion theories are consistent with the experimental phase diagram of a biological system containing casein micelles and EPS, indicating the practical relevance of depletion interaction.

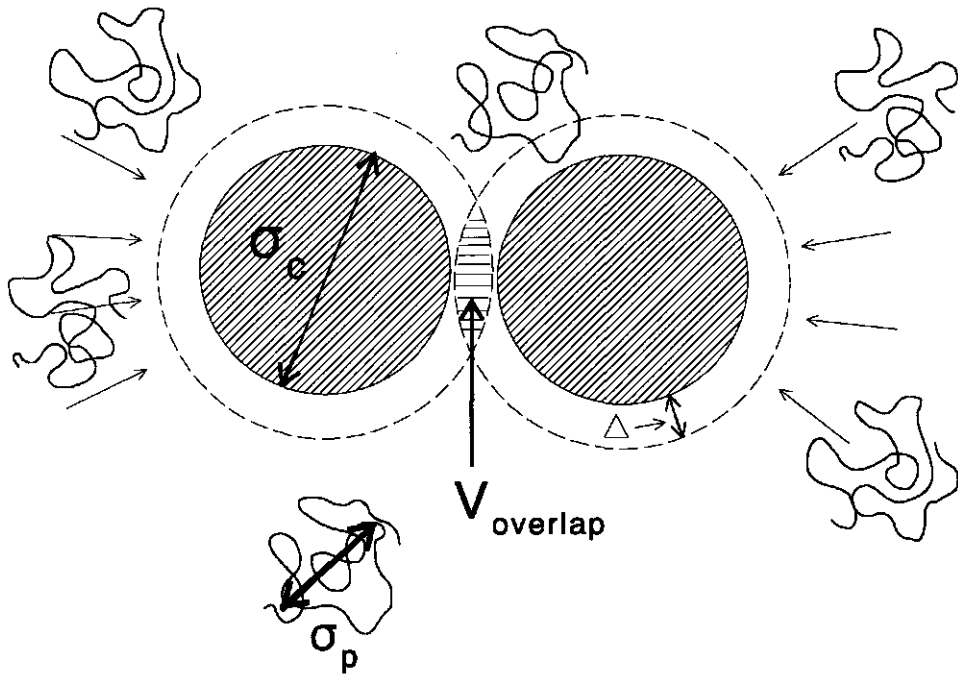


Figure 1 Schematic picture of the depletion interaction mechanism. The colloidal spheres with diameter σ_c are pushed together by the unbalanced osmotic pressure as exerted by the polymer molecules with diameter σ_p .

Theory

Depletion interaction theories

- Vrij theory

A schematic picture of colloidal spherical particles dispersed in a solution of non-adsorbing polymer molecules is sketched in Figure 1. The polymer molecules, with an effective diameter σ_p (twice the depletion layer thickness Δ) are assumed to be freely permeable towards one another (θ -solvent) but are hard spheres for the colloids with diameter σ_c . Vrij [11] derived that then the attractive interparticle potential between two spherical colloidal particles, which behave as hard spheres towards one another, is proportional to the overlap volume V_{overlap} and to the osmotic pressure of the polymer solution Π_p . For the osmotic pressure of the polymer solution Vrij used the limiting Van 't Hoff's law:

$$\Pi_p = c_p R T / M \quad 1$$

where c_p is the polymer concentration, R the gas constant, T the temperature and M the molar mass of the polymer. The overlap volume depends on the distance between the centers of the particles r :

$$V_{\text{overlap}}(r) = \frac{1}{6} \pi (\sigma_c + \sigma_p)^3 \left[1 - \frac{3r}{2(\sigma_c + \sigma_p)} + \frac{r^3}{2(\sigma_c + \sigma_p)^3} \right] \quad 2$$

Equation 2 applies for $\sigma_c < r < (\sigma_c + \sigma_p)$. Now the depletion interaction potential of Vrij is given by [11]:

$$U(r) = \begin{array}{ll} +\infty & 0 < r < \sigma_c, \\ -\Pi_p V_{\text{overlap}}(r) & \sigma_c \leq r \leq (\sigma_c + \sigma_p), \\ 0 & r > (\sigma_c + \sigma_p), \end{array} \quad 3$$

Given the pair potential the equilibrium properties of the system can be evaluated using statistical mechanics [16]. If the polymer-induced attraction between two particles becomes strong enough the system tends to phase separate into a colloid-rich and polymer-rich phase [14]. The calculation of the binodal in a statistical mechanical way is possible but rather involved. Simpler is a calculation of the spinodal the osmotic compressibility $\partial \Pi_c / \partial \phi$ becomes zero [16]:

$$\frac{\partial \Pi_c}{\partial \phi} = 0 \quad 4$$

The spinodal usually lies very close to the binodal and therefore the spinodal can also be taken as an estimation of the phase boundary. The virial expansion of the osmotic pressure of colloids is [17]:

$$\frac{\Pi_c V_c}{k_B T} = \phi + B_2 \phi^2 + B_3 \phi^3 + \dots \quad 5$$

where $V_c (= \pi \sigma_c^3 / 6$ for spheres) is the particle volume of the colloids, B_2 is the second and B_3 the third osmotic virial coefficient. For low volume fractions ($\phi < 0.2$) B_3 and higher-order terms can be neglected. Combining equations 4 and 5 gives the value B_2^{sp} at the spinodal for a given volume fraction:

$$B_2^{sp} = -\frac{1}{2\phi^{sp}} \quad 6$$

where ϕ^{sp} is the volume fraction at the spinodal. The second virial coefficient can be measured in the one-phase region at a given ϕ . On addition of polymer, B_2 will decrease due to attractions. From statistical mechanics a relation between $U(r)$ and B_2 can be derived [16]:

$$B_2 = \frac{2\pi}{V_c} \int_0^\infty r^2 [1 - \exp(-\frac{U(r)}{k_B T})] dr \quad 7$$

which gives $B_2=4$ for the hard sphere interaction potential. For depletion interactions, we calculate B_2 from equation 7 by taking $U(r)$ from equation 3. This then yields B_2 , which becomes negative for sufficiently high polymer concentrations, eventually leading to spinodal demixing. So, for a mixture with a certain volume fraction ϕ of colloidal spheres with diameter σ_c the effect of non-adsorbing polymer molecules on B_2^{sp} can be calculated. This yields the limiting polymer concentration and by doing this at various values of ϕ the phase diagram can be calculated.

Since in the approach of Vrij only pair interactions are involved, which is incorrect above the dilute regime, we have also used an alternative thermodynamic route which takes into account many particle interactions to calculate the spinodal with the interaction potential for depletion interaction given in equation 3. From equation 4 we know that the spinodal corresponds to the point where the osmotic compressibility $\partial \Pi_c / \partial \phi$ equals zero. Therefore use can be made of the relation between the structure factor of a colloidal dispersion $S(Q)$, which can be measured with scattering techniques. The osmotic compressibility and $S(Q)$ are related as follows:

$$S(Q=0) = kT \frac{\partial \rho}{\partial \Pi} \quad 8$$

where $\rho = N_c/V$ is the number density, with N_c the number of particles in a volume V , which is related to the volume fraction by $\phi = N_c V_c / V$. The scattering wave vector Q equals

$4\pi n \sin(\theta/2)/\lambda_0$, where n is the refractive index, θ is the angle under which the scattered intensity is detected and λ_0 is the wavelength in vacuo. Comparison with equation 4 shows that the condition $S(Q=0)^{-1}=0$ gives the spinodal. The structure factor $S(Q)$ is defined as the Fourier transform of $g(r)$:

$$S(Q) = 1 + 4\pi\rho \int_0^{\infty} [g(r) - 1] \frac{\sin(Qr)}{Qr} dr \quad 9$$

where r is the distance between the centers of any two randomly chosen particles, say particle 1 and 2. In order to calculate $S(Q)$ one thus needs an expression for the radial distribution function $g(r)$. The integral equation of Ornstein and Zernike (OZ-equation) gives the total correlation function $h(r)$ [18]:

$$h(r) = c(r_{12}) + \rho \int c(r_{13}) h(r_{23}) dr_3 \quad 10$$

which makes it possible to solve for $g(r)=h(r)+1$ when one has an appropriate closure relation for $c(r_{12})$, the direct correlation function. The OZE defines $g(r)$ as the sum of the direct effect of particle 1 on particle 2 and an indirect effect of 1 on 2 in which all other particles are involved. We have used the hypernetted chain (HNC) closure relation [19]:

$$c(r) = h(r) - \ln(g(r) - U(r)/k_B T) \quad 11$$

We applied a mathematical solution procedure developed by Gillan [20] to solve equations 10 and 11. We can insert equation 3 into the HNC closure and subsequently calculate $g(r)$ and $S(Q)$ by using equations 10 and 9. Hence, $S(Q=0)$ can be obtained as a function of c_p which makes it possible to calculate the spinodal (the polymer concentration for which $1/S(Q=0)$ equals zero).

In the foregoing the depletion layer thickness Δ was left unspecified. Usually, it is identified with the radius of gyration of the polymer molecules: $\Delta = R_g = \sigma_p/2$. De Hek and Vrij [12] numerically calculated the distance r where the particles just start to attract one another and found $\sigma_p \approx 2.25 R_g$, which confirms that $\Delta \approx R_g$. Calculations of Fleer *et al.* [21] for concentrations below overlap give $\Delta \approx R_g$, which also corroborates the general assumption that the radius of gyration is a good measure of the depletion layer thickness in dilute solutions. Fleer *et al.* also calculated the decrease of Δ above coil overlap, but since in our case c_p is below the overlap threshold we do not need these expressions.

In order to illustrate the main trends some model predictions as calculated with the theory of Vrij [11,12] are given in Figure 2. Results are calculated for a mixture of colloidal particles with a radius of 100 nm ($\sigma_c=200$ nm) and polymer molecules with a molar mass of 10^3 kg/mol and three different radii of gyration: 30, 60 and 90 nm ($\sigma_p=60, 120$ and 180 nm), respectively, corresponding to varying the flexibility of the chains.

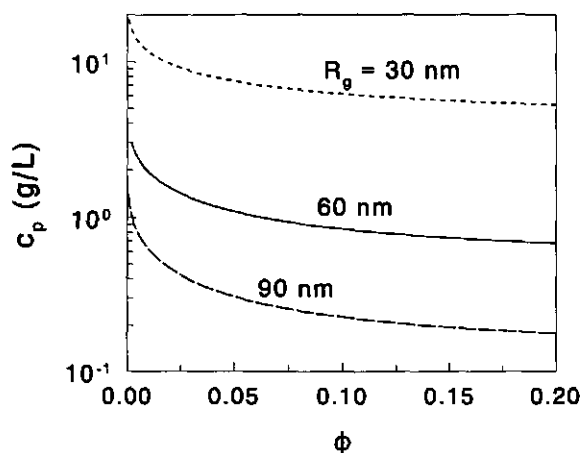


Figure 2 Phase lines as calculated with the theory of Vrij [11] for colloidal spheres with a diameter of 200 nm and polymer molecules with a molar mass of 1000 kg/mol and radii of gyration (R_g) as indicated.

Increasing ϕ gives a lower limiting polymer concentration since according to equation 6 the product $\phi \cdot B_2^{sp}$ is a constant. This indicates that a less negative value of B_2^{sp} , and hence a lower polymer concentration, is required at higher ϕ . By comparing the results for the various sizes of the polymer molecules, we observe a decreasing spinodal demixing curve with increasing depletion layer thickness (larger polymer molecules). This indicates that when the polymer chains are more stiff, leading to a larger R_g , they will have a stronger tendency to induce phase separation by the depletion interaction mechanism.

- *Lekkerkerker theory*

Another way of calculating the phase lines was developed by Lekkerkerker and co-workers. The approach is based upon a grand canonical statistical mechanical description of hard spheres in the presence of freely interpenetrable coils. Lekkerkerker *et al.* [14] derived expressions for both the osmotic pressures and the thermodynamic potentials of the colloidal suspension for the fluid as well as for the crystal phases in order to predict the phase behavior of polymer-colloid mixtures by calculation of the binodal. The polymer concentration acts as perturbation parameter.

Fluid phase

For the fluid phase a dimensionless osmotic pressure Π_f is expressed as:

$$\Pi_f = \frac{\phi}{1-\phi} + 3\left(\frac{\phi}{1-\phi}\right)^2 + 3\left(\frac{\phi}{1-\phi}\right)^3 + \frac{c_p^R \pi \sigma_c^2}{6M\zeta^3} \left(\alpha - \frac{d\alpha}{d\phi}\right) \quad 12$$

where c_p^R is the overall polymer concentration in the reservoir. The fraction α is the fraction of the total volume which is accessible to the polymer molecules, and $\zeta = \sigma_p/\sigma_c$ is the size ratio of the polymer molecules relative to the colloidal spheres. The macroscopic polymer concentration equals $\alpha \cdot c_p^R$. The free volume fraction α can be calculated from [14, 15]:

$$\alpha = (1-\phi) \exp\left[-A \frac{\phi}{1-\phi} - B \left(\frac{\phi}{1-\phi}\right)^2 - C \left(\frac{\phi}{1-\phi}\right)^3\right] \quad 13$$

with $A=3\zeta + 3\zeta^2 + \zeta^3$, $B=4.5\zeta^2 + 3\zeta^3$, and $C=3\zeta^3$. Equation 13 reduces to $\alpha=1-\phi$ for $\zeta \rightarrow 0$. The first three terms on the right-hand side of equation 12 are derived from the Percus-Yevick equation of state [22] and the fourth term is a perturbation factor arising from the presence of the polymer molecules. For the thermodynamic potential μ_f of colloidal spheres in the fluid phase Lekkerkerker *et al.* [14] derived the following equation:

$$\frac{\mu_f}{k_B T} = \ln\left(\frac{\phi}{1-\phi}\right) + 7\left(\frac{\phi}{1-\phi}\right) + \frac{15}{2}\left(\frac{\phi}{1-\phi}\right)^2 + 3\left(\frac{\phi}{1-\phi}\right)^3 - \frac{c_p^R \pi \sigma_c^2}{6M\zeta^3} \frac{d\alpha}{d\phi} \quad 14$$

which has the same physical origin as equation 12.

Solid phase

For the crystal or solid phase, equations analogous to 12 and 14 can be derived. For the osmotic pressure, a simplified version of the equation of state of Hall [23] is used:

$$\Pi_s = \frac{\phi}{1 - \frac{\phi}{\phi_{cp}}} + \frac{c_p^R \pi \sigma_c^2}{6M\zeta^3} \left(\alpha - \frac{d\alpha}{d\phi}\right) \quad 15$$

where ϕ is now the volume fraction of colloidal particles in the solid phase and ϕ_{cp} is the volume fraction at closest packing ($=\pi\sqrt{2}/6$). The thermodynamic potential in the solid phase is given by:

$$\frac{\mu_s}{k_B T} = 2.1306 + 3 \ln\left(\frac{\phi}{1 - \frac{\phi}{\phi_{cp}}}\right) + \frac{3}{1 - \frac{\phi}{\phi_{cp}}} - \frac{c_p^R \pi \sigma_c^2}{6M\zeta^3} \frac{d\alpha}{d\phi} \quad 16$$

where the constant cannot be calculated analytically. The value 2.1306 given above is taken from computer simulations of Frenkel and Ladd [24] and is consistent with experimental values for $\phi=0.494$ and 0.545 at the fluid-crystal transition of a suspension of hard spheres.

Subsequently, the phase behavior can be calculated from the conditions $\Pi_l = \Pi_s$ and $\mu_l = \mu_s$. This gives two sets of equations with two unknowns, ϕ 's for the volume fractions of colloids in the coexisting phases, which can be solved numerically. The model described above makes it is possible to calculate the phase behavior of polymer-colloid mixtures. The coexisting phases which can be found are fluid-solid, and above approximately $\zeta=0.3$ gas-liquid, gas-solid and gas-liquid-solid since the fluid phase then also exhibits a gas-liquid transition.

Adhesive hard sphere model

For skim milk it has been shown [6,7] that casein micelles can be treated as hard spheres under the conditions relevant for this study. When hard spheres become sufficiently attractive a (colloidal) fluid-solid transition takes place which can be regarded as a phase separation. Casein micelles become attractive when EPS is added to skim milk. We use the adhesive hard sphere (AHS) model in order to make a connection between dynamic light scattering experiments and the attraction between colloidal particles.

An interaction potential profile for adhesive spheres has been proposed by Baxter [25] as a square well potential with an infinitely narrow width ($\delta \rightarrow 0$):

$$\frac{U(r)}{k_B T} = \begin{cases} +\infty & 0 < r < \sigma_c, \\ \ln[12\tau_B\delta / (\sigma_c + \delta)] & \sigma_c \leq r \leq (\sigma_c + \delta), \\ 0 & r > (\sigma_c + \delta), \end{cases} \quad 17$$

where τ_B is the Baxter parameter ($0 < \tau_B < \infty$) and τ_B^{-1} is a measure of the attraction between the spheres. A prerequisite for applying the Baxter potential is that the term $\tau_B\delta$ has to remain finite. The experimentally accessible parameter from light scattering and osmotic pressure measurements is B_2 . Combining equations 7 and 17 gives:

$$B_2 = 4 - \frac{1}{\tau_B} \quad 18$$

Using Baxter's approach Watts *et al.* [26] showed that τ_B can be directly related to the volume fraction at the spinodal ϕ^{sp} . For a volume fraction lower than 0.12 Penders and Vrij [27] simplified the expressions of Watts *et al.* [26] to:

$$\tau_B = \frac{\phi^{sp}}{1 - \phi^{sp}} \left(\sqrt{1 + \frac{1}{2} \phi^{sp}} - 1 \right) \quad 19$$

For higher values of ϕ , the PY theory can be used [22,27]. Equation 19 allows us to calculate the volume fraction at which decomposition takes place at a certain adhesiveness. So, when τ_B is determined the spinodal can be calculated. Although strictly speaking the AHS model is not

correct for our system we apply it here since it provides a theoretical framework which allows us to describe the phase separation in terms of τ_B values, which can be calculated from for instance transport properties. The way τ_B is related to the self-diffusion coefficient is treated in the next section.

Phase separation from self-diffusion

Previously [28] we have measured τ_B of skim milk-EPS mixtures by dynamic light scattering. We calculated Baxter parameters from the measured self-diffusion coefficients by applying the following expression from Cichocki and Felderhof [29]:

$$\frac{D_s}{D_0} = 1 - \left(1.832 + \frac{0.295}{\tau_B}\right)\phi \quad 20$$

where D_s is the self-diffusion coefficient and D_0 is its value at $\phi \rightarrow 0$. By calculating τ_B values from equation 20 ϕ^{sp} can subsequently be obtained from equation 19. Hence, scattering data allow calculation of the phase boundary.

However, in the approach given above the viscosity increase due to the addition of B40 EPS to the continuous phase has been neglected. Previously, we have shown [30] that the (zero-shear) specific viscosity $\eta_{sp} = (\eta_0 - \eta_s)/\eta_s$ (where η_0 is the zero-shear solution viscosity and η_s the solvent viscosity) of polysaccharide solutions can be described as:

$$\eta_{sp} = [\eta]c + \frac{1}{25}([\eta]c)^{3.5} \quad 21$$

where $[\eta]$ is the intrinsic viscosity of the polysaccharide solution. For EPS solutions with an ionic strength of 0.10 M, $[\eta]$ equals 3.2 m³/kg. We assume the same value for skim milk, where the ionic strength is close (0.08 M). Equation 21 indicates that the self-diffusion coefficient, which depends on the viscosity of the continuous phase, decreases when EPS is added to skim milk. We have to take this effect into account by applying a correction for the viscosity. However, for systems where the particle size is of the same order of magnitude as the polymer molecules it is not correct to simply replace the solvent viscosity with the viscosity of the continuous phase as measured macroscopically. The macroscopic viscosity overestimates the friction experienced by the colloidal particles [31].

This phenomenon has been examined theoretically by Cukier [32] and De Gennes [33], who found that relatively small colloidal particles tend to 'hunt for holes' in polymer solutions. Microscopically a polymer solution can be regarded as a system containing obstacles (polymer chains) with a high resistance. Since the particles seek a path of minimum resistance, the viscosity as experienced by the diffusing particles is smaller than the macroscopic viscosity. The contribution of the polymers to the effective viscosity of the solution depends on the

hydrodynamic colloidal particle-polymer size ratio, ζ_h , defined as R^p/R^s , where R^s refers to the hydrodynamic radius of the colloidal sphere and R^p to the effective radius of the polymer molecules. We are not aware of a theory which quantitatively describes the relation between the effective viscosity and ζ_h . In the limit $\zeta_h \rightarrow \infty$ the colloidal particles will only experience friction due to interaction with solvent molecules since the polymer molecules are so large that the particles can easily 'hunt for holes'. When the value of ζ_h is very small the colloidal spheres cannot diffuse through the holes since the holes are too small. Therefore the particles will experience the macroscopic viscosity in the limit $\zeta_h \rightarrow 0$. At intermediate values for ζ_h , the friction will lie in between the solvent and the polymer solution viscosity. Tentatively, we introduce an effective viscosity η_{eff} and propose that it depends as follows on ζ_h :

$$\frac{\eta_{\text{eff}}}{\eta_s} = 1 + \eta_{\text{sp}} \exp(-\zeta_h) \quad 22$$

The solvent contribution is given by the first term on the right-hand side, and that of the solute by the second term. This equation describes the data in ref. 31 reasonably well and gives a correct physical description for the limits.

For the sedimentation of colloidal particles through a polymer solution, Tong *et al.* [34] also found that for very large values of ζ_h the particles experience a much lower viscosity than that of the solvent with polymer molecules. The macroscopic viscosity of the solution is only experienced for $\zeta_h \rightarrow 0$. For R^p these authors use the correlation length ξ , which says that in the entangled region even small particles experience the macroscopic viscosity.

The approach given above will be used to account for the effect of the viscosity of the solution on the measured self-diffusion coefficient. Equation 20 can then be replaced by:

$$\frac{D_s}{D_0} \frac{\eta_{\text{eff}}}{\eta_0} = 1 - \left(1.832 + \frac{0.295}{\tau_B}\right) \phi \quad 23$$

where η_{eff} is defined in equation 22.

Experimental

- NIZO B40 EPS

NIZO B40 EPS was obtained after a fermentation and isolation process at the NIZO pilot plant as described elsewhere [5]. EPS was isolated using various filtration steps, freeze-dried and used as such in this study.

- Skim milk

Reconstituted skim milk was prepared as described in ref. 7. The volume fraction of casein micelles in the reconstituted skim milk was determined by Jeurnink and De Kruif [7] as being 0.130.

- *Permeate*

Skim milk permeate (i.e. the 'solvent' of the casein micelles) was prepared from skim milk by a membrane filtration process. An Amicon hollow-cartridge HIMPO 1-43 membrane with a cut-off of 0.1 μm was used. The pH of the permeate was the same as that of the skim milk (6.60 ± 0.10).

- *Mixtures*

The mixtures were prepared by dissolving EPS diluted in permeate and mixing this EPS-skim milk permeate solution with skim milk. All mixtures were studied at room temperature.

- *Preservative*

Since phase separation was sometimes observed only after a few weeks we used anti-microbial agents (preservatives) in order to prevent growth of micro-organisms during the experiments. We used 0.02 % (m/m) sodium ethylmercurithiosalicylate ($\text{C}_2\text{H}_5\text{HgSC}_6\text{H}_4\text{COONa}$ - thiomersal, BDH Chemicals), with which we could not observe any bacterial growth or any pH changes for more than 6 weeks. In the absence of EPS, skim milk and permeate containing thiomersal were stable for months.

Results and discussion

This section contains three parts. Firstly, a description of the observed phase separation phenomena for the skim milk/permeate/EPS mixtures is given. Theoretical predictions of the phase diagram are presented subsequently and compared with the experiments. Further, the Baxter parameters obtained from dynamic light scattering measurements are used to calculate a phase diagram with the AHS model.

Observations and phase diagram

Firstly, we dissolved EPS in low-heat skim milk permeate (skim milk without casein micelles). The highest EPS concentration studied was 10 g/L since EPS is not soluble (on a practical time scale) at higher concentrations. This represents a practical concentration range since lactic acid bacteria produce EPSs up to concentrations of 0.5 g/L. In permeate solutions no phase separation could be observed for months when EPS was added. Apparently, whey proteins and EPS are fully compatible. Therefore we used permeate to dissolve EPS, after which this EPS-permeate solution was mixed with skim milk.

In this way the required final concentration c_p of EPS and the volume fraction ϕ of casein micelles could be adjusted independently in the range $0 < c_p < 10$ g/L and $0 < \phi < 0.13$. Mixtures in this concentration range were prepared, stored, and studied at room temperature. For high

EPS concentrations a two-phase system could be observed after several hours or, occasionally, after several days. The onset of phase separation occurred always within one week. In phase-separated systems the upper phase became clearer with time while the lower phase became highly turbid (white). In Figure 3 a phase diagram is presented describing which mixtures demixed (filled circles) and which remained stable (open circles). The transition points (plusses) are indicated for various ϕ values and a line which guides the eye represents the visually observed phase boundary. The EPS concentration at which the skim milk suspensions phase separate is rather low. The polymer overlap concentration c_p^* , which equals $3M_n/4\pi R_g^3 N_{AV}$, where M_n is the number-averaged molar mass and N_{AV} Avogadro's number, is 0.92 ± 0.09 g/L. This indicates that phase separation occurs in the dilute regime for casein volume fractions above $\phi \approx 0.03$.

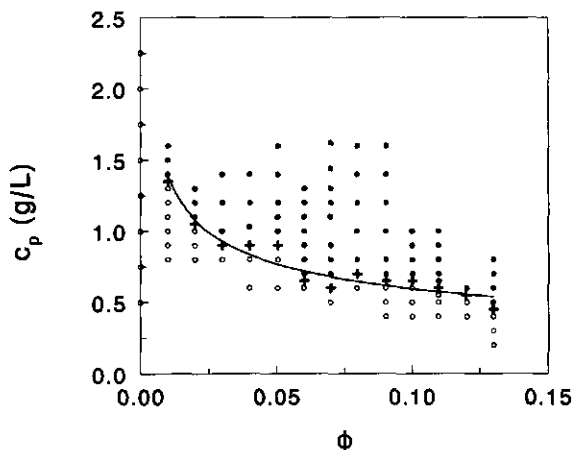


Figure 3 Visually observed phase diagram for various EPS concentrations (c_p) and volume fractions of the casein micelles (ϕ). Indicated are the phase boundaries (plusses), stable mixtures (open circles) and unstable mixtures (filled circles).

In the course of time the upper layer becomes fully transparent. After about one week the upper phase has the same appearance as skim milk permeate. This indicates that the bottom layer is concentrated in casein micelles: their density is slightly higher than that of the permeate. We measured the EPS and casein concentration in the upper layer. For instance at $\phi=0.07$, samples with initial EPS concentrations of 0.75, 1.00 and 1.25 g/L had an EPS concentration in the upper layer of 0.87, 1.03 and 1.33 g/L respectively after phase separation.

The volume fraction of casein micelles in the upper phase was always smaller than $\phi=0.01$. Systematically, there is a slight increase in the EPS concentration in the upper transparent layer while the caseins are highly concentrated in the lower phase. This is the first confirmation that the type of phase separation originates from depletion interaction and not bridging since polysaccharides and proteins are separated into two separate phases. If the mechanism would be bridging flocculation, polysaccharides and proteins are expected to concentrate in one of the two phases.

Another aspect which indicates that we are dealing with depletion flocculation is the fact that the flocculation is reversible. After initial phase separation the system can be mixed, after which it takes some time before the system becomes phase separated again. If a sample prepared with such a composition that it is located just above the phase separation threshold is shaken and subsequently diluted with skim milk permeate it remains stable. In the case of bridging flocculation, sedimentation or creaming is always irreversible. Moreover, in the case of bridging flocculation the limiting polymer concentration increases with increasing ϕ . Also this last characteristic of bridging was not found.

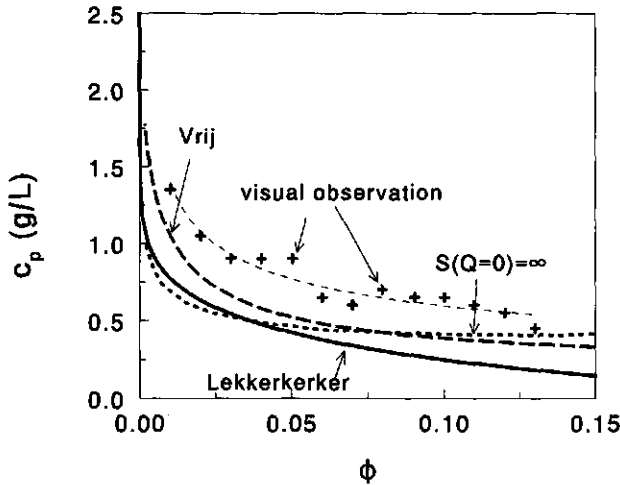


Figure 4 Comparison of theoretically calculated phase lines with the visually observed phase boundary (plusses), which is replotted as a dashed curve to guide the eye. The phase diagrams calculated with the various models are indicated as Lekkerkerker [14], Vrij [11] and $S(Q=0)=\infty$ (obtained by combining Vrij's theory with Gillan's method [20]).

*Theoretical description**- The Vrij model*

We have set the parameters in the model such that they comply with the experimental conditions for casein micelles and EPS: $\sigma_c=200$ nm, $M=1.47 \cdot 10^3$ kg/mol and $\alpha_p=2 \cdot R_g$, with $R_g=86$ nm for the radius of gyration. The resulting spinodal curve is plotted in Figure 4 (long dashes), in which the phase boundary as observed visually is also given (symbols). The calculated phase line lies below the experimental phase boundary, but the difference is small. Also the shapes of the curves are similar. It should be noted that we calculated the phase boundary from independently measured characteristic parameters of the system; there is no data fitting.

As the next step we calculated the polymer concentrations for which $S(Q=0)$ goes to infinity. This was done by insertion of Vrij's interaction potential profile $U(r)$ (equation 3) into equation 11. In order to solve $g(r)$ by combining equations 10 and 11, we used Gillan's approach [20]. From the radial distribution function obtained in this way $S(Q)$ was subsequently calculated with equation 9. By iteration we calculated at which polymer concentration $S(Q=0)$ approaches infinity and the resulting phase diagram (spinodal) is plotted in Figure 4 (short dashes). In this way we implicitly accounted for multiple interactions, whereas Vrij's model is on the pair level. This phase line corresponds reasonably well to those calculated with the Lekkerkerker and Vrij models.

It must be realized that, except for the critical point the spinodal always lies above the binodal. Still, from the above it follows that a reasonable prediction can be made from the Vrij theory, which does not contain any adjustable parameters. The differences between experimental and theoretical phase boundary can further be explained by realizing that the casein micelles (and EPS) are not monodisperse. A model developed by Chu *et al.* [35] indicates that polydispersity of the colloidal particles weakens depletion interaction effects also and thus shifts the theoretical curves upwards.

- Lekkerkerker theory

In the region where we observed phase separation visually the theory of Lekkerkerker *et al.* [14] predicts a colloidal gas-liquid transition. For our system with $\zeta=0.86$, we have calculated the phase diagram. After calculating c_p from the overall reservoir concentration c_p^R by multiplying with α from equation 13, equations 12 and 14-16 allow a calculation of the binodal. The calculated phase diagram is given for the relevant ϕ range in Figure 4. This shows that the Vrij and Lekkerkerker models give approximately the same phase line. The comparison of theoretical predictions of the phase diagram with that of a model colloid-polymer mixture has

already been done by Ilett *et al.* [36]. In this paper it is shown however that the concepts of depletion interaction allow a quantitative description of mixtures of proteins and polysaccharides, illustrating the importance of depletion interaction in biological and food systems.

The calculations given assume that the thickness of the depletion layer Δ is independent of c_p . Fleer *et al.* [21] developed a theory from which the decrease of Δ as a function of c_p can be calculated. In the appendix we have calculated the $\Delta(c_p)$ dependence, which shows that Δ has a constant value in our relevant concentration region. This means that we do not have to incorporate a $\Delta(c_p)$ dependence in our calculations. Any effect would have shifted the calculated curves upward.

Phase diagram from self-diffusion

The diffusion coefficients were determined as described previously [28] for a series of polymer concentrations at various volume fractions. At every volume fraction we calculated the diffusion coefficient at the spinodal by combining equations 19 and 20. For the moment we neglect viscosity corrections as described by equations 22 and 23. Subsequently, we used the measured self-diffusion coefficients to infer at which polymer concentration the spinodal is situated. We plotted these spinodal points in Figure 5 (circles). The data are consistent with the experimental (observed) phase boundary although the phase boundary derived from the self-diffusion coefficient measurements is lower. The discrepancy may originate from the fact that just above the phase boundary nucleations of the new phase are extremely slow (and hence not observable). Another point is that the application of Baxter's sticky sphere model is hardly justified in view of the long range of the depletion interaction potential. Nevertheless, its use helps us to understand the phase behavior.

Another aspect not fully accounted for is the viscosity experienced by the particles. We have calculated an effective viscosity from equation 22 and used equation 23 to correct the self-diffusion coefficient and, hence, the Baxter parameter τ_b . For the calculation of the effective viscosity we took the average end-to-end distance of EPS molecules as 211 nm as calculated from the radius of gyration for R^p . The data in ref. 31 are described in the best way if the end-to-end distance is taken for R^p . With $R^s=100$ nm this gives $\zeta_r \approx 2.11$. Then we used equations 19, 22 and 23 to calculate the corresponding polymer concentration at the spinodal for every measured volume fraction. The result is plotted in Figure 5 (diamonds); it is consistent with the observed phase behavior.

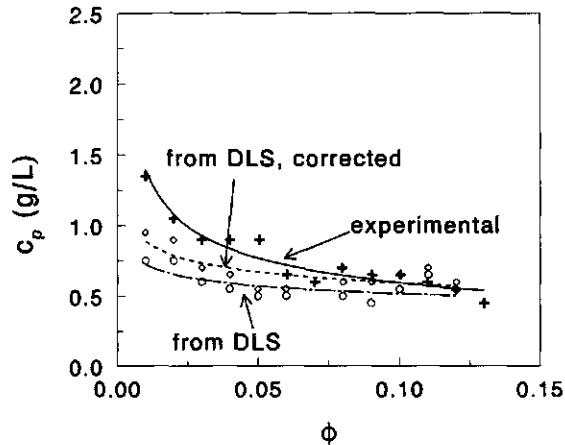


Figure 5 Phase diagram with visually observed phase boundaries (plusses) and phase boundaries calculated from self-diffusion coefficient measurements. The results from the approach which uses equation 19 are given by the circles and those obtained with equation 22 are given by the diamonds. The curves are drawn to guide the eye.

Conclusions

Phase separation caused by depletion interaction is observed when EPS is mixed with casein micelles. This polysaccharide is a non-adsorbing biopolymer with respect to casein micelles. Various theoretical models were compared with the observed phase threshold and gave good predictions of the stability limit. We were also able to calculate a phase diagram from dynamic light scattering experiments, and found it to be consistent with observations.

Acknowledgment

We thank the late Cyril Renaud for doing many experiments. Professor H.N.W. Lekkerkerker and Gerrit Vliegenthart (Van't Hoff laboratory, Debye Institute, Utrecht University) are thanked for encouraging discussion and their help with the calculations of the phase boundary with the Lekkerkerker model. Dr. E. Ten Grotenhuis and Dr. S.P.F.M. Roefs from NIZO food research are thanked for their interest.

Appendix

In this section we will give some results for the depletion layer thickness near a flat plate as can be obtained from self-consistent field (SCF) theory. In the theories of Vrij and Lekkerkerker it is assumed that changing the polymer concentration does not affect the depletion layer thickness Δ . De Gennes [37], however, showed theoretically that the correlation length of concentration fluctuations ξ , which depends on the polymer concentration, is a good measure for Δ and gave the following scaling law for the concentration dependence of ξ :

$$\xi \sim c_p^{-m} \quad \text{A1}$$

where m is a scaling parameter which is zero in the dilute regime and takes values of 3/4 (good solvent) or 1 (θ -solvent) in the semi-dilute regime.

Hence, in the semi-dilute regime Δ is a decreasing function of c_p . This can be understood by realizing that at very high polymer concentrations the osmotic pressure Π_p becomes very high, which will push the polymer molecules into narrower gaps, giving smaller Δ values. Eventually, Δ becomes zero, which agrees with the observation that mixing colloidal spheres with polymer melts often does not give a phase separation.

In order to calculate the concentration dependence of Δ , the self-consistent field (SCF) theory of Scheutjens and Fleer [38] can be used. This theory is based upon a mean-field approach ($m=1/2$) and enables evaluation of the segment density profile of polymer molecules situated between two flat plates as a function of the plate separation at a given adsorption energy. In the SCF theory the polymer chains are described as weighted walks upon a lattice. The polymers are considered to behave as Kuhn chains [39]. For a Kuhn chain, the root-mean-square end-to-end distance, $\langle R^2 \rangle^{1/2}$, follows from the number N_k of Kuhn segments and the length l_k of such a segment as [40]:

$$\langle R^2 \rangle = l_k^2 N_k \quad \text{A2}$$

For long chains the radius of gyration R_g equals $\sqrt{\langle R^2 \rangle / 6}$. However, real chains with N segments, each of length l , cannot be directly described as random-flight chains. The values for l and N can be translated to l_k and N_k by demanding equal contour lengths for the Kuhn chain and the real chain:

$$L \equiv lN = l_k N_k \quad \text{A3}$$

When R_g has been measured, the quantity l_k can then be calculated from equation A2 as $l_k = \langle R^2 \rangle^{1/2} / N_k^{1/2} = 6R_g^2 / L$ and N_k follows as L / l_k .

Fleer *et al.* [21] studied the segment density profile for non-adsorbing polymer in a solution which is near $\chi=0.5$ (θ -solvent), where χ is the Flory-Huggins segment-solvent interaction parameter, and obtained an analytical expression for Δ :

$$\sin^2\left(\frac{\pi/2}{2\Delta/l_k+1}\right) = \left(\frac{1.95}{N_k}\right)\left(1 + \frac{2.84}{\sqrt{N_k}}\right) - \ln(1-\phi_b) - 2\chi\phi_b \quad \text{A4}$$

where ϕ_b is the bulk volume fraction of polymer molecules. We calculated the $\Delta(c_p)$ dependence for $\chi=0.3$ and 0.5 which represent values usually found experimentally for polymers. The results are given in Figure A1. For polymer molecules in a 'good' solvent usually $\chi \approx 0.3-0.4$, leading to a result in between the curves drawn in Figure A1. The calculations were performed with $N_k=153$ and $l_k=17$ nm, calculated from equations A2 and A3 by using the radius of gyration and $L=2.60$ μm as reported previously [5]. Furthermore, the density of a B40 EPS melt was estimated as 1000 kg/m^3 .

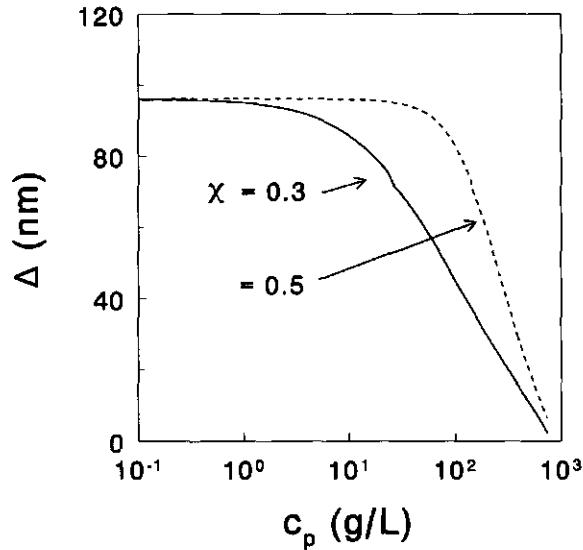


Figure A1 Calculated depletion layer thickness Δ as a function of the polymer concentration according to equation A4 for Flory-Huggins parameters as indicated in the plot.

In Figure A1 it is shown that Δ has a value of 96 nm at $c_p < 1$ g/L, which nearly agrees with $\Delta = R_g$. Above this concentration, Δ decreases as a function of c_p , as can be expected since $c_p^* = 0.92$ g/L. In the concentration region where we observe and calculate phase separation (from 0.3 to 1.5 g/L), the decrease of Δ as a function of c_p can be neglected and Δ has a constant value. This means that we do not have to incorporate a $\Delta(c_p)$ dependence in our calculations.

References

- [1] Beijerinck, M.W., *Zentralbl. Bakteriol. Parasitenkd. Infektionskr. 2 Abt.* **2** (1896) 697.
- [2] Tolstoguzov, V.B., *Food Hydrocolloids* **4** (1991) 429.
- [3] Tolstoguzov, V.B., in: '*Food Colloids and polymers : stability and mechanical properties,*' E.Dickinson, P.Walstra, Eds., Royal Soc. Chem., **113**, 1992.
- [4] Antonov, Yu.A., Soshinskii, A.A., Glotova, Yu.K., *Appl. Biochem. Microbiol.*, **30** (1994) 760.
- [5] Tuinier, R., Zoon, P., Olieman, C., Cohen Stuart, M.A., Fleer, G.J., de Kruif, C.G., *Biopolymers* **49** (1999) 1; Chapter 2 of this thesis.
- [6] De Kruif, C.G., *Langmuir* **8** (1992) 2932.
- [7] Jeurnink, Th.J.M., De Kruif, C.G., *J. Dairy Res.* **60** (1993) 139.
- [8] Traube, J., *Gummi Ztg.* **39** (1925) 434.
- [9] Vester, C.F., *Kolloid Z.* **84** (1938) 63.
- [10] Asakura, S., Oosawa, F., *J. Chem. Phys.* **22** (1954) 1255; *J. Pol. Sci.* **33** (1958) 183.
- [11] Vrij, A., *Pure & Appl. Chem.* **48** (1976) 471.
- [12] De Hek, H., Vrij, A., *J. Colloid Interface Sci.* **84** (1981) 409.
- [13] Lekkerkerker, H.N.W., *Colloids Surf.* **51** (1990) 419.
- [14] Lekkerkerker, H.N.W., Poon, W.C.K., Pusey, P.N., Stroobants, A., Warren, P.B., *Europhys.Lett.* **20** (1992) 559.
- [15] Poon, W.C.K., Pusey, P.N., in: '*Observation and Simulation of Phase Transitions in Complex Fluids,*' M. Baus, L.F.Rull, J-P.Ryckaert (Ed.) , Kluwer, Dordrecht, The Netherlands, 1995, p. 3.
- [16] McQuarrie, D.A., *Statistical Mechanics*, Harper & Row, New York, 1976.
- [17] Lyklema, J., '*Fundamentals of Colloid and Interface Science,*' Volume 1, Chapter 2, Academic press, 1991.
- [18] Ornstein, L.S., Zernike, F., *Proc. Koninkl. Nederland Akad. Wetenschap, Amsterdam*, **17** (1914) 793.
- [19] Hansen, J.P., McDonald, I.R., '*Theory of simple liquids,*' Academic Press, New York, 1976.
- [20] Gillan, M.J., *Mol. Phys.*, **38** (1979) 1781.
- [21] Fleer, G.J., Scheutjens, J.M.H.M., Vincent, B., in: '*Polymer adsorption and dispersion stability,*' ACS Symp. Ser. **240** (1984) 245.

- [22] Percus, J.K., Yevick, G.J., *Phys. Rev.* **110** (1958) 1.
- [23] Hall, K. R., *J. Chem. Phys.* **57** (1972) 2252.
- [24] Frenkel, D., Ladd, A., *J. Chem. Phys.* **81** (1981) 3188.
- [25] Baxter, R.J., *J. Chem. Phys.* **49** (1968) 2770.
- [26] Watts, R.O., Henderson, D., Baxter, R.J., *Adv. Chem. Phys.* **21** (1971) 421.
- [27] Penders, M.H.G., Vrij, A., *Adv. Colloid Interface Sci.* **36** (1991) 185.
- [28] Tuinier, R., de Kruij, C.G., In: 'Gums and Stabilisers for the Food Industry,' P.A. Williams, G.O. Phillips, Eds., p. 222, 1998.
- [29] Cichocki, B., Felderhof, B.U., *J. Chem. Phys.* **93** (1990) 4427.
- [30] Tuinier, R., Zoon, P., Cohen Stuart, M., A., Fleer, G.J., de Kruij, C.G., submitted; Chapter 3.
- [31] Hoogveen, N.G., Hoogendam, C.W., Tuinier, R., Cohen Stuart, M.A., *Int. J. Pol. Anal. Char.* **1** (1995) 315.
- [32] Cukier, R.I., *Macromolecules* **17** (1984) 252.
- [33] De Gennes, P.G., *Macromolecules* **9** (1976) 594.
- [34] Tong, P., Ye, X., Ackerson, B.J., Fetters, L.J., *Phys. Rev. Lett.* **79** (1997) 2363.
- [35] Chu, X.L., Nikolov, A.D., Wasan, D.T., *Langmuir* **12** (1996) 5004.
- [36] Ilett, S.M., Orrock, A., Poon, W.C.K., Pusey, P.N., *Phys. Rev. E* **51** (1995) 1344.
- [37] De Gennes, P.G., *Macromolecules* **14** (1981) 1637; **19** (1982) 492.
- [38] Scheutjens, J.M.H.M., Fleer, G.J., *J. Phys. Chem.* **83** (1979) 1619; *J. Phys. Chem.* **84** (1980) 245.
- [39] Kuhn, W., *Kolloid Z.*, **68** (1934) 2.
- [40] Flory, P.J., 'Principles of Polymer Chemistry,' Cornell University Press, New York, 1953.

Phase separation, creaming, and network formation of oil-in-water emulsions induced by an exocellular polysaccharide

Abstract

We have investigated the effect of an exocellular polysaccharide (EPS) on the phase behavior and the rheology of oil-in-water emulsions. Already at low EPS concentrations the phase separation occurs. The phase line can be described by depletion interaction theory. At high EPS concentrations and dispersed phase volume fractions above 10% there is a stable 'gel'-like region in the phase diagram.

A kinetic study showed that the rate of creaming decreases with increasing oil content due to hydrodynamic effects. This rate depends strongly on the concentration of EPS, which is related to the strength of the depletion interaction and the viscosity of the continuous phase. At low EPS concentration the creaming rate strongly increases with EPS concentration because of the stronger attraction. At higher EPS concentrations creaming is slowed down by the viscosity increase of the continuous phase and of the particle network which is formed. At high EPS concentrations this network becomes so strong that the gel prevents creaming. The rheological behavior of the "gel" was studied by measuring flow curves, which could be interpreted by a theoretical model for weakly aggregating particles.

hydrodynamic interaction and the corrected creaming/sedimentation velocity u_h for hard spheres becomes:

$$\frac{u_h}{u} = 1 - \phi \left(\frac{5 - 3\phi + \phi^2}{1 + 2\phi} \right) \quad 2$$

where ϕ is the volume fraction of the hard spheres.

In the following we assume that the relative creaming velocity u_h/u equals the relative displacement rate v_h/v [24]. The displacement rate v is the rate of the boundary between the cream (oil-rich) upper phase and the lower (clear) phase during creaming. An increase in the volume fraction of oil slows down the creaming rate as predicted by equation 2. An increase of the EPS concentration can affect the creaming rate in various ways. A hydrodynamic effect upon adding EPS is the increase of the macroscopic shear viscosity of the continuous phase. EPS also induces depletion interaction between the oil droplets, which in turn increases the creaming velocity u_h since the particles become mutually attractive. In order to calculate u_h for suspensions in the stable region in the presence of polymer we use the generalized Stokes-Einstein equation [25]:

$$\frac{u_h(c_p)}{u_h(c_p=0)} = \frac{S(Q=0)D_c(Q=0)}{S(Q=0)_{HS}D_0} \quad 3$$

where $u_h(c_p=0)$ is the creaming velocity in the absence of EPS, and $S(Q=0)$ is the value of the structure factor at zero wavevector Q ; it is proportional to the osmotic compressibility. $S(Q=0)_{HS}$ is the structure factor of hard spheres (without attractions). The parameter D_0 is the diffusion coefficient of the particles in a solvent without EPS and $D_c(Q=0)$ is the short-time collective diffusion coefficient of the creaming particles at $Q=0$. We calculate $S(Q=0)$ from the second osmotic virial coefficient $B_2(c_p)$, which follows from the theory of Vrij [20] by using the approximation:

$$S(Q=0) = \exp(-2B_2(c_p)\phi) \quad 4$$

which is valid for hard spheres [26] and adhesive hard spheres [27] up to $\phi=0.4$. For hard spheres equation 4 becomes $S(Q=0)_{HS} = \exp(-8\phi)$. The diffusion coefficient is approximated by dividing D_0 by the relative viscosity of the polymer solution:

$$D_c(Q=0) = \frac{D_0}{1 + [\eta]c_p + \frac{1}{25} \{[\eta]c_p\}^{3.5}} \quad 5$$

where $[\eta]$ is the intrinsic viscosity. This correction factor is motivated by the work of Imhof *et al.* [28], Kops-Werkhoven [29], and van der Werff and De Kruijff [30]. These authors showed that for a suspension of hard spheres the relative diffusion coefficient is very well approximated by the inverse relative viscosity of the dispersion.

At the binodal, $S(Q=0)$ reaches a certain value and it is uncertain how $S(Q=0)$ behaves in the unstable regions. Simplistically, we assume that in the unstable region $S(Q=0)$ does not depend on the polymer concentration:

$$S(Q=0) = \exp(-2B_2(c_p^{\text{bin}})\phi) \quad 6$$

where c_p^{bin} is the polymer concentration at the binodal for the given value of the oil volume fraction ϕ . The driving force of the phase separation process is then constant, and no longer a function of c_p . The friction, however, increases with c_p as shown in equation 5. We assume that this equation is still valid in the unstable region, even though in the unstable regions clusters will be formed consisting of aggregated oil droplets. These clusters thus feel a friction during creaming which is equal to that in the EPS solution (the continuous phase).

The viscosity of weakly aggregated dispersions

We measured the viscosity of the emulsions as a function of the shear rate in order to characterize the attractive forces between the oil droplets in the emulsions as induced by the EPS. When these forces are strong enough the system no longer phase separates but behave as "weak gels". The behavior of such so-called weakly flocculated suspensions can be described with the model of Potanin *et al.* [31] for dispersions of aggregating particles. This model considers an aggregate as a fractal structure with a radius R_{agg} containing N primary particles:

$$N = \left(\frac{R_{\text{agg}}}{a} \right)^{d_f} \quad 7$$

where a is the radius of the primary particles and d_f is the fractal dimensionality. The fractal concept is only used here to describe the dimensionality of the network. When the shear rate is increased it is assumed that the aggregates break down, which leads to a shear-rate-dependent volume fraction of the aggregates. For the viscosity of the dispersions Krieger's equation is used [32]:

$$\eta(\dot{\gamma}) = \eta_c \left(1 - \frac{\phi_a(\dot{\gamma})}{\phi_{\text{max}}} \right)^{-2.5\phi_{\text{max}}} \quad 8$$

where $\eta(\dot{\gamma})$ is the viscosity at a shear rate $\dot{\gamma}$, η_c the viscosity of the continuous phase, $\phi_a(\dot{\gamma})$ the volume fraction of the aggregated flocs ($\approx \phi$ for $\dot{\gamma} \rightarrow \infty$), and ϕ_{max} the maximum volume fraction (0.63 for random close packing).

Furthermore, Potanin *et al.* [31] introduced a break-up criterion: the maximum stress an aggregate can withstand. This gives a second relation between the variables $\eta(\dot{\gamma})$ and ϕ_a :

$$\eta(\dot{\gamma})\dot{\gamma} = \frac{2C_{rup}k_{el}}{5\pi a \left(K^{-d_f} \frac{\phi_a(\dot{\gamma})}{\phi} \right)^{3/(3-d_f)}} \quad 9$$

where C_{rup} is a numerical coefficient characterizing the fragility of the bond between the primary particles, and K is defined below. The parameter k_{el} is the spring constant between the particles, which equals $d^2U(r)/dr^2$ at $r=r_{min}$, where r_{min} is the distance from the center of the particle where the interaction potential has its minimum. The exact value of k_{el} depends on the details of the repulsive part of the potential. In a simple approach we assume:

$$k_{el} \sim c_p \quad 10$$

for particles interacting through depletion. The quantity K in equation 9 is defined as:

$$K = \frac{0.72}{\sqrt{1 + \frac{2}{d_f}}} \quad 11$$

Using equations 8-11 it is possible to solve η as a function of $\dot{\gamma}$. In our case we are dealing with a polymer solution which is also shear thinning, affecting the value of η_c . We use Bueche's theory for the shear-rate dependence [33], which gives a good description of the shear-rate dependence of the viscosity of (B40) EPS solutions in 0.10 M salt solutions [34]. For η_c we can write:

$$\frac{\eta_c(\dot{\gamma}) - \eta_s}{\eta_0 - \eta_s} = 1 - \frac{6}{\pi^2} \sum_{p=1}^{10} \frac{(\dot{\gamma} \tau_1)^2}{p^2(p^4 + \dot{\gamma}^2 \tau_1^2)} \left(2 - \frac{(\dot{\gamma} \tau_1)^2}{p^4 + \dot{\gamma}^2 \tau_1^2} \right) \quad 12$$

where η_s is the solvent viscosity, η_0 the viscosity at zero shear, and τ_1 the longest relaxation time from the theory of Rouse [35]:

$$\tau_1 = \frac{6(\eta_0 - \eta_s)M}{\pi^2 RT c_p} \quad 13$$

The zero shear viscosity η_0 of the EPS solution can be calculated from [34]:

$$\eta_0 = \eta_s \left(1 + [\eta] c_p + \frac{1}{25} [\eta]^{3.5} c_p^{3.5} \right) \quad 14$$

The EPS concentration was corrected for the oil volume fraction ($c_p^R = c_p / (1 - \phi)$).

Materials

The experiments were carried out with an emulsion prepared from sunflower oil (Reddy), demineralized water and NaNO_3 added to achieve a ionic strength of 0.10 M. As emulsifier we used 10 g/L Bipro, a whey protein isolate containing 71% (w/w) β -lactoglobulin, 12% α -lactalbumin, 5% immunoglobulin, 5% bovine serum albumin, 2% salt, 1% lactose and 4 % water. The whey protein isolate (WPI) powder was purchased from Domo Food Ingredients, Beilen, The Netherlands. Thiomersal (sodium ethylmercurithiosalicylate, BDH Chemicals), was added (0.03 % (w/w)) to prevent bacterial growth.

The EPS was produced at the pilot-plant facility at NIZO [36]. *Lactococcus lactis* subsp. *cremoris* NIZO B40 was used to inoculate a whey permeate medium. After EPS production EPS was isolated using a sequence of filtration steps [36]. This preparation was freeze-dried and used as such in this study. The EPS has a (number-averaged) molar mass (M) of $1.47 \cdot 10^6$ g/mol and a number-averaged radius of gyration (R_g) of 86 nm, and has a small polydispersity [36]. The polymer overlap concentration c_p^* , which equals $3M/4\pi R_g^3 N_{AV}$, where N_{AV} is Avogadro's number, is 0.9 ± 0.1 g/L.

Methods

Preparation of the emulsion mixtures

The emulsifier was dissolved in demineralized water with salt (NaNO_3 , 0.1 M) and the oil was added under continuous stirring. This pre-emulsion was mixed with an Ultra Turrax (Polytron, Switzerland) for one minute and subsequently homogenized with a Rannie (type 8.30 H). The emulsion obtained in this way was stored at 5°C .

Mixtures of emulsion and EPS were prepared by dissolving EPS in 0.10 M NaNO_3 solution and mixing it (Vortex) with an appropriate amount of the emulsion so as to obtain the required composition. The samples were stored at 5°C.

Experimental techniques

The particle size distribution (PSD) of the emulsion droplets was measured with a Malvern Master Sizer X (MSX) using a He/Ne laser with a wavelength of 632.8 nm. The forward scattering intensity is used to calculate the particle size distribution by Malvern's proprietary software.

The density of the emulsion was measured at 5.0°C with a DMA 45 Digital Density Meter (Anton Paar, Austria). The measuring principle of this instrument is based on the change of the frequency of a hollow oscillator when filled with a liquid or gas. A simple relationship between the density of the sample and the natural frequency of the filled oscillator makes it possible to determine the density of samples which are injected into the oscillator.

Turbidity measurements were made with a Turbiscan MA 1000. This instrument measures the intensity of the back-scattered light along the height of the 1 cm diameter glass tubes containing the emulsion mixtures.

For the rheological measurements, a controlled stress CSL² 500 Rheometer (TA Instruments™) was used. The Rheometer is connected to a water bath which was set at 5.0°C. We used a concentric (Couette type) cylinder geometry with radii of 8.60 and 9.33 mm. The bottom of the cylinder is tapered and the gap was set at 5.0 mm. We applied a shear-rate ramp, and determined the viscosity at shear rates in the measurable range from 10 to 550 s⁻¹. The ramp lasted 30 minutes but a ramp of 15 or 45 minutes gave the same result. We tested whether there was wall slip using a roughened concentric cylinder geometry and found that it was absent.

Emulsion stability

In order to check whether the emulsion droplets themselves were stable, we regularly measured the size distribution of the emulsion droplets with the Malvern Master Sizer X. The average diameter (and the size distribution) will change when the emulsion droplets coalesce. A stock emulsion with $\phi=0.5$ was prepared. At this volume fraction no significant creaming takes place within 6 weeks. Every month a new emulsion was prepared. We prepared emulsions with a σ_{21} ($\sigma_{ab} = \sum N_i \sigma_i^a / \sum N_i \sigma_i^b$) of $0.9 \pm 0.2 \mu\text{m}$ and a σ_{32} of $1.3 \pm 0.3 \mu\text{m}$, indicating rather polydisperse emulsions. The particle size distribution did not change in time within 6 weeks after preparation. We checked that slight size differences between the various batches did not significantly change the creaming rate.

The density of emulsion was measured for different volume fractions. Measurements were made at 5.0°C. For the pure oil we found 930.7 kg/m³ and for water 999.7 kg/m³, and the volume fraction dependence was found to be approximately linear ($\rho \approx \rho_o \phi + \rho_w [1 - \phi]$).

Results and discussion

Phase diagram

All emulsions with a volume fraction of 0.40 and lower containing no or a small amount of EPS demixed. Demixing is here defined as the concentration of oil droplets in one phase, and covers both creaming and phase separation. In some mixtures, depending on the concentration of EPS and the volume fraction of oil droplets ϕ , a phase separation can be observed. A phase separation is characterized by a sharp interface, whereas there is no interface if there is only creaming; there is only a gradient in the oil droplet concentration. If there is a phase separation, the mixture separates into two phases: an upper phase enriched in oil and a lower phase enriched in EPS. As the interface rises the lower (EPS-rich) phase becomes more transparent. An example of the phase separation process is given in Figure 1. These pictures show that the emulsion droplets cluster with time. It is also shown that the droplets do not coalesce. Their clustering is attributed to the depletion force exerted by the EPS.

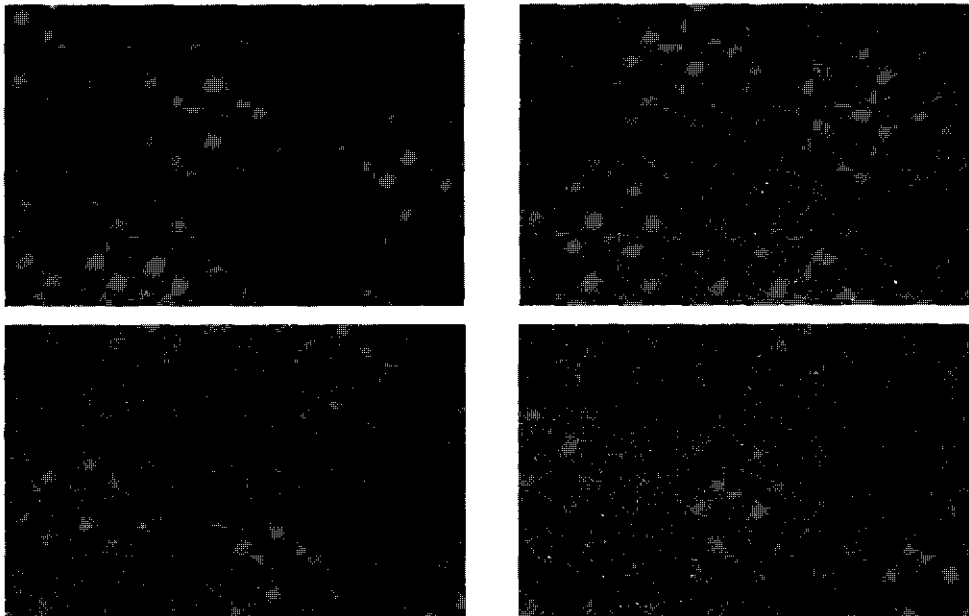


Figure 1 Photomicrographs of a mixture of EPS (0.13 g/L) and emulsion droplets (1%) at $t=0$ (upper left) and after 4.5 (upper right), 10 (lower left) and 20 minutes (lower right); 320 times magnification.

At high ϕ (>0.2) it is difficult to observe a phase separation because the volume of the EPS-rich phase is small for such systems. In order to distinguish between a phase separation and creaming we used the results obtained with the Turbiscan. We take the demixing as a phase separation when the two phases are separated by a sharp interface, whereas (enhanced) creaming is recognized as a more gradual change of the back-scattering signal along the sample height. Mathematically, when the slope $d\Sigma/dh$, where Σ is the intensity of the back-scattering signal and h is the sample height, is infinite at the interface, the sample is phase separated, whereas only creaming occurs when $d\Sigma/dh$ has a finite value for all h in the range $0 < h < h_t$, where h_t is the total sample height.

The phase behavior is presented in Figure 2. Filled squares refer to systems which exhibit only creaming (at low c_p) or belong to the stable 'gel' region (high c_p). The open circles refer to systems undergoing a phase separation. The solid line was calculated from the theory of Vrij [20], using $\sigma_{32}=1.3 \mu\text{m}$, $R_q=86 \text{ nm}$ and $M=1460 \text{ kg/mol}$ [36] and gives a good estimate for the phase line, taking into account the large dispersion in emulsion droplet size. Since the phase line lies below the overlap concentration (0.9 g/L) it is reasonable to approximate the osmotic pressure as $c_p RT/M$.

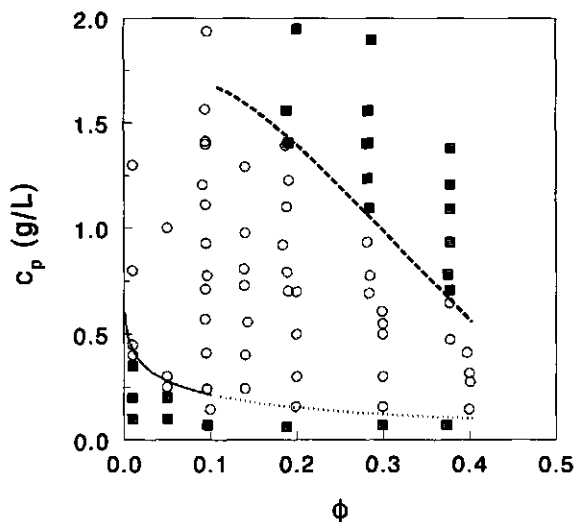


Figure 2 Phase diagram of an emulsion mixed with EPS. Filled squares refer to the stable regions and open circles to phase-separated systems. The dashed curve indicates the 'gel'-line and the solid curve (followed by a dotted curve) corresponds to the spinodal as calculated from the theory of Vrij [20].

In the theory of Vrij the colloidal particles are assumed to behave as hard spheres, whereas the emulsion droplets may be somewhat adhesive initially. For adhesive spheres B_2 , the second osmotic virial coefficient, is smaller than 4 (the value for hard spheres) as used in the theory of Vrij [20]. For adhesive spheres phase separation will be attained at lower concentrations than calculated from the Vrij theory. At high values of ϕ (where the calculated phase line is indicated as a dashed curve) the Vrij theory may no longer be valid since then higher-order virial coefficients have to be taken into account.

'Gel'-region

At high volume fractions the system no longer phase separates when the EPS concentration exceeds a certain value, as indicated by the filled squares in Figure 2 at high ϕ and high c_p . These mixtures have a (weak) gel-like consistency which agrees with the results of Verhaegh [37], Pusey *et al.* [38] and Poon *et al.* [39], who observed gelation in model colloid-polymer mixtures with a short-range attraction. It is found theoretically that, if the range of the attractions between the particles is narrow, a colloidal aggregation can interfere with the phase separation process when the potential well is sufficiently deep.

The process of colloidal aggregation creating a space-filling network of aggregated particles is called percolation. The percolated phase consists of an infinitely large cluster of Brownian particles. The percolation line was calculated by Chiew and Glandt [40] from the Ornstein-Zernike equation [41] in the Percus-Yevick [42] approximation. At this percolation threshold the following equation holds:

$$\tau_B = \frac{19\phi^2 - 2\phi + 1}{12(1-\phi)^2} \quad 15$$

where τ_B is the Baxter parameter [43] which is inversely proportional to the strength of attraction and which is thus related to c_p . Kranendonk and Frenkel [44] performed Monte Carlo simulations of suspensions of sticky hard spheres (given τ_B) and their results were consistent with equation 15. Since the emulsion droplets are relatively large compared to the EPS (the relative range of attraction equals $2R_d/\sigma_{32} \approx 0.13$) we may compare our system with a suspension of sticky spheres for which the attraction is infinitely narrow. Previously we found an exponential dependence of τ_B on c_p : $\tau_B \sim c_2 \exp(-c_p/c_1)$ [45], where c_1 is a reference concentration and c_2 is a constant. Hence, we have fitted the polymer concentration c_p^{gel} at the 'gel'-line to $c_1 \ln[c_2 12(1-\phi)^2 / (19\phi^2 - 2\phi + 1)]$, where c_1 and c_2 are used as fitting parameters. The result is plotted in Figure 2 (dashed curve); in this case $c_1 = 0.825$ g/L and $c_2 = 0.642$. The experimental 'gel'-line agrees quite well with equation 15 combined with $\tau_B \sim c_2 \exp(-c_p/c_1)$.

It must be realized that the space-filling network of weakly aggregating oil droplets has a dynamic, statistical character. Bonds are broken and formed spontaneously. At very low volume fraction ($\phi < 0.20$), the concentration of EPS has to be very high to induce a gel. For $\phi = 0.10$, a lower phase with a small volume is observed at an EPS concentration > 2 g/L. It seems that a sort of network is formed but it is not yet strong enough to withstand the creaming process. In order to get an idea of the time scales involved to induce phase separation we studied the kinetics of demixing.

Demixing kinetics

From the back-scattering measurements we analyzed the change in position of the interface in time and we calculated the relative volume R_l of the lower phase, defined as $R_l = V_l/V_{tot}$, where V_l is the volume of the lower phase and V_{tot} is the total volume of the mixture. First, we studied the creaming behavior of the emulsion (without EPS). In Figure 3 R_l is plotted as a function of time for $\phi = 0.10, 0.20, 0.30$ and 0.40 . The upper phase (enriched in oil droplets) acquires a larger volume with increasing ϕ , which can be understood since the maximum value of R_l , R_l^{max} , is a function of ϕ : $R_l^{max} = 1 - \phi_0/\phi_{max}$, where ϕ_0 is the initial volume fraction and ϕ_{max} the volume fraction of the oil droplets at close packing. The time scale of creaming can be estimated by calculating the creaming velocity u with equation 1. For $\rho_o = 930$ kg/m³, $\rho_w = 1000$ kg/m³, $g = 9.81$ m/s², $\eta_c = 1.50 \times 10^{-3}$ Pa·s (water at 5.0°C), and σ_c (for which we took σ_{32}) = 1.3 μ m, we find $v = 4.3 \times 10^{-9}$ m/s. Roughly estimating we can say that an average oil droplet has moved 3.0 cm (half the sample height of 6.0 cm) when R_l has become $\frac{1}{2} R_l^{max}$, which takes approximately 8 days; this is a reasonable guess for $\phi = 0.10$ in Figure 3. The curves drawn in Figure 3 are not directly comparable in terms of kinetics, because the maximum volume of the lower phase is different for each sample. Therefore we have fitted the curves to:

$$R_l(t) = R_l^{max} \left(1 - e^{-v_h t} \right) \quad 16$$

which can be used to describe first-order rate processes. In equation 16 v_h has the units s⁻¹ (the length scale is normalized by using the dimensionless volume R_l/R_l^{max}). By fitting $R_l(t)$ with this equation, v_h can be determined. The parameter v_h equals the initial creaming rate since:

$$\left[\frac{d}{dt} \left(\frac{R_l}{R_l^{max}} \right) \right]_{t \rightarrow 0} = v_h \quad 17$$

It is remarkable how well this ad hoc description fits the data. We can now compare the samples because only one parameter describes the characteristics of the demixing kinetics.

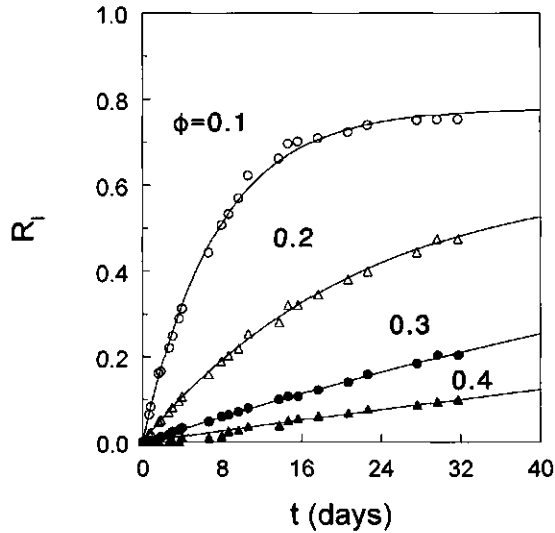


Figure 3 Creaming behavior of the emulsion, represented by the relative volume of the lower phase R_1 , for various ϕ values as a function of time. The drawn curves were fitted using equation 16.

In Figure 4 we plotted v_h as a function of ϕ (symbols), which shows that v_h strongly decreases with increasing ϕ . The dashed curve is calculated from the empirical relation:

$$\frac{v_h}{v} \approx (1-\phi)^\beta \quad 18$$

If $\beta=5$, this equation corresponds to the first-order term of the linear expansion of equation 2. However, $\beta=5$ does not give a good description of our data. By using $\beta=9$ our system is described in a better way. The theory of Brady and Durlinsky [23] also does not fit very well with our result quantitatively. The difference between the theory and the experimental results can be explained by the fact that our colloidal spheres are not hard spheres and are rather polydisperse. Buscall [46] reported that for practical suspensions β deviates from 5 and that other theories predict a higher value for β . Walstra and Oortwijn [47] found $\beta=8.6$ for milk fat globules which is very well comparable to our finding.

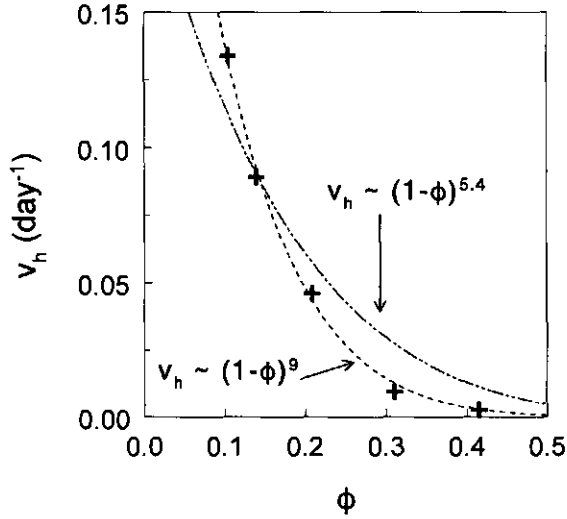


Figure 4 The initial creaming rate v_h as a function of the volume fraction of oil droplets in the emulsion (symbols). The dashed curves are predicted from equation 18.

By following the same method as in the previous paragraph we determined $R_c(t)$ of mixtures with EPS added to the emulsions. Firstly, we analyzed a set of mixtures at different volume fractions and fixed EPS concentration. The exponential equation 16 fits the experimental points fairly well (see Figure 5).

In general, the rise of the interface is much faster than for the emulsions without EPS. The increase in the creaming rate is due to aggregated oil droplets which cream faster (the effective radius of the particles in equation 1 is larger).

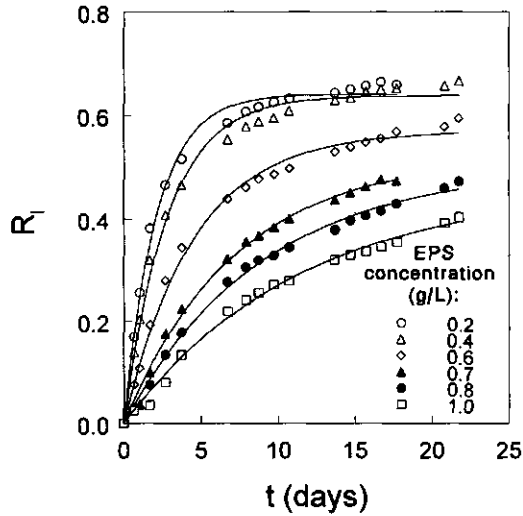


Figure 5 Demixing of emulsion ($\phi=0.14$) at varying EPS concentrations as indicated.

In Figure 6 the v_h parameters as calculated from equation 16 are given as a function of the EPS concentration for various values of ϕ . When EPS is added v_h increases at all volume fractions. It reaches a maximum value at the concentration at the binodal, c_p^{bin} . Beyond that concentration v_h decreases with c_p because the relative viscosity increases strongly above ~ 0.5 g/L.

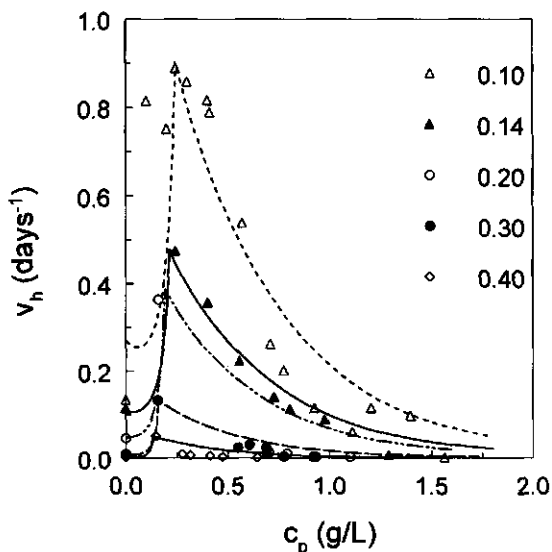


Figure 6 The initial demixing rate v_h , as a function of the EPS concentration for various volume fractions as indicated. The drawn curves are calculated from equations 3-5 ($c_p < c_p^{bin}$) and from equations 3, 5 and 6 ($c_p > c_p^{bin}$).

The drawn curves in Figure 6 ($c_p < c_p^{bin}$) are calculated from equations 3-5 and the parts for $c_p > c_p^{bin}$ from equations 3, 5 and 6. The simplified theoretical approach gives a remarkably good description of the experimental data. At high volume fractions the value of v_h becomes so low that the system no longer phase separates on a practical time scale; this can be explained by the creation of the transient 'gel'-like network [3,10,37-39]. Parker *et al.* [10] and Manoj *et al.* [19] could identify this network by delayed creaming upon increasing the polymer concentration, but we could not detect any initial delay in the creaming process.

Rheology

When a sufficient amount of EPS is added, a stable region can be detected at $\phi > 0.10$, as shown in Figure 2. Just after mixing EPS and the emulsion the suspension is liquid-like, but after storage (1 day) it becomes gel-like. As soon as shear is applied to the gel it flows, but it returns to a gel-like system after storage. In order to characterize the mixtures in this region we have studied their rheological behavior. We added concentrated EPS solutions to emulsions with a volume fraction of 0.3 and 0.4, and measured the viscosity as a function of the shear rate after three days of storage. The results are plotted in Figures 7 (a) and (b). It is clearly demonstrated that the mixtures are shear thinning, which is characteristic for a suspension of aggregating particles, but also for a concentrated polysaccharide solution.

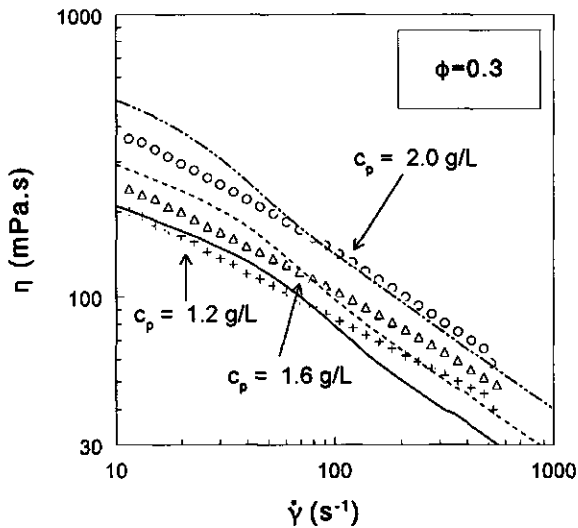


Figure 7 (a) The shear-rate dependence of the viscosity for an emulsion with $\phi=0.30$ for EPS concentrations as indicated. The theoretical predictions were made from the theory of Potanin et al. [31], combined with the shear-rate dependence for polymer solutions from Bueche [33] and Rouse [35].

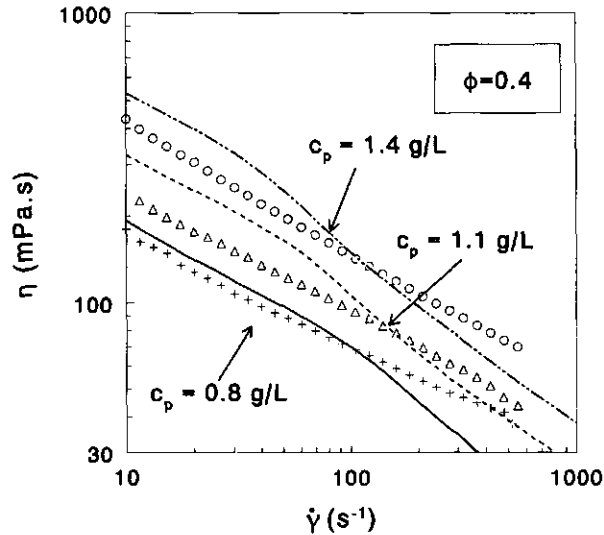


Figure 7 (b) As 7 (a) but for $\phi=0.40$.

We tried to describe the rheological behavior by combining equations 8 and 12 (assuming that there are no interactions between the oil droplets; $\phi_d(\dot{\gamma})=\phi$) but this gave poor results: the predicted viscosities were far too low. For instance, for 0.8 g/L EPS and $\phi=0.40$ the zero-shear viscosity would be approximately 84 mPa.s, whereas it is almost 200 mPa.s at $\dot{\gamma}=10 \text{ s}^{-1}$ (and even higher in the zero-shear limit).

The drawn curves in Figures 7 (a) and (b) represent the theoretical predictions from the Potanin model for suspensions of weakly aggregated spherical particles [31]. In the calculations, we used $\phi_{\text{max}}=0.63$, $a=650 \text{ nm}$, $d_r=2.50$ (this fractal dimensionality gave the best description of the slope of the data points) and k_{el} was simply taken proportional to c_p . The only parameter left is the product of numerical coefficient C_{rup} times the prefactor of the elasticity constant k_{el} . This product was fitted to the data series with 1.4 g/L EPS and $\phi=0.30$ at $\dot{\gamma}=10 \text{ s}^{-1}$ and was kept constant for the other calculations. The model curves follow the experimental trends of varying the EPS concentration and the volume fraction rather well. It should be noted that the theory of Bueche [33] overestimates the shear-rate thinning of EPS solutions to some extent for EPS concentrations below 3 g/L [34]. Therefore the calculated viscosity at high shear rates is too low, which explains the deviation between experiment and

theory at higher shear rates. Nevertheless, the theoretical description is reasonable, taking into account the complexity of the system. The more EPS is added, the stronger the gel (k_{el} is higher). The creation of a gel-like particle network in emulsions by adding polysaccharides is in accordance with the findings of Parker *et al.* [10].

When the shear rate was decreased after the experiment from 500 to 10 s^{-1} , hysteresis was found: the viscosity had decreased and did not return to its initial value. In terms of the Potanin model, this can only be explained if one assumes that the fractal dimension has increased during breakdown of the aggregates, giving a smaller effective volume fraction of aggregates in the system. The same kind of hysteresis was reported by Wolthers *et al.* [48] for a model system containing colloidal particles and non-adsorbing polymers. They found that the height $\eta(\dot{\gamma})$ -curves decreased in subsequent ramps. All curves, however, followed the Potanin model description if it was assumed that d_f increased.

Conclusions

When EPS is added to an emulsion, phase separation occurs due to a depletion mechanism. The phase separation threshold can satisfactorily be predicted by the Vrij theory. The time scale of demixing strongly depends on the volume fraction of oil, which can be explained by hydrodynamic interactions. Addition of EPS initially increases the creaming rate due to attractions between the droplets in the presence of EPS. The creaming rate reaches a maximum at the EPS concentration corresponding to the binodal, and this rate can be described by a simple theory derived from the generalized Stokes-Einstein equation. The rheological behavior can be reasonably interpreted by considering the mixture as a suspension of weakly aggregating particles. The increase in the viscosity of the mixture observed upon increasing the EPS concentration is too large to be explained only by the thickening properties of the EPS in the continuous phase; it must also be due to the creation of a network.

Acknowledgment

Fanny Weinbreck is acknowledged for doing many experiments and for her pleasant co-operation. We thank Alan Parker, Firmenich, Switzerland, and Dr. H.T.M. van den Ende, Twente University, The Netherlands, for discussions and critical reading of the manuscript. Jan Klok is thanked for taking the micrographs. Dr. Erik ten Grotenhuis, Martine van den Berg, and Franklin Zoet at NIZO food research are acknowledged for encouraging discussions.

References

- [1] Mulder, H., Walstra, P., *The Milk Fat Globule*, 1974.
- [2] Cerning, J., *FEMS Microbiol. Rev.*, **87** (1990) 113.
- [3] Cao, Y., Dickinson, E., Wedlock, D.J., *Food Hydrocolloids* **4** (1990) 185.
- [4] Dickinson, E., Goller, M.I., Wedlock, D.J., *Colloids Surf. A* **75** (1993) 195.
- [5] Dickinson, E., Ma, J.G., Povey, M.J.W., *Food Hydrocolloids* **8** (1994) 481.
- [6] Dickinson, E., Goller, M.I., Wedlock, D.J., *J. Colloid Interface Sci.*, **172** (1995) 192.
- [7] Dickinson, E., Golding, M., *Food Hydrocolloids* **11** (1997) 13.
- [8] Gunning, P.A., Hibberd, D.J., Howe, A.M., Robins, M.M., *Food Hydrocolloids* **2** (1988) 119.
- [9] Bergenst ahl, B., In: '*Gums and Stabilisers for the Food Industry*,' Phillips, G.O., Wedlock, D.J., Williams, P.A. (Eds.), IRL Press, Oxford, volume 4, 1988.
- [10] Parker, A., Gunning, P.A., Ng, K., Robins, M.M., *Food Hydrocolloids* **9** (1995) 333.
- [11] Manoj, P., Watson, A.D., Hibberd, D.J., Fillery-Travis, A.J., Robins, M.M., *J. Colloid Interface Sci.*, **207** (1998) 294.
- [12] Precht, D., Peters, K.-H., Petersen, J., *Food Hydrocolloids* **2** (1988) 491.
- [13] Walstra, P., De Roos, A. L., *Food Rev. Int.*, **9** (1993) 503.
- [14] Tuinier, R., Dhont, J.K.G., De Kruijff, C.G., submitted, 1999; Chapter 5 of this thesis.
- [15] Dickinson, E., *J. Dairy Sci.*, **80** (1997) 2607.
- [16] Dickinson, E., Pawlowsky, K., *J. Agric. Food Chem.* **45** (1997) 3799.
- [17] Bibette, J., Roux, D., Pouligny, B., *J. Phys. II France*, **2** (1992) 401.
- [18] Steiner, U., Meller, A., Stavans, J., *Phys. Rev. Lett.* **74** (1995) 4750.
- [19] Manoj, P., Fillery-Travis, A.J., Watson, A.D., Hibberd, D.J., Robins, M.M., *J. Colloid Interface Sci.*, **207** (1998) 283.
- [20] Vrij, A., *Pure & Appl. Chem.* **48** (1976) 471.
- [21] Gast, A.P., Hall, C.K., Russel, W.B., *J. Colloid Interface Sci.*, **96** (1983) 251.
- [22] Lekkerkerker, H.N.W., Poon, W.C.K., Pusey, P.N., Stroobants, A., Warren, P.B., *Europhys.Lett.* **20** (1992) 559.

- [23] Brady, J.F., Durlofsky, L.F., *Phys.Fluids*, **31** (1988) 717.
- [24] Dhont, J.K.G., 'An Introduction to Dynamics of Colloids,' Elsevier Science, Amsterdam, 1996.
- [25] Kops-Werkhoven, M.M., Vrij, A., Lekkerkerker, H.N.W., *J. Chem. Phys.* **78** (1983) 2760.
- [26] De Kruijff, C.G., Briels, W.J., May, R.P., Vrij, A., *Langmuir* **4** (1988) 668.
- [27] De Kruijff, C.G., Rouw, P.W., Briels, W.J., Duits, M.H.G., May, R.P., Vrij, A., *Langmuir* **5** (1989) 422.
- [28] Imhof, A., van Blaaderen, A., Maret, G., Mellema, J., Dhont, J.K.G., *J. Chem. Phys.* **100** (1994) 2170.
- [29] Kops-Werkhoven, M.M., Ph.D. Thesis, Utrecht University, 1982.
- [30] van der Werff, J.C., De Kruijff, C.G., *J. Rheol.* **33** (1989) 421.
- [31] Potanin, A.A., De Rooij, R., van den Ende, D., Mellema, J., *J. Chem. Phys.* **102** (1995) 5845.
- [32] Krieger, I.M., *Adv. Colloid Interface Sci.*, **3** (1972) 111.
- [33] Bueche, F., *J. Chem. Phys.*, **22** (1954) 1570.
- [34] Tuinier, R., Zoon, P., Cohen Stuart, M.A., FLeer, G.J., de Kruijff, C.G., submitted 1999; Chapter 3 of this thesis.
- [35] Rouse, P.E., *J. Chem. Phys.*, **21** (1953) 1272.
- [36] Tuinier, R., Zoon, P., Olieman, C., Cohen Stuart, M.A., FLeer, G.J., de Kruijff, C.G., *Biopolymers* **49** (1999) 1.
- [37] Verhaegh, N., 'Structure and kinetics of phase separating colloidal suspensions,' Ph.D. Thesis Utrecht University, 1996.
- [38] Pusey, P.N., Pirie, A.D., Poon, W.C.K., *Physica A*, **201** (1993) 322.
- [39] Poon, W.C.K., Pirie, A.D., Pusey, P.N., *Faraday Disc.*, **101** (1995) 65.
- [40] Chiew, Y.C., Glandt, E.D., *J. Phys. A: Math. Gen.* **16** (1983) 2599.
- [41] Ornstein, L.S., Zernike, F., *Proc. Koninkl. Nederland Akad. Wetenschap, Amsterdam*, **17** (1914) 793.
- [42] Percus, J.K., Yevick, G.J., *Phys. Rev.* **110** (1958) 1.
- [43] Baxter, R.J., *J. Chem. Phys.* **49** (1968) 2770.
- [44] Kranendonk, W.G.T., Frenkel, D., *Mol. Phys.* **64** (1988) 403.
- [45] Tuinier, R., ten Grotenhuis, E. Holt, C., Timmins, T.A., de Kruijff, C.G., *Phys. Rev. E*, in press, 1999.
- [46] Buscall, R., *Colloids Surf.*, **43** (1990) 33.
- [47] Walstra, P., Oortwijn, H., *Neth. Milk Dairy J.* **29** (1975) 263.
- [48] Wolthers, W., Duits, M.H.G., van den Ende, D., Mellema, J., *J. Rheol.* **40** (1996) 799.

Practical implications and future work

The key question posed in this thesis is 'what determines the viscosity of exocellular polysaccharide (EPS) solutions and the phase behavior of EPS-protein mixtures?' The characterization and physical properties of an exocellular polysaccharide (EPS) were described in Chapters 2-4. Subsequently, the interactions of EPS with components in milk were investigated: with whey proteins (Chapter 5), casein micelles (Chapters 6 and 7) and emulsion droplets (Chapter 8). In this concluding Chapter the practical relevance of this work is outlined.

Viscosity of EPS solutions

Investigations on the rheological properties of polysaccharides produced in fermented products are required in order to characterize the thickening effect of EPSs in food products. When 'new' EPSs are isolated, their properties need to be checked and compared with commercial types, which may eventually lead either to improvement of products or to less expensive ingredients.

Various studies on EPSs have focused on the physiology of production [1,2] or on the genetic engineering of the EPSs [3-6]. Independent chemical studies have been made of the primary structure of EPSs [e.g. 7-10]. Indeed, chemical information about the repeating unit of an EPS may be very useful in order to predict the efficiency of the EPS as a thickener when one knows how this chemical structure is related to the physical properties of the polysaccharides in solution. Attention has also been paid to the measurement of the viscosities of EPSs [11-16], with variables such as temperature [14], salt concentration [15] and the different stages of growth [12]. However, in most cases the relation with molecular properties is not clear and poorly quantified.

In Chapter 3 of this thesis a general approach was introduced and further developed to describe the contribution of a random coil polysaccharide to the solution viscosity. A similar approach can be used to characterize new polysaccharides, which then helps to answer questions from the industry such as: what type of polysaccharide would increase the viscosity the most at a given polymer weight concentration? or: what characteristics make a polysaccharide solution more shear-thinning? From the results of this thesis it follows that the intrinsic viscosity is the key quantity required to answer these questions. The intrinsic viscosity, which equals the hydrodynamic volume per unit mass and is thus an "effective voluminosity" of the polymer, may be expressed in terms of the radius of gyration (R_g), and, hence, depends on

the molar mass (M), on the solvent quality, and on the chain stiffness of the polymer. The chain stiffness, in turn, depends on the primary structure of the polysaccharide: the chemical nature of the monomers and, more importantly, the types of linkage between the monomers in the backbone. This means that, to obtain a higher intrinsic viscosity, in genetic engineering of EPSs it is more relevant either to increase the chain length or to make the polysaccharide stiffer rather than to vary the type of sugar monomers. Also branching changes the rheological properties since an increase in the number of branches decreases the hydrodynamic volume of the chains of a given molar mass.

By way of illustration the result for B40 EPS is compared with B891 EPS from another strain of *Lactococcus lactis* subsp. *cremoris* from the NIZO collection. The radius of gyration and the molar mass were measured experimentally and the intrinsic viscosity was theoretically predicted (see Chapter 3) and compared with experiment. The results are given in Table 1.

Table 1 Some characteristics of the EPSs produced by *L. lactis* B40 and B891.

EPS	B40	B891
M_n (10^3 ·kg/mol)	1.47 ± 0.06	2.38 ± 0.08
R_g (nm)	86 ± 2	91 ± 2
M_w/M_n	1.13	1.17
ν	0.57 ± 0.02	0.51 ± 0.01
l_k (nm)	17 ± 2	11 ± 2
$[\eta]_0$ (m ³ /kg) calculated	2.7 ± 0.3	2.0 ± 0.2
$[\eta]_0$ (m ³ /kg) measured	3.2 ± 0.2	2.0 ± 0.3

Table 1 shows that although B40 EPS has the lower molar mass, its radius of gyration is only slightly smaller than that of B891 EPS for two reasons: higher stiffness, and higher expansion (better solvency). For polymers with a high chain stiffness the hydrodynamic volume per unit mass is relatively large. In order to quantify the chain stiffness, the Kuhn lengths of the EPSs were calculated (as described in Chapter 2) from the measured radii of gyration and molar masses, also given in Table 1, using the geometry of the repeating unit, as analyzed by van Casteren [17]. The Kuhn lengths are given in Table 1 and indicate that the chain stiffness of B40 EPS ($l_k=17$ nm) is larger than that of B891 EPS ($l_k=11$ nm).

As the primary structure of B891 EPS has not yet been fully determined one can only speculate on the reasons for the difference in flexibility. It is known, for instance, that monosaccharides connected by β -(1-4) bonds make a stiffer backbone than chains with α -(1-4) or β -(1-3) bonds [18-20]. Furthermore, charged groups (absent in B891 EPS) may enhance the solvent quality of the polysaccharide, thereby increasing the value of ν (the scaling exponent relating radius of gyration to the molar mass: $R_g \sim M^\nu$), and l_k .

Subsequently, the intrinsic viscosities of the EPSs were determined from low shear measurements and also calculated from the measured radius of gyration and molar mass (see Chapter 3). The magnitude of the calculated and measured $[\eta]_0$ correspond very well, which thus confirms that the combination of the molar mass and size in solution determines the intrinsic viscosity. Since the concentration dependence of the viscosity can be described in terms of $[\eta]_0$ only (see references 21 and 22 plus Chapter 3 of this thesis) the analysis can be used as a tool to predict the suitability of an EPS as thickener. Understanding the relation between primary structure and R_g (for a given M) requires additional research. Better insight into this relation is essential for genetic engineers aiming at controlling the physical properties of EPSs by changing their primary structure. Work is in course to determine the chemical (primary) structures of a range of EPSs. With the result of these in hand, the 'structure-function'-correlation can be further determined.

Dynamic rheological properties of EPS solutions

A remarkable property of acidified milk products with in-situ produced EPS is that they often allow a liquid thread to be drawn out of the solution. This behavior is typical for sufficiently concentrated polymer solutions, because these become visco-elastic liquids, and develop normal stresses. Phenomena such as the slimy character of acidified milk products can therefore be attributed to high local EPS concentrations. The rheological behavior can be manipulated by increasing η_0 and M , as shown theoretically in Chapter 4. Further work should lead to a better understanding of the complex behavior of stirred yogurts in which EPS plays an important role [2,3]. The relation between sliminess and normal stresses could be tested by investigating the elongational flow properties of EPS solutions and EPS-containing acidified milk products.

EPS and its interactions with proteins

The second part of this thesis addresses the interactions of EPS with the main constituents of milk: whey proteins, casein micelles, and milk fat particles (Chapters 5-8). As a model for fat particles we used sunflower oil droplets covered with whey proteins. In comparison with pure EPS solutions, mixtures of EPS and proteins are more like many real foods, where polysaccharides, proteins, and fat or oil are present together. The bio-colloids chosen for this work were well-defined in composition in order to be able to quantify the physical properties of mixed systems; they were derived from milk constituents. Milk proteins have similar structures and functionalities as flour proteins. According to Tolstoguzov [23] polysaccharides mixed with skim milk proteins behave very much like wheat dough.

An example of a two-phase system obtained after mixing (heated) whey proteins and EPS is given in Figure 1. It can be seen that the protein-rich phase (lower phase) behaves as a liquid, which is to be expected for colloidal aggregates.

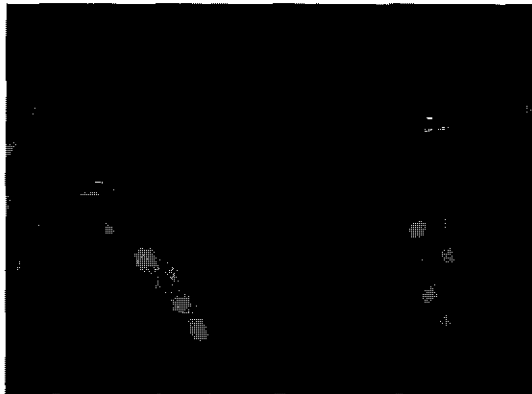


Figure 1 Photographs of a phase-separated whey protein/EPS mixture.

Figure 2 depicts tubes of skim milk having a volume fraction of 7% casein micelles; the one on the left also contained 1.2 g/L EPS. It is seen in this photograph how strongly casein micelles can be concentrated in a separate phase when sufficient EPS is added, with EPS present in the upper phase. A practical application of such phase separation is currently used at NIZO to separate and concentrate protein fractions.

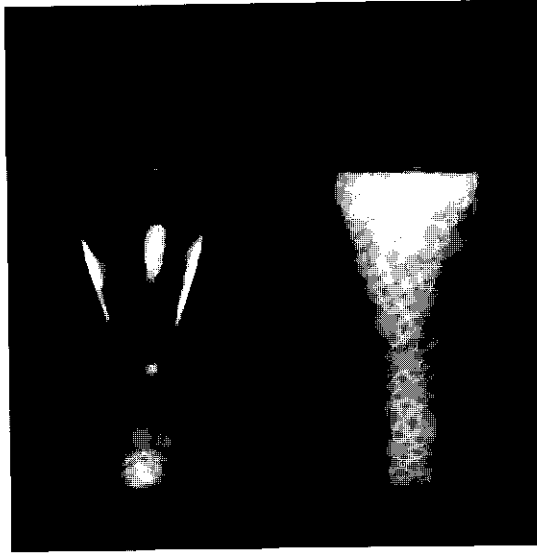


Figure 2 Photograph of tubes of skim milk (volume fraction 7%), left with added EPS (1.2 g/L).

When adding EPS to an oil-in-water emulsion various types of instability can be observed, as shown in Figure 3.



Figure 3 Photograph of an emulsion (volume fraction 20%) with EPS concentrations (increasing from left to right).

At low concentrations a distinct phase separation takes place but upon further increase of the EPS concentration the phase separation rate is slowed down, eventually leading to a stable gel-like network.

In Chapters 5-8 the properties of the mixtures were described in terms of depletion interactions. The presence of depletion interaction in polysaccharide-protein mixtures is very common due to a usually segregative interaction between these types of biopolymers [24,25]. It has been shown that mixing EPS with (not too small) protein particles and emulsion droplets leads to a phase separation. Figure 4 shows typical experimental phase lines of some investigated systems. The measured phase behavior could almost quantitatively be accounted for by using an appropriate theory (Chapters 5, 7 and 8). Figure 4 illustrates the strong effect of the ratio of the particle sizes on the phase boundary; especially at low colloidal volume fraction ϕ , the EPS concentrations c_p required for phase separation of very small (AWC) and of very large (oil) particles differ by an order of magnitude.

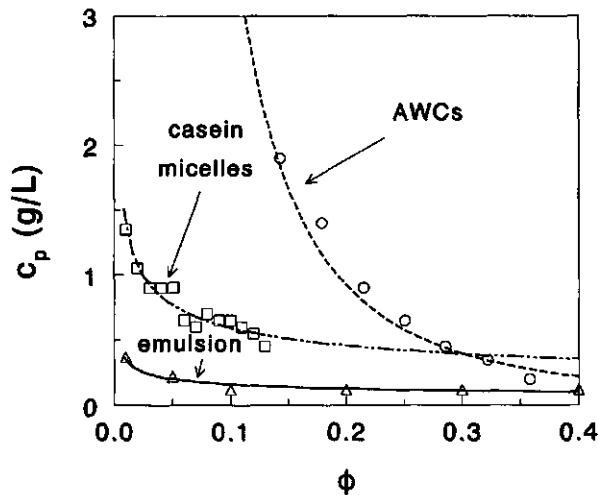


Figure 4 Phase diagrams of the mixtures investigated in this thesis: EPS mixed with aggregated whey protein colloids (AWCs), with casein micelles and with emulsions. Systems below the curves are stable; those above phase separate.

In consumer products, phase separation is usually unwanted. However, many aspects related to interactions between EPS (or polysaccharides in general) and proteins or emulsions can be used for improving the products. Firstly, a fundamental understanding of the interactions leads to predictions of the phase line and interpretation of the measured phase behavior. The unwanted effect of phase separation can then be suppressed by using only biopolymer concentrations in the stable regions. The theory for depletion interaction allows the phase lines to be predicted from the sizes and molar masses of the particles involved. In the stable region the system does not behave ideally; as has been shown in Chapters 5, 7 and 8 the equilibrium and transport properties of the proteins change when EPS is added. The transport properties, such as diffusion and especially the viscosity, affect aspects such as mouthfeel. An understanding of the biopolymer interactions may thus also lead to a more intelligent manipulation of the properties of food dispersions.

From the interactions of EPS with emulsion droplets it was found that a gel phase can form when the attraction between the oil droplets is large and the volume fraction of oil droplets is sufficiently high. This is an 'arrested' phase separation which behaves macroscopically as a stable highly viscous/gel-like mixture. In products such as salad dressings this mechanism gives the product its characteristic consistency.

Knowledge of the interactions between biopolymers will allow the manipulation of food sensory properties by adjusting the interaction in a desirable way. Adjustment can be done by a proper selection of biopolymers and process conditions. The detailed quantitative description of the interactions between model biocolloids in this thesis may serve as an approach for monitoring and adjusting interactions in (food) biopolymer mixtures.

In separation technology the concepts of phase separation can be used to lower the energy consumption of the process. For example, concentration of caseins can be achieved easily by adding the right polysaccharide dose. Industrial applications of depletion interactions have been proposed before [26,27] but with increasing knowledge of the fundamentals it becomes easier to tune these processes. At NIZO food research the depletion mechanism is now exploited to separate large and small biocolloids, thereby replacing the more cumbersome procedure of acidification and centrifugation.

Suggestions for future work

The concepts developed for describing the rheological properties of EPSs and polysaccharides in general may be further tested for a series of well-defined polysaccharides, differing in chain stiffness, molar mass, charged groups and degree of branching. A direct measurement of the elongational properties of both EPS/polysaccharide solutions as well as

acidified milk products would be useful for gaining more insight into another important textural attribute of stirred yogurt: ropiness.

Considering the interactions with proteins we mainly investigated the repulsive interactions between EPS and milk proteins. We restricted ourselves to the conditions prevailing in native milk. There is, however, a great variety of dairy products, such as acidified milk drinks and yogurts, where the conditions and processing variables are vastly different. At low pH EPSs might also take part in specific associative phenomena like bridging flocculation. EPS may serve as a model research compound to unravel the behavior of less well-defined polysaccharides, such as pectin and carrageenan. Future work could be directed to this aspect of specific interactions. Work on the properties of stirred yogurt, already begun by van Marle [28] will, together with the work on interactions at low pH, lead to a better understanding of the contribution of EPS to the texture of fermented products and to the possibility of controlling texture by modifying EPS.

In order to make progress there is a need for experimental methods which can distinguish between segregative and associative behavior. One method could be nuclear magnetic resonance solvent relaxation, $^1\text{H-NMR}$, which for model systems can detect whether or not polymer adsorption occurs, as shown by van der Beek *et al.* [29]. This method is based on a change in the magnetic relaxation behavior of protons in water molecules: when a polymer adsorbs a part of the 'bound'-water is set free which decreases the relaxation efficiency.

Dynamic light scattering (DLS) is also a very useful tool for determining whether a polymer adsorbs onto a colloidal particle, as shown for instance by van der Beek and Cohen Stuart [30]. Recently it was shown that DLS is also very suited for probing polysaccharide-protein interactions [31]. By measuring the radius of the protein particles in dilute protein solutions one can distinguish between segregative and associative interactions. In the case of associative interactions the effective radius of the particles increases due to an adsorbed layer of polysaccharides whereas the radius remains unaffected in the case of segregative interactions.

One way of manipulating depletion interactions to help structure a product is by inducing a gel-like network as in the case of EPS mixed with emulsion droplets. The precise nature of the network formed is not yet clear and could be studied, for instance, by confocal laser microscopy (CSLM) and/or diffusing wave spectroscopy (DWS). If such a network consists of percolated oil droplets, CSLM will show rigid strands of aggregated particles in which the droplets hardly move. The diffusion of such droplets will thus be very low, and can then be monitored by DWS.

Acknowledgments

Remi den Broeder and Jan van Riel (NIZO food research) are thanked for performing various experiments. Ellen Looijesteijn is thanked for her help with the production of B891 EPS. I am indebted to Dr. C. Holt, Hannah Research Institute, UK, for a critical reading of the manuscript. Professor J. Mellema and Dr. M.H.G. Duits, Department of Rheology of Twente University, are acknowledged for making accessible the Contraves low-shear rheometer.

References

- [1] Cerning, J., Renard, C.M.G.C., Thibault, J.F., Bouillanne, C., Landon, M., Desmazeaud, M., Tropisirovic, P., *Appl. Environ. Microbiol.*, **60** (1994) 3914.
- [2] Marshall, V. M., Cowie, E.N., Moreton, R.S., *J. Dairy Res.* **62** (1995) 621.
- [3] Hötte, B., Rath-Arnold, I., Pühler, A., Simon, R., *J. Bacteriol.*, **172** (1990) 2804.
- [4] Glucksmann, M.A., Reuber, T.L., Walker, G.C., *J. Bacteriol.*, **175** (1993) 7045.
- [5] Huang, J., Schell, M., *Mol. Microbiol.*, **16** (1995) 977.
- [6] van Kranenburg, R., Marugg, J.D., van Swam, I.I., Willem, N.J., de Vos, W.M., *Mol. Microbiol.*, **24** (1997) 387.
- [7] O' Neill, M.A., Morris, V.J., Selvendran, R.R., Sutherland, I.W., Taylor, I.T., *Carbohydr. Res.*, **148** (1986) 63.
- [8] Gruter, M., Leeflang, J., Kuiper, J.P., Kamerling, J.P., Vliegthart, J.F.G., *Carbohydr. Res.*, **239** (1993) 209.
- [9] Robijn, G.W., Thomas, J.R., van den Berg, D.J.C., Haas, H., Kamerling, J.P., Vliegthart, J.F.G., *Carbohydr. Res.*, **276** (1995) 137.
- [10] van Casteren, W.H.M., Dijkema, C. Schols, H.A., Beldman, G., Voragen, A.G.J., accepted for publication in *Carbohydr. Pol.*, 1998.
- [11] Lapasin, R., Pricl, S., Bertocchi, C., Navarini, L., Cesaro, A., De Philippis, R., *Carbohydr. Pol.*, **17** (1992) 1.
- [12] Ridout, M.J., Brownsey, G.J., Morris, V.J., Cairns, P., *Int. J. Biol. Macromol.*, **16** (1994) 324.
- [13] Britten, M., Morin, A., *Lebensm.-Wiss. U. -Technol.*, **28** (1995) 264.
- [14] Calvo, C., Ferrer, F., Martinez-Checa, Bejar, V., Quesada, E., *Appl. Biochem. Biotechnol.*, **55** (1995) 45.
- [15] Eteshola, E., Gottlieb, M., Arad, S., *Chem. Engin. Sci.*, **51** (1996) 1487.
- [16] Fishman, M.L., Cescutti, P., Fett, W.F., Osman, S.F., Hoagland, P.D., Chau, H.K., *Carbohydr. Pol.*, **32** (1997) 213.
- [17] van Casteren, W.H.M., to be published, 1999.

- [18] Ring, S.G., l'Anson, Morris, V.J., *Macromolecules*, **18** (1985) 182.
- [19] Rees, D.A., *Polysaccharide Shapes, Outline Studies in Biology*, Chapman & Hall, London, 1977.
- [20] Bianchi, E., Ciferri, A., Conio, G., Lanzavecchia, L., Terbojevich, M., *Macromolecules*, **19** (1986) 630.
- [21] Robinson, G., Ross-Murphy, S.B., Morris, E.R., *Carbohydr. Res.*, **107** (1982) 17.
- [22] Morris, E.R., Cutler, A.N., Ross-Murphy, S.B., Rees, D.A., Price, J., *Carbohydr. Polymers*, **1** (1981) 5.
- [23] Tolstoguzov, V.B., *Food Hydrocolloids* **11** (1997) 181.
- [24] Tolstoguzov, V.B., *Food Hydrocolloids* **4** (1991) 429.
- [25] Syrbe, A., Bauer, W.J., Klostermeyer, H., *Int. Dairy J.*, **8** (1998) 179.
- [26] Polson, A., Potgieter, G.M., Largier, J.F., Mears, G.E.F., Joubert, J., *Biochim. Biophys. Acta.*, **82** (1964) 463.
- [27] Antonov, Yu, A., Grinberg, V. Ya., Tolstoguzov, V.B., *Coll. Pol. Sci.*, **255** (1977) 937.
- [28] Van Marle, M.E., PhD Thesis Twente University, 1998.
- [29] van der Beek, G., Cosgrove, T., Cohen Stuart, M.A., *Langmuir* **5** (1989) 1180.
- [30] van der Beek, G., Cohen Stuart, M.A., *J. Phys. (Paris)* **49** (1988) 1449.
- [31] Langendorff, V., Cuvelier, G., Michon, C., Parker, A., de Kruijff, C.G., submitted to *Food Hydrocolloids*, 1999.

Summary

In the food industry polysaccharides are used as thickening or gelling agents. Polysaccharides are usually extracted from plants. Micro-organisms are also capable of excreting polysaccharides: exocellular polysaccharides (EPSs). In some cases EPSs are produced in-situ in food products, notably in acidified milk products. These EPSs function effectively as food thickeners but do not need to be declared in the food label.

Systematic physical analysis of an exocellular polysaccharide produced by a lactic acid bacterium has hardly been performed until now. In order to obtain a better understanding of the role of EPS in (acidified) milk products the physical properties of an EPS from the lactic acid bacterium strain *Lactococcus lactis* subsp. *cremoris* B40 were studied (Chapters 2-4) as well as its interactions with milk proteins (Chapters 5-8). The ionic strength of the EPS solutions was always set at 0.10 M, about the ionic strength in milk.

In Chapter 2 the isolation, purification and analysis of the molecular properties of EPS from *L. lactis* B40, our 'model' EPS, are investigated. The polysaccharide was separated from most low molar mass compounds in the culture broth by filtration processes. Gel permeation chromatography (GPC) was used to size-fractionate the polysaccharide. Fractions were analyzed by multi-angle static light scattering in aqueous solutions from which a number- (M_n) and weight-averaged (M_w) molar mass of $(1.47 \pm 0.06) \cdot 10^3$ and $(1.62 \pm 0.07) \cdot 10^3$ kg/mol, respectively, were calculated so that $M_w/M_n \approx 1.13$. The number-averaged radius of gyration was found to be 86 ± 2 nm. The hydrodynamic radius as determined from dynamic light scattering was consistent with the radius of gyration.

The viscosity of the EPS solutions was studied in simple shear flow as described in Chapter 3. Firstly, the zero-shear viscosity was determined as a function of the concentration. The intrinsic viscosity was determined from the data in the low concentration range. The intrinsic viscosity and the concentration dependence of the (zero-shear) viscosity of the B40 EPS could be predicted from the molar mass and the hydrodynamic radius. In addition the shear-thinning behavior was measured at several concentrations. The shear rate at which the viscosity starts to decrease scales with polymer concentration in accordance with the Rouse theory. By combining existing theories (Rouse and Bueche) it is possible to predict the intrinsic viscosity, concentration dependence of the viscosity, and shear-thinning behavior in terms of the molar mass and the hydrodynamic radius.

The measurements and theoretical description of the dynamic rheological properties of the EPS are presented in Chapter 4. Dynamic rheological measurements were performed as a function of frequency and EPS concentration. The dynamic properties could be described by the bead-spring model of Rouse. Concentrated EPS solutions have a significant elasticity at

Summary

high concentrations and high frequencies, which is indicative of the presence of significant normal stress differences. It is suggested that these normal stresses may explain the contribution of the EPSs to the ropy behavior of yogurts.

Having characterized the EPS in aqueous solution, its interaction with the most relevant colloidal (protein) particles present in milk products was studied. As the polysaccharide studied in this thesis occurs in dairy products our focus was on the interactions and phase behavior of EPS with the colloidal components in milk. There are three distinctly different types of particles in the colloidal size range in milk: fat globules, casein micelles and whey proteins. Smaller molecular species (over 100,000 in milk) are considered as part of the continuous phase.

In Chapter 5 the interactions with whey proteins are described. Native whey proteins and EPS were co-soluble; they could be mixed in all proportions. However, an effective attraction (a depletion interaction) is induced between aggregated-whey-protein colloid (AWC) particles when they are mixed with the EPS. This depletion interaction originates from a loss of conformational entropy of the EPSs near the surface of neighboring AWC particles and leads to a phase separation at high enough EPS and/or AWC concentrations. The effect of the depletion interaction on the properties of the mixtures of EPS and AWC particles was first studied in the stable, i.e. one-phase region. The strength of attractions was characterized by small-angle neutron scattering (SANS) and dynamic light scattering (DLS). The SANS results could be described quantitatively by the Vrij theory and integral theory (Ornstein-Zernike with HNC closure) in combination with the Schaink-Smit theory and allowed a determination of the position of the spinodal. The DLS results could be described reasonably well by using a theory of Dhont and Kawasaki.

Furthermore, the experimental phase boundary was determined and compared with the Schaink-Smit theory, a mean-field theory which evaluates the free energy of a mixture of colloids and large non-adsorbing polymers. The spinodal so calculated was found to be consistent with the experimentally determined position of the phase boundary.

Spinodal phase separation kinetics was investigated by small-angle light scattering (SALS). At low Q a scattering peak was detected which shifted to lower Q 's with time, in agreement with other experimental data and theoretical predictions for spinodal decomposition. Both the scaling of the scattered intensity with Q and the scaling of the Q -position of the peak with time agree with theoretical predictions of Furukawa and Siggia.

The interactions between EPS B40 and casein micelles are treated in in Chapter 6. Casein micelles become mutually attractive when the EPS is added to skim milk. The attraction can be explained as a depletion interaction between the casein micelles induced by the non-adsorbing EPS. We used three scattering techniques (SANS, turbidity measurements and DLS) to measure the attraction. The Vrij theory in combination with integral theory and all the

experiments showed that casein micelles became more attractive upon increasing the EPS concentration.

The phase separation arising from depletion interaction in mixtures of casein micelles and EPS is described in Chapter 7. We have determined a phase diagram that describes the separation of skim milk with EPS into a casein-micelle-rich phase and an EPS-rich phase. We compared the phase diagrams with those calculated from theories developed by Vrij, and by Lekkerkerker and co-workers, showing that the experimental phase boundary can be predicted quite well. From measurements of the self-diffusion of the casein micelles in the presence of EPS the spinodal was calculated, which corresponds to the visual observations.

The effect of adding the EPS to an oil-in-water emulsion, stabilized with whey proteins, is reported in Chapter 8. Even at low EPS concentrations the emulsion phase separates. The phase line could be described by depletion interaction theory of Vrij. At high EPS concentrations and dispersed phase volume fractions above 10% we found a stable 'gel'-like region in the phase diagram. In that region the oil droplets attract one another so strongly that a space-filling network is formed at sufficient oil volume fractions.

A kinetic study showed that the rate of creaming/demixing decreases with volume fraction of oil of the system (hydrodynamics) and strongly depends on the concentration of EPS (strength of depletion interaction and continuous-phase viscosity). At low EPS concentration the creaming rate strongly increased with EPS concentration since attractions enhance creaming. At higher EPS concentrations creaming was slowed down by the viscosity increase of the continuous phase and the particle network which was created. This network became so strong at high EPS concentrations that creaming was absent in the 'gel' region. The rheological behavior of the 'gel' was studied by measuring flow curves which could be interpreted by the Potanin model, which describes the rheology of a dispersion of weakly aggregating particles.

In Chapter 9 the practical implications of this work are described. In order to understand the thickening effect of EPSs the molar mass, radius of gyration, and their interrelation are very important. It is indicated how the effectivity of a polysaccharide can be analyzed on the basis of the molar mass and the radius of gyration. The relation between the radius of gyration and the molar mass depends on the kind of monosaccharide residues, the linkage type, and the solvent. Further it is addressed how a fundamental understanding of the interactions between polysaccharides and proteins leads to predictions of the phase line and interpretation of the measured phase behavior. The unwanted effect of phase separation can then be suppressed by using only biopolymer concentrations at which the system is still stable. An understanding of the biopolymer interactions may thus make it possible to adjust the properties of food dispersions. Finally, some suggestions for further research are given.

Samenvatting

Polysacchariden worden in de voedingsmiddelenindustrie gebruikt als verdikkings- of geleermiddel. Ze worden meestal uit planten geëxtraheerd, maar ook micro-organismen zijn in staat om polysacchariden uit te scheiden: exocellulaire polysacchariden (EPSen). In levensmiddelen worden EPSen soms geproduceerd tijdens fermentatie (in-situ productie). Zo worden er EPSen geproduceerd in verzuurde melkproducten zoals yoghurt. Op die manier wordt er tijdens het fermentatieproces op een natuurlijke wijze verdikkingsmiddel aan het product toegevoegd, zodat EPS niet hoeft te worden aangegeven op de verpakking als hulpstof.

Een systematische analyse van de fysische eigenschappen van EPSen is noodzakelijk om de rol van EPS als verdikkingsmiddel in zuivelproducten beter te begrijpen. In dit proefschrift staan de fysische eigenschappen van een EPS geproduceerd door de melkzuurbacterie-stam *Lactococcus lactis* subsp. *cremoris* NIZO B40 centraal. Dit EPS is geïsoleerd en in waterige oplossing gebracht. De ionsterkte van de waterige oplossing is steeds ingesteld op 0.10 M, ongeveer de ionsterkte in melk. In hoofdstukken 2 tot en met 4 zijn enkele fysische eigenschappen van dit EPS beschreven. Vervolgens zijn de interacties tussen EPS en de belangrijkste disperse deeltjes van melkproducten beschreven in de hoofdstukken 5 tot en met 8.

In hoofdstuk 2 worden de productie, isolatie en analyse van de moleculaire eigenschappen van het EPS besproken. Het polysaccharide werd gescheiden van bacteriecellen en laagmoleculaire componenten met behulp van filtratieprocessen. Gelpermeatiechromatografie (GPC) is gebruikt om het polysaccharide te scheiden in fracties met verschillende molmassa's. De verschillende fracties zijn geanalyseerd met behulp van lichtverstrooiing. Dit levert een aantalsgemiddelde (M_n) en gewichtsgemiddelde (M_w) molmassa op van respectievelijk $(1.47 \pm 0.06) \cdot 10^3$ en $(1.62 \pm 0.07) \cdot 10^3$ kg/mol wat leidt tot een polydispersiteit, M_w/M_n , van 1.13. De gevonden (aantalsgemiddelde) gyratiestraal is 86 ± 2 nm. De hydrodynamische straal is bepaald met dynamische lichtverstrooiing en bleek overeen te komen met de gyratiestraal.

De metingen en de interpretatie van de viscositeit in eenvoudige afschuifstroming van de EPS oplossingen staan in hoofdstuk 3. Allereerst is de viscositeit bij lage afschuifsnelheid bepaald als functie van de concentratie. Uit de metingen in het lage concentratieregime is de intrinsieke viscositeit bepaald. De viscositeit bij lage afschuifsnelheid blijkt volledig beschreven te kunnen worden op basis van de intrinsieke viscositeit en de concentratie EPS. Vervolgens is de afschuifsnelheids-afhankelijkheid bepaald bij verschillende EPS concentraties. Door verschillende bestaande theorieën (Rouse en Bueche) te combineren bleek dat de intrinsieke viscositeit, de concentratie-afhankelijkheid en de afschuifsnelheidsafhankelijkheid volledig konden worden beschreven op basis van de molmassa en de hydrodynamische straal.

De resultaten van de dynamisch reologische experimenten staan in hoofdstuk 4. Deze experimenten zijn uitgevoerd om de dynamische moduli te bepalen als functie van de frequentie en de EPS concentratie. De dynamische moduli kunnen worden beschreven met het kraal-veer model van Rouse. Het blijkt dat geconcentreerde EPS oplossingen relatief erg elastisch worden bij hoge EPS concentraties en hoge frequenties. Dit geeft aan dat er significante normaalspanningen worden opgebouwd in deze oplossingen en dat zou een verklaring kunnen zijn voor het feit dat EPSen soms een slijmvormende bijdrage leveren aan yoghurt en de yoghurt dradentrekkend maken.

Na de karakterisatie van het EPS in oplossing volgen de studies naar de interacties van het EPS met de kolloïdale deeltjes in melk. Deeltjes worden kolloïdaal genoemd wanneer ze groter zijn dan ruwweg 1 nm terwijl de bovengrens ligt bij enkele microns. Kleinere deeltjes in melk worden gezien als behorende tot het oplosmiddel. Er kunnen drie typen kolloïdale deeltjes worden onderscheiden in melk: melkvetbolletjes, caseïne-micellen en wei-eiwitten.

De interacties met wei-eiwitten zijn bestudeerd in hoofdstuk 5. Verse melk bevat natieve wei-eiwitten. Bij verhitten denatureren de wei-eiwitten en deze gaan vervolgens aggregeren. Mengsels van natief wei-eiwit en EPS zijn stabiel bij alle onderzochte mengverhoudingen. EPS is ook gemengd met kolloïdale geaggregeerde wei-eiwit deeltjes (GW deeltjes), aggregaten verkregen door natief wei-eiwit te verhitten. Mengsels van GW deeltjes en EPS ontmengen bij een zekere concentratie. Het blijkt dat de GW deeltjes elkaar effectief gaan aantrekken indien ze worden gemengd met EPS, als gevolg van depletie van het polymeer. Deze depletie-interactie ontstaat doordat het aantal realiseringmogelijkheden van de EPSen sterk afneemt nabij een GW deeltje. De attracties tussen de GW deeltjes is allereerst bestudeerd in het gebied waar geen fasenscheiding optrad (het stabiele gebied). De sterkte van de attracties is gekarakteriseerd met behulp van kleine-hoek neutronenverstrooiing (NV) en dynamische lichtverstrooiing (DLS). De NV resultaten kunnen kwantitatief worden beschreven met behulp van de depletie-interactie potentiaal van Vrij en integraaltheorie (Ornstein-Zernike met HNC sluiting) in combinatie met de theorie van Schaink en Smit: een gemiddeld-veld benadering die is ontwikkeld om de vrije energie uit te rekenen van een mengsel van kleine bolvormige kolloïden en lange polymeren. Tevens zijn er enkele punten op de spinodaal bepaald met behulp van de NV resultaten. Het blijkt dat de DLS resultaten goed zijn te beschrijven op basis van een recente theorie van Dhont en Kawasaki voor de diffusie van bolvormige kolloïden die elkaar aantrekken.

Vervolgens is de experimentele fasengrens bepaald en vergeleken met de resultaten van de Schaink-Smit theorie. De aldus berekende spinodaal komt overeen met de experimentele fasengrens. De spinodale ontmengingskinetiek van ontmengende GW-EPS mengsels is bestudeerd met behulp van kleine-hoek statische lichtverstrooiing. Bij kleine golfvector (Q)

werd een verstrooiingspiek waargenomen en deze piek schuift naar lagere waarden van Q als functie van de tijd. Dit komt overeen met experimentele studies aan andere systemen die spinodale ontmenging vertonen. Zowel het schalingsgedrag van de verstrooide intensiteit met de golfvector als de top van de verstrooiingspiek als functie van de tijd komen overeen met theoretische voorspellingen van Furukawa en Siggia.

De interacties tussen EPS en caseïne-micellen zijn beschreven in hoofdstuk 6. Caseïne-micellen gaan elkaar aantrekken als EPS wordt toegevoegd aan ondermelk. Deze attractie kan worden beschreven als een depletie-interactie tussen de caseïne-micellen geïnduceerd door niet-adsorberend EPS. Er zijn drie verstrooiingstechnieken gebruikt om de attracties aan te tonen in het stabiele gebied: kleine-hoek neutronenverstrooiing (NV), turbiditeitsmetingen en dynamische lichtverstrooiing (DLS). Zowel voorspellingen op basis van de theorie van Vrij, integraaltheorie en theorie voor plakkende bollen als de experimentele resultaten geven aan dat de attractie tussen de caseïne-micellen toeneemt met toenemende EPS concentratie.

Indien de attracties sterk genoeg worden gaat het systeem ontmengen in een fase rijk aan caseïne-micellen en een fase rijk aan EPS. Het fasengedrag is beschreven in hoofdstuk 7. Allereerst is de experimentele fasenlijn bepaald en deze is vergeleken met verschillende theoretische voorspellingen op basis van theorie voor depletie-interactie van Vrij en van Lekkerkerker en medewerkers. De theoretische voorspellingen zijn consistent met de experimentele fasenlijn. Dit betekent dat de fasenlijn van zulke systemen goed kan worden voorspeld, met als enige parameters de straal van de kolloïdale deeltjes en de gyrationstraal en molmassa van het polymeer. Met behulp van DLS metingen aan caseïne-micellen in de aanwezigheid van EPS is de spinodaal berekend die goed overeenkomt met de visueel waargenomen fasengrens.

Het effect van EPS op de eigenschappen van een olie-in-water emulsie, gestabiliseerd met wei-eiwit, is in hoofdstuk 8 weergegeven. Bij relatief lage EPS concentratie is reeds een fasenscheiding waargenomen van de emulsie met EPS in een fase rijk aan EPS en een fase geconcentreerd in emulsiedruppels. De fasenlijn kan goed worden beschreven met behulp van de theorie van Vrij voor depletie-interactie. Bij hoge EPS concentratie en volumefracties van emulsiedruppels hoger dan 10% wordt een kolloïdale 'gel'-fase waargenomen. De oliedruppels trekken elkaar daar zo sterk aan dat ze bij voldoende hoge volumefracties aan bolletjes een ruimtevullend netwerk vormen.

Onderzoek naar de ontmengingskinetiek liet zien dat de ontmengingssnelheid afneemt met toenemende volumefractie aan olie en tevens sterk afhangt van de EPS concentratie. Bij lage EPS concentratie neemt de ontmengingsnelheid eerst sterk toe met de EPS concentratie aangezien een toename van de attractie leidt tot een verhoging van de ontmengingssnelheid. Bij hogere EPS concentraties neemt de ontmengingsnelheid weer af ten gevolge van de

toename van de viscositeit van de continue fase en het ontstaan van het netwerk van disperse deeltjes. De ontmengingssnelheid kan goed worden beschreven met behulp van de gegeneraliseerde Stokes-Einstein relatie. Het reologische gedrag van deze gelfase is geanalyseerd door de viscositeit te bepalen als functie van de afschuifsnellheid. Deze resultaten kunnen goed worden beschreven met behulp van een reologisch model voor een zwak aggregerende dispersie, gegeven door Potanin.

In hoofdstuk 9 zijn de praktische implicaties van dit onderzoek beschreven. Voor de verdikkende werking van EPSen blijkt de relatie tussen molmassa en gyrationstraal van groot belang te zijn. Deze relatie hangt van de ketenstijfheid af en dus van de aard van de monosaccharide residuen, het bindingstype tussen de residuen en het oplosmiddel. Er is aangegeven hoe de effectiviteit van een polysaccharide geanalyseerd kan worden op basis van molmassa en gyrationstraal. Vervolgens is aangetoond hoe kennis van de interacties tussen EPS en de kolloïdale componenten in melk kan worden gebruikt in praktische toepassingen. De grootte-verhouding tussen polymeer en kolloïdaal deeltje blijkt van groot belang te zijn voor de ligging van de fasenlijn. Aangezien het fasengedrag redelijk voorspeld kan worden kan rekening worden gehouden met ontmengingsverschijnselen in produktformuleringen. Tenslotte zijn er enige suggesties gegeven voor verder onderzoek.

List of symbols

Latin

a	sphere radius (m)
a_H	hydrodynamic radius (m)
a_{low}	lower length scale limit (m)
a_{up}	upper length scale limit (m)
b	path length through the sample (m)
B_2	second virial coefficient
B_2^{sp}	second virial coefficient at the spinodal
B_3	third virial coefficient
c	particle or polymer concentration (g/L) (Chapters 2-4)
c_i	cross-over polymer concentration between regimes i and j (g/L)
$c(r)$	direct correlation function
c_p	polymer concentration (g/L) (Chapters 5-8)
c_p^R	polymer concentration in the reservoir (g/L)
c_p^{bin}	polymer concentration at the binodal (g/L)
C	constant which depends on branching and polydispersity of polymer
C_{rup}	numerical coefficient characterizing the fragility of the bond between the primary particles
C_1	constant which reflects the hydrodynamic interactions between particles
C_2	unknown proportionality constant (L/g)
d_f	fractal dimension
D	diffusion coefficient ($m^2 \cdot s^{-1}$)
D_c	collective diffusion coefficient ($m^2 \cdot s^{-1}$)
$D(Q)$	apparent diffusion coefficient ($m^2 \cdot s^{-1}$)
D_0	diffusion coefficient at infinite dilution ($m^2 \cdot s^{-1}$)
D_s	short-time self-diffusion coefficient ($m^2 \cdot s^{-1}$)
$\langle D \rangle_z$	z-averaged diffusion coefficient ($m^2 \cdot s^{-1}$)
dn/dc	refractive index increment (m^3/kg)
$f_p^{tot}(r)$	total local free energy density of the polymer solution as a function of the distance from a sphere (J)
$f_p^{ex}(r)$	contribution of the excluded volume interactions between disconnected polymer segments to $f_p^{tot}(r)$ (J)
$f_p^{sq}(r)$	square gradient contribution neighborhood of the spheres to $f_p^{tot}(r)$ (J)

F_c	free energy of the hard spheres (J)
F_p	spatial integral of the local free energy density $f_p^{\text{tot}}(r)$ (J)
F_{tot}	total free energy (J)
$g(r)$	radial distribution function
$g^{(2)}(\tau)$	auto-correlation function
$G^{(2)}(Q, \tau)$	intensity auto-correlation function
G'	storage modulus (Pa)
G''	loss modulus (Pa)
$h(r)$	total correlation function
$I(Q)$	scattered intensity at a wave vector Q (a.u. or $\text{J}\cdot\text{m}^{-5}$)
$I_0(Q)$	scattered intensity of the proteins (without EPS) (a.u.)
I_0	scattering intensity of the primary beam ($\text{J}\cdot\text{m}^{-2}$)
k_1	constant describing the first-order volume fraction dependence of the self-diffusion coefficient
k'	Huggins constant (m^3/kg)
k_B	Boltzmann's constant (J/K)
k_{el}	spring constant between the particles (N/m)
K	material constant (m^2/g^2)
l	segment length (m)
l_K	length of a Kuhn segment (m)
L	contour length (m)
m	mass of a polymer molecule (kg)
M	molar mass (kg/mol)
M_n	number-averaged molar mass (kg/mol)
M_w	weight-averaged molar mass (kg/mol)
M_z	z-averaged molar mass (kg/mol)
n	refractive index of the continuous phase
n_0	refractive index of the solvent
N	number of polymer segments
N_1	first normal stress difference (Pa)
N_{AV}	Avogadro's number (mol^{-1})
N_c	number of colloidal particles
N_K	number of Kuhn segments
$p^2(r)$	polymer concentration near a particle relative to the polymer bulk concentration
$P(Q)$	particle scattering form factor
Q	scattering wave vector (m^{-1})

List of Symbols

Q_m	wave vector where the scattered intensity has its maximum (m^{-1})
r	distance between the centers of the colloidal spheres (m)
R	gas constant (J/K)
R_{agg}	radius of an aggregate (m)
R_g	radius of gyration (m)
R_l	relative volume of the lower phase
R_H	hydrodynamic radius (m)
R_L	radius of the spherical cell (m)
$\langle R^2 \rangle^{1/2}$	root-mean-square end-to-end distance (m)
$R(Q)$	Rayleigh ratio
$S(Q)$	structure factor
$S_0(Q)$	structure factor of protein particles in absence of EPS
t	transmission (Chapter 6)
t	time (s)
T	temperature (K)
$U(r)$	interaction potential (J)
u	sedimentation/creaming velocity (m/s)
u_h	corrected sedimentation/creaming velocity (m/s)
U_0	minimum of the interaction potential (J)
v	creaming rate (s^{-1})
v_h	corrected creaming/sedimentation rate (s^{-1})
v_{sp}	specific volume of spherical particles (m^3/kg)
V_c	particle volume (m^3)
$V_{overlap}$	overlap volume (m^3)
$V_{free}(r)$	volume of the spherical shell accessible for the polymers (m^3)
V_{shell}	volume of the shell (m^3)
$V_{ov}(\sigma_c, R_L)$	sphere-shell overlap volume (m^3)

Greek

α	linear expansion coefficient
β	constant linked to the signal-to-noise ratio in light scattering
Σ	system-dependent constant
χ	Flory-Huggins segment-solvent interaction parameter
δ	range of the attraction/depletion layer thickness (m)
Δ	depletion layer thickness (m) (Chapters 6 and 7)

μ_c	thermodynamic potential of the colloidal suspension (J)
μ_f	thermodynamic potential of colloidal spheres in the fluid phase (J)
μ_p	thermodynamic potential of polymer solution (J)
μ_s	thermodynamic potential of colloidal spheres in the solid phase (J)
ζ	σ_p/σ_c
ζ_h	ratio between the effective polymer radius and sphere radius
Γ_n	nth order cumulant
η_{∞}	limiting viscosity at infinitely high shear rate (Pa.s)
η_0	dynamic viscosity in the Newtonian plateau regime (Pa.s)
η_r	relative viscosity
η_{r0}	relative viscosity in the Newtonian plateau regime
η_c	viscosity of the continuous phase (Pa.s)
η_e	elongational viscosity (Pa.s)
η_{eff}	effective viscosity
η_s	solvent viscosity (Pa.s)
η_{sp}	specific viscosity ($=\eta_r-1$)
$[\eta]$	intrinsic viscosity ($=\eta_{\text{sp}}/c_p$ at $c_p \rightarrow 0$) (m^3/kg)
$[\eta]_0$	intrinsic viscosity in the Newtonian plateau regime (m^3/kg)
$\dot{\gamma}$	shear rate (s^{-1})
$\dot{\gamma}_R$	inverse of the Rouse time (s^{-1})
λ	wavelength (m)
λ_0	wavelength in vacuo (m)
ν	scaling exponent relating the molar mass to the radius of gyration
θ	angle under which scattered light is detected
Π_c	osmotic pressure of the colloidal particles (Pa)
Π_f	dimensionless osmotic pressure of the colloidal fluid phase
Π_p	osmotic pressure of the polymer solution (Pa)
Π_s	dimensionless osmotic pressure of the colloidal solid phase
ρ	number density of the particles (m^{-3})
ρ_c	density of the colloidal phase (kg/m^3)
ρ_p	density of the polymer in the molten state (kg/m^3)
ρ_w	density of the aqueous phase (kg/m^3)
σ_c	colloid diameter (m)
σ_p	effective diameter of the polymers (m)
τ	decay time (s)
τ_1	longest relaxation time (s)

List of Symbols

τ_B	Baxter parameter
τ_i	i-th characteristic relaxation time (s)
τ_p	relaxation time corresponding to mode p (s)
τ_R	longest relaxation time (s)
ξ	ratio between the radius of gyration and the hydrodynamic radius of a polymer (Chapter 2)
ξ	friction coefficient ($N \cdot m^{-1} \cdot s$)
ξ	correlation length (Chapter 5)
ω	frequency (rad/s)
$\Psi_{1,0}$	first normal stress coefficient ($Pa \cdot s^2$)
ϕ	volume fraction of spheres
$\phi_a(\dot{\gamma})$	volume fraction of aggregated flocs
ϕ_{cp}	volume fraction at closest packing
ϕ_{max}	maximum volume fraction
ϕ^{sp}	volume fraction at the spinodal
ϕ_p	polymer volume fraction
$\phi_p(\mathbf{r})$	local volume fraction of polymer molecules
Λ	typical length scale of the fastest growing density variation (m)

List of Publications

1. Hoogeveen, C.W. Hoogendam, Tuinier, R., Cohen Stuart, M.A., Adsorption of weak polyelectrolytes on amphoteric oxide surfaces, *Int. J. Pol. Anal. Char.* **1** (1995) 315.
2. Tuinier, R., Bisperink, C.G.J., van den Berg, C., Prins, A., Transient foaming behavior of aqueous alcohol solutions as related to their dilational surface properties, *J. Colloid Interface Sci.* **179** (1996) 327.
3. Hoogendam, C.W., Peters, J., Tuinier, R., de Keizer, A., Cohen Stuart, M.A., Bijsterbosch, B.H., Effective viscosity of polymer solutions: relation to the determination of the depletion thickness of the adsorbed layer of cellulose derivatives, *J. Colloid Interface Sci.* **207** (1998) 309.
4. Tuinier, R., de Kruif, C.G. Depletion flocculation of casein micelles induced by the EPS of a lactic acid bacterium, In: "Gums and Stabilisers for the Food Industry", P.A. Williams, G.O. Phillips, Ed., 1998, p. 222 (parts of Chapters 6 and 7).
5. Tuinier, R., Zoon, P., Olieman, C., Cohen Stuart, M.A., Fleer, G.J., de Kruif, C.G., Isolation and physical characterization of an exocellular polysaccharide, *Biopolymers* **49** (1999) 1.
6. Tuinier, R., ten Grotenhuis, E., Holt, C., Timmins, P.A., de Kruif, C.G., Depletion interaction of casein micelles and an exocellular polysaccharide, accepted for publication in *Phys. Rev. E* (Chapter 6).
7. Tuinier, R., de Kruif, C.G., Phase behavior of casein micelles/exocellular polysaccharide mixtures; experiment and theory, accepted for publication in *J. Chem. Phys.* (Chapter 7).
8. Tuinier, R., Zoon, P., Cohen Stuart, M.A., Fleer, G.J., de Kruif, C.G., Concentration and shear-rate dependence of an exocellular polysaccharide, submitted (Chapter 3).
9. Tuinier, R., de Kruif, C.G., Phase separation, creaming, and network formation of oil-in-water emulsions induced by an exocellular polysaccharide, submitted to *J. Colloid Interface Sci.* (Chapter 8).
10. Tuinier, R., Dhont, J.K.G., de Kruif, C.G., Depletion induced phase separation of aggregated whey protein colloids by an exocellular polysaccharide, submitted to *Langmuir* (Chapter 5).
11. Tuinier, R., Oomen, C.J., Zoon, P., Cohen Stuart, M.A., de Kruif, C.G., Viscoelastic properties of a polysaccharide produced by a *Lactococcus lactis*, submitted (Chapter 4).

Dankwoord

Na het afronden van een proefschrift is het een goede traditie om verschillende mensen te bedanken die je hebben ondersteund. Allereerst denk ik daarbij aan Mieke. Ik ben haar dankbaar voor alle ruimte die ze mij heeft gegeven om tijd te besteden aan het onderzoek. Het is niet altijd even gezellig als iemand met tensoren op het strand ligt. Haar liefde is van groot belang geweest voor de rust die ik had voor het schrijven van dit proefschrift. Mijn ouders wil ik bedanken voor hun nooit aflatende steun, zeker ook ten behoeve van mijn ontwikkeling.

Met mijn wetenschappelijke begeleiders heb ik het getroffen; vier verschillende mensen van wie ik veel heb geleerd. Nel Zoon heeft mij op de juiste momenten de extra zetten gegeven die nodig waren om de vaart erin te krijgen en heeft me de vrijheid gegeven om me te verdiepen in theorie om de experimentele resultaten te kunnen kwantificeren. Kees de Kruif heeft me veel geleerd over fysische chemie en aan de nuttige brainstormsessies op zijn kamer waarbij de ballen letterlijk en figuurlijk rondvlogen denk ik met plezier terug. De neutronenverstrooiings-experimenten die we hebben uitgevoerd in Grenoble hebben veel indruk op me gemaakt. Martien Cohen Stuart heeft mij vanaf het moment dat ik startte met een afstudeervak op "FYSKO" altijd het vertrouwen gegeven. Toen ik in mijn eerste AIO-jaar nog 'zoekende' was en mijn twijfel uitte kon hij me met zijn fysisch-chemische kennis en creativiteit weer motiveren. De kritische blik van Gerard FLeer op mijn schrijfsels en bedenksels heeft me geholpen onderzoekswerk veel beter onder woorden te brengen en er kritischer naar te kijken. Een opmerking als 'het is geen roman!' zal me nog lang heugen.

I would like to thank Dr. Carl Holt and Dr. Peter Timmins for their collaboration and help with the neutron scattering experiments in Grenoble. Verschillende medewerkers van de reologie-groep van de universiteit Twente en het van't Hoff lab in Utrecht ben ik dankbaar voor hun hulp bij het onderzoek. Met name wil ik Jan Dhont voor zijn hulp bij hoofdstuk 5 en professor Vrij voor het kritisch lezen van het proefschrift na mijn start in Utrecht. De contacten met NIZO food research collega's van de afdeling Product Technology zijn zeer prettig en nuttig geweest. Speciaal wil ik Jan Klok en Saskia de Jong noemen voor de uitstekende verzorging van de apparatuur en Erik ten Grotenhuis die mij (o.a.) heeft geholpen met de berekeningen aan structuurfactoren. De samenwerking met de NIZO EPS-club, en met name met Ellen Looijesteijn, was prettig.

Mijn leuke tijd op NIZO is ook te danken aan mijn kamergenoten: Marieke, Edwin en Marja. Marieke, bedankt voor je hulp in mijn moeilijke startperiode. En denk eraan: "an apple a day helps to keep the doctor away !" Edwin zorgde voor veel gezelligheid en hield mij scherp met zijn relativerende ("according to FYSKO the world is a cube") en kritische ("als er maar een kromme lijn uit komt") opmerkingen.

Op het FYSKO lab heb ik me altijd welkom gevoeld, zeker ook bij de AIO's. De VLAG-ABON groep wil ik graag bedanken, en in het bijzonder Willemieke van Casteren en Henk Schols, voor de prettige samenwerking. Jeannette bedank ik voor het ontwerpen van de omslag en Mariska voor het maken van de symbolenlijst.

Finally, I have been very privileged with the undergraduate students who performed a large amount of work which is a part of this thesis. In chronological order: Cyril Renaud, Blandine Oudin, Clasien Oomen, *Dominique Ginapé*, *Fanny Weinbreck*, *Remi den Broeder*, and *Alexandra Le Roy*. I would like to thank you for all your help and friendship. Unfortunately, Cyril died far too early in March 1998. Cyril was a special friend; I dedicate this thesis to the memory of Cyril.

Remco Tuinier, april 1999

Curriculum Vitae

Op 3 maart 1971 ben ik geboren in ziekenhuis 'Zonnegloren' te Soest. Na in 1989 het VWO diploma te hebben behaald aan 'Het Baarnsch Lyceum' te Baarn begon ik met de studie levensmiddelentechnologie aan de Landbouwniversiteit Wageningen. Na een afstudeervak Levensmiddelennatuurkunde over het schuimgedrag van alcohol-water systemen in de groep van professor A. Prins heb ik een stage gedaan bij Quest International te Naarden op het gebied van emulsiestabiliteit. Eind 1994 werd de studie afgerond met een afstudeervak Kolloïden grensvlakchemie over laagdikten van geadsorbeerd polymeer. Vervolgens ben ik gestart met een promotie-onderzoek bij NIZO food research en het laboratorium voor Fysische Chemie en Kolloïdkunde van de Landbouwniversiteit Wageningen waarvan de resultaten zijn beschreven in dit proefschrift. Vanaf februari 1999 ben ik werkzaam bij het Van 't Hoff laboratorium voor Fysische- en Colloïdchemie, Debye instituut, Universiteit Utrecht.